DOCTORAL DISSERTATION
NAGAOKA UNIVERSITY OF TECHNOLOGY

Variability of Flood Peak due to Rainfall Spatial Distribution in Middle and Lower Yom Basin, Thailand

Name Pawee Klongvessa
ID number 13701486

December, 2017

Supervisor: Prof. Dr. Minjiao Lu

Chief examiner:	Dr. Minjiao Lu	Professor
Examiner:	Dr. Tokuzo Hosoyamada	Professor
Examiner:	Dr. Toshiro Kumakura	Associate Professor
Examiner:	Dr. Kazuyoshi Takahashi	Associate Professor
Examiner:	Dr. Takahiro Yamamoto	Associate Professor

External publication:

1. Klongvessa, P.; Lu, M.; Chotpantarat, S. (2017): Variation of characteristics of consecutive rainfall days over northern Thailand. Theoretical and Applied Climatology. in press. DOI 10.1007/s00704-017-2208-4

2. Klongvessa, P.; Lu, M.; Chotpantarat, S. (2017): Variation of critical rainfall duration upon its magnitude in middle and lower Yom basin, Thailand. Journal of Water Resource and Hydraulic Engineering 6(3): 34-42. DOI 10.5963/JWRHE0603001

Abstract

Variability of flood peak due to rainfall spatial distribution has been found in basins which have non-uniform characteristics. However, there is still lack of relevant information on prioritization of each characteristic of the basin. This study identified spatial characteristics of rainfall over the northern Thailand, investigated the variability of flood peak in Suhkothai city due to rainfall spatial distribution in Yom basin, and discussed the effect of basin characteristics on the variability.

In identifying the spatial characteristics of rainfall, Markov chain probability model and chi-square test of independence were applied to study consecutiveness of >0.0, >10.0, and >35.0 mm rainfall days during May-October 1981-2010. The results reveal that >10.0 mm rainfall days are consecutive all over the northern Thailand and >35.0 mm rainfall days are obviously consecutive over the joint between mountainous region and plain area. Then, student-t test was applied to investigate the rainfall amount on >10.0 mm rainfall days and the result reveals that the mountainous region has lower rainfall amount on >10.0 mm rainfall days than the plain area. Therefore, the characteristics of consecutive rainfall days over the mountainous region, plain area, and joint area are established.

In flood peak investigation, floods from designed rainfalls were simulated by HEC-RAS and HEC-HMS models. In the model, basin parameters over the mountainous region and plain area were calibrated separately. The area was divided into 4 zones for distributing the rainfall. The spatially random 1,000 rainfalls were simulated for each of 2-, 5-, and 10-y rainfall under the durations of 24-, 48-, and 72-h. The randomization used the Monte Carlo analysis and Cholesky randomization to generate rainfalls under the observed mean, variance and spatial correlation. The results reveal different characteristics between flood peaks from short and long duration rainfalls. Flood peaks from short duration rainfalls are usually low but highly variable and respond to the rainfall over the upstream area while flood peaks from long duration rainfalls are usually high but not very variable and respond to the rainfall over the joint area. However, because the rainfall tends to concentrate over the joint and downstream areas rather than the upstream area, the flood peaks from long duration rainfall are more common. Nevertheless, when the short duration rainfall concentrates over the upstream area, it can give an extremely high flood peak.

The flood peaks from short duration rainfalls respond to the rainfall over the upstream area because the upstream area has low surface storage which is dominant when the rainfall is small and has high steepness which is dominant when the rainfall is large. For the long duration rainfall, the flood peak mainly responds to the soil percolation rate. With this reason, the response of the flood peak to the rainfall in the most upstream area is weak. For both short and long duration rainfalls, the response of the flood peak to the rainfall in the most downstream area is weak because that area has long distance to the main channel.

Keywords: Flood peak, Rainfall spatial distribution, Prioritization, Basin characteristics, Yom basin, Consecutive rainfall days, Rainfall duration.

Contents

List of Figures

List of Tables

Chapter 1

Introduction

1.1 Background

It has been found that when a basin is non-uniform and rainfall duration is shorter than a time to equilibrium, a peak discharge of the basin responds to rainfall spatial distribution [Ogden and Julien, 1993, Singh, 1997, Bell and Moore, 2000]. Recently, there were many studies which emphasized an importance of rainfall spatial distribution on flood simulation [Golian et al., 2010, 2011, Tramblay et al., 2011, Zoccatelli et al., 2011, Saghafian et al., 2014]. Nevertheless, those studies focused on development of simulation technique and assessment of simulation result. Even though some studies discussed the physical mechanisms regarding the basin characteristics, there is still lack of information on prioritization of each characteristic.

Our study aims to investigate the variability of flood peaks due to rainfall spatial distribution for short and long duration rainfalls in middle and lower Yom basin, Thailand, and investigate the physical mechanism behind this variability. The Yom basin appears to be a suitable location for studying flood from spatial rainfall because this basin has a very long main stream, has different characteristics between upstream mountainous region and downstream plain area, and has no large scale control structure to control the flow of flood water. In terms of flood management, this basin is one of the upstream areas of the Chao Phraya basin, the largest and most populated basin in Thailand which frequently has flood during the southwest monsoon period, May-October. Since 1980, at least 5 major flood events, in 1983, 1995, 1996, 2006, and 2011, have been recorded. The losses and damages from these events are on the scale of at least ten millions US dollar [Prajamwong and Suppataratarn, 2007, The World Bank, 2012]. The area which is well pronounced for being inundated by flood in the Yom basin is Sukhothai city which is located in the plain area closed to the mountainous region.

According to the historical records, most major flood events are coincide with consecutive rainfall days [Hydro and Agro Informatics Institute, 2008a,b, 2009]. The reason is that the main stream of the Yom basin is long. Therefore, it takes several days for flood water to travel along this river until it reaches the flood area [Royal Irrigation Department, 2015]. As a result, the water from consecutive rainfall days can get accumulated and causes a severe flood. However, the currently available studies on consecutive rainfall days in the area [Dahale et al., 1994, Szyniszewska and Waylen, 2012] still do not show the spatial characteristics of the consecutive rainfall days even though the topography has been proved to play an important role on rainfall [Okumura et al., 2003, Yokoi and Satomura, 2008, Kuraji et al., 2009, Takahashi et al., 2010, Takahashi, 2010, Mahavik et al., 2014]. Therefore, it is useful to identify the spatial characteristics of the consecutive rainfall days.

In our study, we first identified a spatial pattern of consecutive rainfall days. Then, we developed the conceptual rainfall-runoff model which can take rainfall spatial rainfall and non-uniform basin characteristics into account. Next, we designed a large number of rainfalls with various spatial distributions according to the observed pattern and simulated these rainfalls in the model to investigate the variability of flood peak. Finally, the influences of basin characteristics and rainfall spatial distribution on flood peaks were discussed.

1.2 Objectives

Objectives of this study include the following,

1. Establishment of spatial characteristics of consecutive rainfall days over the northern Thailand.
2. Determination of characteristics of floods from spatially distributed short and long duration rainfalls.
3. Identification of mechanisms behind the flood characteristics.

1.3 Structure of dissertation

In chapter 1, background and objectives are mentioned. Then, theory and literature review are mentioned in chapter 2. Next, details of the study area are mentioned in chapter 3. After that, methods and results are mentioned in chapters 4 and 5. The chapter 4 covers the part of identification of spatial rainfall while the chapter 5 covers the part of flood simulation. Finally, the chapter 6 concludes our study.

Chapter 2

Theory and literature review

2.1 Rainfall-related climatology

2.1.1 Precipitation

Precipitation is a product of a condensation of water vapor in the atmosphere which falls into the Earth surface by the gravity. It can occur when the following 3 conditions are satisfied [Leewatjanakul, 2009],

1. The air is saturated.

2. There is a condensation mechanism which transforms the water vapor to water droplet. Usually, the condensation occurs when the air moves upwards. A lowering of temperature according to the height from the Earth surface causes the condensation in an upper level.

3. There are condensation nuclei for an aggregation of the water droplet which causes the water droplet to become heavy enough to fall into the Earth surface. In the atmosphere, the condensation nuclei are particles in the air.

The aggregation of the water droplet can be due to the collision-coalescence process (warm rain process), ice crystal process (cold rain process), and lightning process. In the collision-coalescence process, the aggregation is caused by a collision of the water droplets to one another. In the ice crystal process, the aggregation occurred in a cloud which consists of supercooled water and ice. The vapors and supercooled water are frozen over the ice crystal and cause the ice to become larger. In the lightning process, the lightning causes positive and negative charges in the water droplets which lead to an attraction.

Depending on the condition, the precipitation can be in forms of drizzle, rain, snow, snow grains (granular snow), snow pellets (graupel), hail, sleet, and freezing rain [Ahrens, 2009]. The drizzle consists of very small water droplets with circumferences of approximately 0.1-0.5 mm. It has a very slow falling rate, usually $\leq$1 mm/h. It usually occurs when the upward movement of the air is slow. The rain consists of the water droplets with longer circumferences than those in the drizzle. It is the most common form of precipitation in the areas where temperatures are suitable for the water to be in the liquid state. The snow is the precipitation in the form of ice crystal. It occurs due to the ice crystal process when the cloud droplet is very small. The ice crystals in the snow can be called snowflakes. The snow grains are similar to the drizzle but they occur in the colder air. The difference of characteristics between the snow grains and the drizzle is that the snow grains are frozen while the drizzle is not. The snow pellets are small balls of rime, an ice particle. They occur when supercooled water droplets freeze on snowflakes. The hail is the precipitation in form of ice with the circumference of >1 cm. It occurs when the height of the freezing level is

low and the upward movement of the air is strong enough to bring the falling precipitation upwards to the freezing level. Over the freezing level, the precipitation becomes ice and the condensation causes the growth of the ice. The sleet is the rain which passes the cold air while falling and becomes ice before it reaches the ground. The freezing rain is the rain which remains liquid before reaching the ground but becomes ice when it hits the cold ground.

In Thailand, due to the location of the country which is in the tropical area and the low elevation topography, the temperature is suitable for the precipitation to be in the form of rain throughout the year. Even though there are some drizzle and hail, the precipitation amounts from these drizzle and hail are small and negligible. Therefore, the rain is the only form of precipitation which brings the significant amount of water to the country.

2.1.2 Rainfall occurrence mechanism

The rainfall can be classified according to the occurrence mechanisms into convective rainfall, orographic rainfall, and frontal rainfall [Leewatjanakul, 2009]. All of these rainfalls are caused by the upwards movement of the air and the condensation in the upper level. However, these types of rainfalls occur from the different upwards movement mechanisms which result in different rainfall characteristics.

2.1.2.1 Convective rainfall

The convective rainfall is caused by a difference of near surface air temperatures among areas. With this difference, the hotter air rises due to the lower density than the cooler air and condenses. The convective rainfall usually covers a small area and has short duration but high intensity. It is the most common type of rainfall in Thailand.

2.1.2.2 Orographic rainfall

The orographic rainfall is caused by a moist air which is blown towards a high elevation area by wind. The moist air is lifted according to the topography and condenses. The orographic rainfall usually concentrates over the windward side of a mountain. Since the mountain acts as a blockage to the wind, the leeward side of the mountain usually has lower rainfall amount than the windward side.

In Thailand, the effect of the mountain on rainfall can be found in some parts of the country where the mountain ranges lie against the southwest monsoon which brings the moist air from the southern oceanic area to the country.

2.1.2.3 Frontal rainfall

The frontal rainfall is caused by a confrontation of air masses with different temperatures. With this confrontation, the warmer air mass rises over the colder air mass. The characteristic of the frontal rainfall depends on the movements of the cold and warm air masses. If the warm air mass moves towards the cold air mass, the warm air will rise slowly and the rainfall will not be intense but cover a large area along the confrontation zone which is called a warm front. This kind of rainfall can be called a stratiform rainfall. If the cold air mass moves towards the warm air mass, the warm air will rise rapidly and the rainfall will be intense but have short duration and cover a small area along the confrontation zone which is called a cold front. There is another case which is the confrontation between the cold air mass and another colder air mass. The warm air mass between these 2 air masses

will rise and causes a heavy rainfall long the confrontation zone which is called an occluded front. This type of confrontation can cause a cyclone.

In Thailand, the frontal rainfall is not very common because the high temperature in the tropical area is not suitable for an existence of the cold air mass. However, around April, there is a possibility that a cold air from the northern continental area intrudes a local warm air and causes a thunderstorm. Nevertheless, floods are not very well pronounced during this period.

2.1.3 Wind

Wind has a role on the rainfall since it controls a movement of the vapor which is used to produce the rainfall [Leewatjanakul, 2009]. Generally, the wind is caused by the difference of temperatures between the areas. In the warmer area, the air is lifted and the pressure is low, and then, the air from the cooler area which has higher pressure moves to replace the air in the warmer area. This movement of the air is the wind blowing from the cooler area to the warmer area. On the Earth, there are many systems of winds.

2.1.3.1 Prevailing wind

The prevailing wind is the annual wind on the Earth surface. This wind occurs because of a difference of temperatures between equatorial and polar zones and the rotation of the Earth. Between the latitudes of 30°N and 30°S, the prevailing wind blows from the east to the west towards the equator. The prevailing wind in this zone is called a trade wind. Between the latitudes of 30° and 60° both in the northern and southern hemispheres, the prevailing wind blows from the west to the east towards the 60° latitude. The prevailing wind in this zone is called a prevailing westerly wind. Between the latitude of 60° and the polar both in the northern and southern hemispheres, the prevailing wind blows from the east to the west towards the 60° latitude. The prevailing wind in this zone is called a polar wind.

As a result of the trade wind, prevailing westerly wind, and polar wind, there is a convergence of the trade wind at the equator and a convergence between the westerly wind and polar wind at the 60° latitude. Over these convergence zones, there are upward movements of the air from the Earth surface to the upper level which lead to condensations, and therefore, the rainfall can occur. The location where the trade wind converges is called an Inter Tropical Convergence Zone and the location where the prevailing westerly wind converges with the polar wind is called a polar front. At the 30° latitude, where both the trade wind and prevailing westerly wind blow outwards, the wind is calm and the pressure is high. That area is called horse latitude.

Due to the leaning Earth axis and the orbiting of the Earth around the sun, at each location, an amount of heat received from the sun varies upon the time in the year, and therefore, the locations of the Inter Tropical Convergence Zone, horse latitude, and polar front vary throughout the year.

The another role the trade wind on rainfall is that it brings warm surface water in the Pacific Ocean to the Australian side of the ocean and causes the air around that area to be warm and moist. Over another side of the ocean, the South American side, there is an upwelling of cold water from the deep ocean, and therefore, the air is colder and drier. Sometimes, there is a weakening of the trade wind which causes the air on the Australian side to be colder and drier than usual and causes the air on the South American side to be warmer and moister than usual. Therefore, the rainfall amount on the Australian side is lower than usual while that on the South American side is higher than usual. This weakening

of the trade wind is called El Niño. Conversely, sometimes, there is a strengthening of the trade wind which causes the air on the Australian side to be warmer and moister than usual and causes the air on the South American side to be colder and drier than usual. This strengthening of the trade wind is called La Niña. It results in more rainfall than usual on the Australian side and less rainfall than usual on the South American side. Not only over the Pacilific ocean, there are also interactions between the atmosphere and ocean over others area, and hence the El Niño and La Niña affect rainfalls in many parts of the Earth [Ahrens, 2009].

In Thailand, the Inter Tropical Convergence Zone passes from the south to the north during May-June and passes from the north to the south during July-October. During these months the Inter Tropical Convergence Zone causes high rainfall amounts. The rainfall amount is even higher when there is the La Niña but lower when there is the El Niño due to the location of the country which is near the Australian side of the Pacific Ocean.

2.1.3.2 Jet stream

The jet stream is the wind at the tropopause, the boundary of the lowest portion of the atmosphere (troposphere), which blows from the west to the east at the latitudes of 30° and 60°. It is caused by a strong temperature gradient and the rotation of the Earth. The flow of the jet stream is sinuous. Even though the jet stream is not a surface wind, its sinuous movement can induce a cyclone on the Earth surface which causes the rainfall.

2.1.3.3 Cyclone

The cyclone is a system of winds which rotate inwards to a low pressure area. The rotation of the cyclone is the result of the rotation of the Earth. In the tropical area, the cyclone can occur due to a high temperature which causes an occurrence of a low pressure area. In the mid-latitude area, the cyclone can occur along a front between warm and cold air masses. Sometimes, the sinuous movement of the jet stream can induce to rotation of the air and cause the cyclone. The cyclone causes an intense rainfall along its path.

In Thailand, the influence of the cyclone can be seen in May and during August-October.

2.1.3.4 Seasonal wind

The seasonal wind is caused by the leaning Earth axis and the orbiting of the Earth around the sun. Around July, the northern hemisphere faces towards the sun while the southern hemisphere does not face towards the sun. Therefore, the northern hemisphere is heated while the southern hemisphere is cooled. Because the heating and cooling rates over the continent are faster than those over the ocean, the continent is warmer than the ocean in the northern hemisphere while the ocean is warmer than the continent in the southern hemisphere. With these reasons, the seasonal wind blows from the ocean to the continent in the northern hemisphere and blows from the continent to the ocean in the southern hemisphere. Around January, the southern hemisphere faces towards the sun while the northern hemisphere does not face towards the sun. Due to the similar mechanism, the seasonal wind blows from the continent to the ocean in the northern hemisphere and blows from the ocean to the continent in the southern hemisphere.

In Thailand, the rainfall is strongly influenced by the seasonal wind due to the location of the country which is between the southern oceanic area and northern continental area. From mid-May to mid-October, the seasonal wind blows from the southern oceanic area and brings

the moist air to the country. This seasonal is called a southwest monsoon. Its direction is deflected from south to southwest because of the rotation of the Earth. From mid-October to mid-February, the seasonal wind blows from the northern continental area and bring the dry air to the country. This seasonal is called a northeast monsoon. Its direction is deflected from north to northeast because of the rotation of the Earth. With these reasons, the seasonal wind causes the high rainfall amount from mid-May to mid-October and the low rainfall amount from mid-October to mid-February.

2.1.3.5 Local wind

The local wind is caused by heating and cooling of the Earth surface during the day and night, respectively, and differences of heating and cooling rates among areas on the surface. It has been found to affect the variation of rainfall locations in the daily scale [Takahashi et al., 2010]. Well-known local wind systems are a system of land and sea breezes and a system of mountain and valley winds.

In the system of land and sea breezes, the land has higher cooling and heating rates than the sea. During the day, the land is warmer than the sea, and therefore, the wind blows from the sea to the land. This wind is called a sea breeze. During the night, the land is cooler than the sea, and therefore, the wind blows from the land to the sea. This wind is called a land breeze.

In the system of mountain and valley wind, the mountain has higher cooling and heating rates than the valley. During the day, the mountain is warmer than the valley, and therefore, the wind blows from the valley to the mountain. This wind is called a valley wind. During the night, the mountain is cooler than the valley, and therefore, the wind blows from the mountain to the valley. This wind is called a mountain wind.

2.2 Concept of hydrology

2.2.1 Hydrologic cycle

The hydrologic cycle describes a circulation of water among atmosphere, surface, and subsurface. It has neither the beginning nor the end. The vapor in the atmosphere precipitates and becomes the water on the surface or infiltrates to the subsurface. Then, the water moves along the surface and subsurface to the ocean. After that, the water in the ocean evaporates and becomes the vapor in the atmosphere again [Leewatjanakul, 2009]. However, there are lots of processes which control the hydrologic cycle as shown in Fig. 2.1.

2.2.1.1 Processes from the atmosphere to the surface

From the atmosphere to the surface, the precipitation is partially intercepted by plants and evaporates back to the air. The maximum amount of the water which can be intercepted on the plant depends on coverage area and type of plants. However, the interception is usually small and negligible during a period of flood-induced rainfall.

2.2.1.2 Processes from the surface to the stream and groundwater

Over the ground surface, some part of the rainwater infiltrates to the subsurface and becomes subsurface runoff while the remaining part becomes surface runoff. Both subsurface and surface runoffs lead the water to a stream. However, along the way to the stream, the

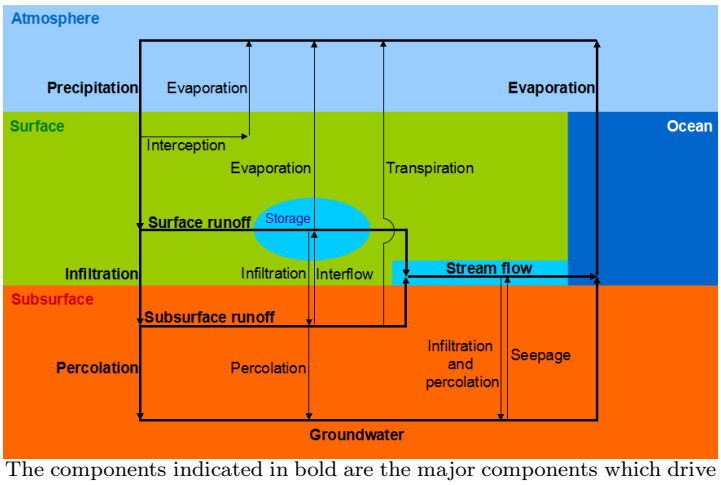

The components indicated in bold are the major components which drive the hydrologic cycle.

Figure 2.1: Hydrologic cycle.

surface runoff can be partially stored on a surface storage and evaporates back to the air, while the subsurface runoff can be partially absorbed by roots of plants and loss to the air by transpiration or partially percolate to the deep soil layer and become groundwater. Moreover, there can be an infiltration of the water from the surface runoff to the subsurface runoff and an interflow of the water from the subsurface runoff to the surface runoff.

The infiltration is controlled by infiltration capacity which is the maximum rate that the ground can absorb the water. It depends on soil characteristics, soil surface condition, moisture content, vegetative cover, and soil temperature [Subramanya, 2008]. Usually, the dry soil has higher infiltration rate than the wet soil. Therefore, the infiltration rate is high when the rainfall begins. After that it decreases due to the wetting by the rainwater.

The difference between the infiltration and percolation is that the infiltration refers to absorption of the water on the surface by the soil while the percolation refers to a descending movement of the water through the soil. The percolation is controlled by soil characteristics and the infiltration.

The surface runoff is controlled by surface roughness, slope, and hydraulic radius. The hydraulic radius is the ratio between the wetted perimeter and flow area. In the wide open waterway, the hydraulic radius can be estimated as the flow depth. Therefore, simply, the runoff on the flood plain is controlled by surface roughness, slope, and flow depth.

The surface storage is controlled by the characteristics of the surface. Usually, the water is stored in ponds or reservoirs.

The subsurface runoff in this section refers to the flow in an unsaturated soil. It is controlled by volumetric water content, matric pressure, and hydraulic conductivity [Nimmo, 2009]. The volumetric water content is a ratio between a volume of water and a bulk volume of soil. The matric pressure is a ratio between pressure of the water in the soil and pressure of the air. The hydraulic conductivity indicates the ability of the soil to conduct the water which will be mentioned in detail in the explanation of groundwater in the section 2.2.1.3. Usually, the flow in the subsurface is much slower than the flow over the surface.

The evaporation and transpiration (evapotranspiration), in comparison to the precipitation, may be small and negligible during each rainfall event. However, in the multiple rainfall events, the evapotranspiration can remove the water from the sub-surface and surface storage after each rainfall event. This removal affects the infiltration and storage of the water from the subsequent rainfall events. Therefore, the evapotranspiration can be important

during a period of multiple rainfall events. It is controlled by solar radiation, temperature, and humidity [Leewatjanakul, 2009].

2.2.1.3 Processes from the stream and groundwater to the ocean

Both stream and groundwater flows lead the water to the ocean. However, if the groundwater level is higher than the stream water level, there can be seepage of the water from the groundwater to the stream. Conversely, if the groundwater level is lower than the stream water level, there can be an infiltration of the water from the stream to the subsurface. Therefore the flow in the stream can be gained or loss.

The stream flow is controlled by channel roughness, slope, and hydraulic radius similarly to the surface runoff in the section 2.2.1.2. However, in comparison between the stream and the floodplain, the stream usually has lower roughness and higher hydraulic radius. The lower roughness and higher hydraulic radius cause the flow in the stream to be faster than that over the flood plain.

The groundwater is this section refers to the flow in a saturated soil. It is controlled by hydraulic gradient and saturated hydraulic conductivity. The hydraulic gradient is a slope of a hydraulic head, a summation of pressure head and elevation head. The hydraulic conductivity is the ability of the soil to conduct the water under a unit of hydraulic gradient. Usually, the hydraulic conductivity increases with the volumetric water content and is highest when the soil is saturated [Nimmo, 2009]. The saturated hydraulic conductivity refers to the hydraulic conductivity when the soil is saturated.

2.2.2 Basin and water budget

In hydrology, a basin is an area which all parts drain the water out of the area through the same outlet. When the rainfall reaches the ground, the movement of the water is controlled by topography. The water moves according to the elevation from the high elevation area to the low elevation area. With this reason, the water cannot cross the mountain ridge, and therefore, the mountain ridge is used as a basin boundary [Subramanya, 2008].

The basin receives the water from the rainfall and discharges the water through its outlet. From the rainfall to the basin discharge, there are many processes involved as mentioned in section 2.2.1. As the result of those processes, the water budget in the basin can be written as the equation 2.1 [Subramanya, 2008],

$$P - R - G - E - T = \Delta S \tag{2.1}$$

where P is the precipitation, R is the net discharge from the surface or runoff, G is the net discharge from the subsurface or groundwater, E is the evaporation, T is the transpiration, and S is the storage.

The basin may be divided into subbasins according to the mountain ridges within the basin. In that case, the water in each subbasin is discharged to an outlet of each subbasin, and then, the discharge from each subbasin is discharged to the outlet of the main basin.

2.2.3 Discharge hydrograph

Flood can be determined from the discharge (R in the equation 2.1). When there is no rainfall, sources of the discharge are the seepage of the groundwater and the interflow of the subsurface runoff. When there is a rainfall, the rainwater will support the water from the

baseflow and causes the discharge to rise. The rising begins when the rainwater reaches the outlet of the basin.

However, it should be noted that, in the hydrologic cycle, some part of the rainwater infiltrates or is stored on the surface (see section 2.2.1.2). That part of the rainwater does not become surface runoff. Therefore, only the part of rainfall which is remained from the infiltration and surface storage can produce the runoff. It is called an excess rainfall. A graph showing the rainfall intensity at each time is called a rainfall hyetograph and a graph showing the excess rainfall intensity at each time can be called an excess rainfall hyetograph.

For a long duration rainfall, after the excess rainfall reaches the outlet, the rising of the discharge continues until the excess rainwater which falls into the most remote part of the basin reaches the outlet. After that the discharge is constant, and then, it decreases after the rain stops. The time that the rainwater which falls into the most remote part takes to reach the outlet is called a concentration time. If the rainfall is uniform, the concentration time can be called a time to equilibrium because the outgoing discharge is balanced with the incoming rainwater when the concentration time is reached. If the rainfall duration is short, it is possible that the discharge decreases before the equilibrium is reached.

The graph which shows the discharge rate at each time is called a discharge hydrograph. Regardless of the rainfall duration, the hydrograph has rising limb, peak, and recession limb. The area under the hydrograph represents the discharge volume. It consists of the runoff and baseflow. The runoff is represented by the area between the rising and falling limbs while the baseflow is represented by the remaining underlying area. If the rainfall hyetograph and discharge hydrograph are considered together, the time from the beginning of the excess rainfall to the peak discharge is called a time to peak, and the time from the center of mass of the excess rainfall hyetograph to the peak discharge is called a lag time. The components of the discharge hydrograph are shown in the Fig 2.2.

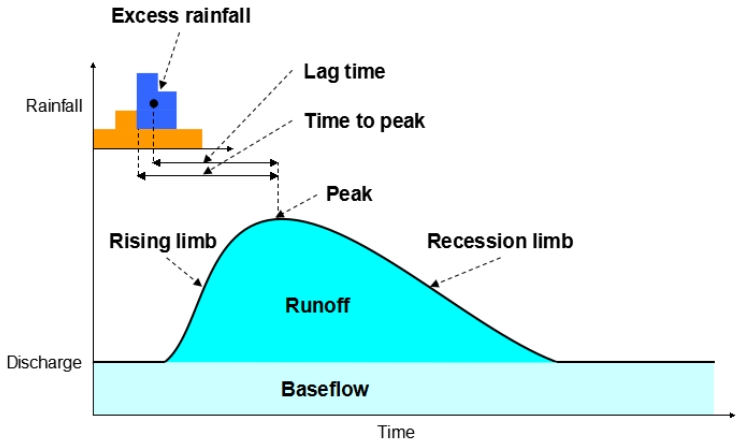

Figure 2.2: Components of discharge hydrograph.

Depending on the basin characteristics, the rainwater can reach the outlet quickly or slowly. If the rainwater reaches the outlet quickly, the hydrograph will have high peak and short lag time. Conversely, if the rainwater reaches the outlet slowly, the hydrograph will have low peak and long lag time. Whether the rainwater can reach the outlet quickly or slowly depends on basin shape, basin size, basin slope, friction, and coverage of streams. Usually, the smaller basin size, shorter basin shape, steeper basin slope, lower friction, and dense coverage of streams cause the rainwater to reach the outlet more quickly [Leewatjanakul, 2009].

2.3 Measurement of hydrological data

Since the movement of the water is controlled by the hydrologic cycle. It is important to measure the movement of the water in each part of the hydrologic cycle accurately. However, for our study, only rainfall, evaporation, water level, and discharge were measured. Therefore, only the measurements of these 4 data are mentioned.

2.3.1 Rainfall

The rainfall can be measured by raingauge, radar, and satellite. The raingauge directly measures the rainfall which falls to the ground at a specific location in where it is located. In the measurement by the radar, the radar emits a pulse of electromagnetic energy and measures an echo intensity which occurs when the pulse hits an obstacle. The rain is one of the obstacles which can cause the echo. In the measurement by the satellite, the satellite measures visible and infrared radiation. This measured radiation reveals properties of a cloud, which is a source of the rain.

In comparison among the raingauge, radar, and satellite, the raingauge can measure the rainfall at a specific point while the radar and satellite can measure the distribution of the rainfall in the area. However, the rainfall amount measured by the raingauge is usually more accurate than those measured by radar and satellite. With this reason, the rainfall measured by the raingauge is widely used for flood simulations.

The raingauge can be divided into 2 types, non-recording raingauges and recording raingauges. The non-recording raingauge simply collects the rainwater which falls into the raingauge. The rainfall amount can be measured by the amount of the collected rainwater. This type of raingauge can measure only total rainfall amount and cannot measure the rainfall continuously. With this reason, the recording raingauge, which can measure the rainfall continuously, was developed. The widely used recording raingauges are as the followings [Leewatjanakul, 2009],

1. Weighing bucket raingauge. This raingauge collects the rainwater in a bucket and records the rainfall by the weight of the collected rainwater at each time. However, the disadvantage of this raingauge is that it can no longer collect the rainfall when the bucket is full, and therefore, the water should be drained manually.

2. Tipping bucket raingauge. This raingauge has a seesaw with a bucket on each side. On the one side, bucket collects the rainwater and tips when the collected rainwater reaches a certain volume. The tip causes the bucket empty, and brings a bucket on the other side to the position to receive the subsequent rainwater instead. Then, similarly to the previous process, the rainwater is collected on that bucket on the other side and that bucket tips when the collected rainwater reaches a certain volume. The rainfall can be recorded by the time of the tip.

3. Float type raingauge. This raingauge collects the rainwater and records the rainfall by the level of the collected water at each time. There is a syphon to drain the water when its level reaches a certain height. Therefore, this raingauge does not require a manual drainage.

Practically, it is possible that the rainfall data at some raingauge is missing in some period. In that case, the missing data can be interpolated from the data at nearby stations using an inverse distance method as the equation 2.2,

$$P_X = \frac{\sum_{i=1}^{N} P_i \left(1/d_i^2\right)}{\sum_{i=1}^{N} \left(1/d_i^2\right)} \tag{2.2}$$

where P_X is the interpolated value at the raingauge with the missing data, N is a count of nearby raingauges used for the interpolation which should not be more than 5, P_i is the measured data at the i-th raingauge, and d_i is the distance from the raingauge with the missing data to the i-th raingauge.

Apart from the problem of missing data, it is possible that the change of the condition of the raingauge or the environment near the raingauge causes an inconsistency of the recorded data. The inconsistency of the data can be checked by the slope of the plot between an accumulated rainfall at each raingauge and an average accumulated rainfall among the nearby raingauges for all timesteps. The inconsistency is shown as a difference between the slopes as shown in the Fig. 2.3. When there is an inconsistency, the data should be adjusted by multiplying with the ratio between the slopes to eliminate the different.

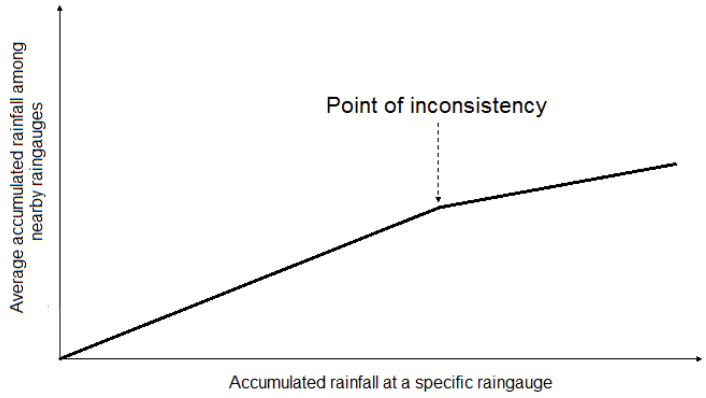

Figure 2.3: Concept of consistency analysis.

The basin rainfall can be calculated from the raingauge rainfall which is the point data by the following methods [Leewatjanakul, 2009],

1. Arithmetic-mean method. In this method, the rainfall amounts from all raingauges are averaged with equal weights. This method can calculate the rainfall amount quickly. However, the calculated rainfall amount can be inaccurate when the raingauges are not uniformly distributed.

2. Thiessen method. In this method, the area was divided into parts according to the nearest raingauge. Each part is called a Thiessen polygon. The basin rainfall is calculated as the average rainfall from all raingauges weighted by the size of their Thiessen polygon. This method can be used when the raingauges are not uniformly distributed. However, the topography, which may affect the rainfall, is not fully taken into account.

3. Isohyetal method. In this method, the area was divided into parts according to the isohyetal lines, rainfall contours, which were drawn according to topography and some climatological data. The basin rainfall is calculated as the average rainfall from all parts of the area weighted by its size. This method can be used when the raingauges are not uniformly distributed. This method takes to topography into account.

Theoretically, the isohyetal method can give a good calculated basin rainfall amount because the topography is taken into account. However, practically, it is difficult to determine the isohyetal line, and therefore, the Thiessen method is still widely used even though the topography is not fully taken into account.

2.3.2 Evaporation

The evaporation can be measured by an instrument called evaporation pan. The water is filled in a pan and the loss of water due to the evaporation can be determined as a decreasing of the water level in the pan. However, due to the heat of the pan, the evaporation rate inside the pan is usually higher than the actual rate. With this reason, the measured evaporation is called pan evaporation (E_P) and should be adjusted by a constant called pan coefficient (C_P) to represent the actual evaporation (E_r) as the equation 2.3.

$$E_r = C_P E_P \tag{2.3}$$

The pan coefficient depends on the type of the pan. In Thailand, the Thai Meteorological Department (TMD) uses the Class A evaporation pan as of the standard of the United States Weather Bureau the pan coefficient of which can be estimated as 0.7 [Leewatjanakul, 2009].

2.3.3 Water level

The water level can be measured by staff gauge, wire-weight gauge, floating-gauge recorder, and bubble gauge [Leewatjanakul, 2009]. The staff gauge directly measures the water level in the channel. The wire-weight gauge measures the water level by releasing a weight which is tied to the gauge by a wire from a specific height to a water surface. The length of the wire from the gauge to the water surface can be used to calculate the water level. In the measurement by the floating gauge recorder, water from the channel is diverted to a pond with static water and a float is used to measure the water level in that pond. The water level in that pond is equal to the water level in the channel. The bubble gauge measures the water level by releasing a bubble of dry nitrogen under the water surface and measures the pressure at the point the bubble is released. The measured pressure can be used to calculate the water level.

2.3.4 Discharge

A discharge in a stream can be calculated as a multiplication of a flow area by a flow velocity. The flow area is determined from cross section data and water level. Therefore, for each cross section, the water level and flow velocity is required to determine the discharge. The measurement of the water level is mentioned in the section 2.3.3. The measurement of the velocity can be done by a cup-type current meter and a propeller-type current meter. The measurements by these current meters are based on the same principle. The difference is that a propeller-type one is generally stronger than a cup-type one.

These current meters measure a velocity by a movement of a cup or a propeller around an axis and use a count of rounds in a unit time to calculate the flow velocity as the equation 2.4,

$$V = aN + b \tag{2.4}$$

where V is a velocity, N is a count of rounds, and a and b are constants which depend on instruments.

However, since the flow velocity varies upon distance from a bank and depth, the velocities should be measured at various points and various depths. Divide a flow area into N parts from the left bank to the right bank. For the i-th part, given a channel bottom depth of d meters, the mean flow velocity ($\bar{V}_i$) can be calculated as the equation 2.5,

$$\bar{V}_i = \begin{cases} V_{0.6d} & \text{for } d \leq 0.60 \\ \frac{V_{0.2d}+V_{0.8d}}{2} & \text{for } 0.60 < d \leq 3.05 \\ \frac{V_{0.2d}+2V_{0.6d}+V_{0.8d}}{4} & \text{for } 3.05 < d \leq 6.10 \\ \frac{V_{0.3}+3V_{0.2d}+2V_{0.6d}+3V_{0.8d}+V_{d-0.3}}{10} & \text{for } d > 6.10 \end{cases} \tag{2.5}$$

where V_x ($x \in \{0.3, 0.2d, 0.6d, 0.8d, d-0.3\}$) is the flow velocity at the depth of x meter(s). The mean flow velocity of the stream flow ($\bar{V}$) and the discharge (Q) can be calculated as the equations 2.6 and 2.7, respectively,

$$\bar{V} = \frac{\sum_{i=1}^{N} A_i \bar{V}_i}{\sum_{i=1}^{N} A_i} \tag{2.6}$$

$$Q = \bar{V} \sum_{i=1}^{N} A_i = \sum_{i=1}^{N} A_i \bar{V}_i \tag{2.7}$$

where N is a count of the divided parts and A_i is a flow area for the i-th part. In order to calculate the mean flow velocity accurately, the count of the divided parts (N) should be large enough to make the flow volume in each part less than 10% of the total flow volume.

2.4 Rainfall spatial distribution and basin discharge

The effects of rainfall spatial distribution as well as temporal distribution and basin characteristics on basin discharge have been studied by many researchers and were reviewed in Singh [1997]. That review suggested that peak discharge is affected by the rainfall temporal distribution and spatial hydraulic conductivity of the basin while the rainfall spatial distribution seems to affect the runoff timing rather than peak discharge. In a small area, Lee et al. [2009] also supported that the rainfall spatial distribution does not affect peak discharge. In that study, the observed rainfall in each grid was moved diagonally to the opposite side of the area and the runoff was simulated. The result showed that relocating the grid rainfall affects flood sources rather than basin discharge.

Nevertheless, Ogden and Julien [1993] studied the variability of the peak discharge from spatially distributed rainfall under different duration and found that the effect of spatial distribution is dominant when the rainfall duration is shorter than the time to equilibrium, the time at which an outgoing discharge from the area begins to be equal to an incoming discharge from rainfall. This result coincides with the study of Bell and Moore [2000]. In that study, the discharges from convective and stratiform rainfalls were simulated under different spatial resolutions. The result shows that the sensitivity of discharge to spatial rainfall is larger for convective rainfall, which is usually of a shorter duration than the stratiform rainfall. Since a large or long basin usually has long time to equilibrium, the variability of flood peak due to rainfall spatial distribution can be expected easier in the larger or longer basin.

The effect of non-uniform basin characteristics on the response of flood peak from spatial rainfall has been confirmed by Golian et al. [2010, 2011], and Saghafian et al. [2014]. These studies simulated rainfalls with different spatial distribution over the non-uniform basin and found that the peak discharge and rainfall thresholds, the rainfall amount which causes critical water level for a given soil moisture condition, varies upon rainfall location. Moreover, some studies also found that simulations of lumped rainfall and spatially distributed rainfall gave different flood peaks [Tramblay et al., 2011, Zoccatelli et al., 2011].

The basin characteristics which affect the response of flood peak to rainfall spatial distribution discussed in those previous studies are hydraulic conductivity, slope, basin shape. Nevertheless, there is still lack of information on a comparison among influences of these characteristics.

2.5 Rainfall in northern Thailand

Many studies have established the rainfall characteristics in the Chao Phraya basin and northern Thailand. Most of them have identified the effect of topography as well as wind on rainfall location.

Okumura et al. [2003] investigated the radar echo over the Dawna range, the boundary between the Chao Phraya basin and Andaman sea. They have found the phase delay corresponding to the distance from this mountain range. During May-July, when the monsoon comes from the Andaman sea side, the phase delay appears over the Chao Phraya basin side. On the other hand, in October, when the monsoon comes from the Chao Phraya basin side, the phase delay appears over the Andaman sea side. Therefore, the result suggested the occurrence of the phase delay over the leeward side of this mountain range. Yokoi and Satomura [2008] investigated the intraseasonal variations of the radar data in the same area during May-October. They have found that the 30-60 days variation is dominant over the Andaman sea side while the 10-20 days variation is dominant over the Chao Phraya basin side. The variations over both sides of the mountain range coincide with a cyclonic circulation, but only that over the Andaman sea side coincides with a zonal wind. Therefore, this mountain range acts as a blockage to the zonal wind. The altitude also affects the rainfall since Kuraji et al. [2009] studied the spatial characteristics of annual rainfall in Mae Chaem basin, the small basin over the upstream part of the Chao Phraya basin, and have found that the rainfall hours increase with altitude. However, the rainfall intensity shows no clear trend toward the altitude.

In large scale, Takahashi et al. [2010] investigated the diurnal rainfall pattern during May-October and have found that the rainfall concentrates over mountain crest in the afternoon and over the plain in the evening. This finding can be described by the diurnal wind which flows towards the upslope direction in the afternoon and downslope direction in the evening. Takahashi [2010] investigated the data during the pre-monsoon period (April-May), the first half of the monsoon period (June-July), and the second half of the monsoon period (August-September). The monsoon period has more rainfall amount than the pre-monsoon period because of monsoon onset and the second half of the monsoon period has more rainfall amount than the first half because of higher tropical disturbance activities. However, even though the surface winds among these periods are different, the rainfall diurnal cycle is still the same. Only the rainfall amounts are different. Recently, Mahavik et al. [2014] applied the principle component analysis to the radar data and discussed the magnitudes of each component with the wind data. The result shows that rainfall is likely to concentrates over the windward side of the mountain range.

About the consecutive rainfall days, Dahale et al. [1994] applied the Markov chain to rainfall data over India, Sri Lanka, and Thailand. They suggested that the likelihood that whether a particular day is a dry or rainfall day is related with whether the previous day is a dry or rainfall day. A Markov chain of order 1 appears to be enough to describe this likelihood in Thailand and dry zones of Sri Lanka while the order of more than 1 is required in India and wet zones of Sri Lanka. Szyniszewska and Waylen [2012] conducted the study in the central and northeastern Thailand by applying the Markov chain to daily rainfall data

separately for each month during April-October. They have found that the probability of consecutive rainfall days increases with monthly rainfall amount.

It can be seen that the studies on consecutive rainfall days mostly provide the information on the relation between climate and consecutive rainfall days while the information on the relation between topography and consecutive rainfall days still has not been provided even though the topography has been proved to play the role on rainfall distribution.

2.6 Flood in Yom basin

The main characteristics of the Yom basin are that the upstream part is the mountainous region while the downstream part is the plain area, and the water flows naturally with less influence of control structures. With these characteristics, the upstream part cannot retain much flood water and the downstream part cannot drain much flood water. Moreover, a narrow section of the river in the downstream area causes the drainage capacity to be even lower [Kure and Tebakari, 2012]. Therefore, flood occurs frequently in the downstream part of the Yom basin.

Most of floods occur in the southwest monsoon period, during May-October. In the latest climatological period, 1981-2010, there has been at least 4 major flood events, in 1983, 1995, 1996, and 2006 [Prajamwong and Suppataratarn, 2007]. Moreover, in 2011, there was a devastating flood which causes losses and damages worse than those from the 4 previously mentioned events [The World Bank, 2012]. Some studies also pointed out that the flood situation will be even worse in the future due to the climate change [Hunukumbura and Tachikawa, 2012, Kure and Tebakari, 2012].

In terms of relation between rainfall and flood, Kotsuki and Tanaka [2013] has found that in natural flood years, rainfalls during June-August bring the water to fill the storage capacity, and then, heavy rainfalls during September-October provide runoff which become flood in the area. Sayama et al. [2015] suggested that the peak inundation is correlated with total rainfall in 6 months more obviously than that in others duration.

There have been some studies which proposed the model to predict flood as well as estimating losses and damages. Tingsanchali and Karim [2010] proposed flood and hazard maps from 20-, 50-, 100-, and 200-year rainfalls in the Yom basin. Sriariyawat et al. [2013] proposed the method to calculate the damage from flood in the Sukhothai province by using the model to simulate flood area and using the relation between flood area and damage to calculate the damage. Sayama et al. [2017] proposed the model to predict flood in the near real-time by prioritizing the input data. They suggested that the most important data is evapotranspiration followed by dams and cross sections of the river.

Currently, the flood estimation follows the plan developed by Royal Irrigation Department [2015]. This plan has proposed the estimation of a peak discharge in the downstream area from an observed peak discharge in the upstream area using an observed historical data. According to this plan, after the peak discharge is observed in Phrae city (see Fig.3.2), the peak discharge in Sukhothai city can be expected in 2-3 days and the larger flood takes more time to travel than the smaller flood.

2.7 Flood modelling

2.7.1 Distributed and semi-distributed models

Many studies have developed the model to simulate flood in the Chao Phraya basin as well as the Yom basin. In order to take rainfall spatial distribution into account, the distributed model is widely used such as in Hunukumbura and Tachikawa [2012], Kotsuki and Tanaka [2013], Sriariyawat et al. [2013], Sayama et al. [2015], and Sayama et al. [2017]. In the distributed model, the basin is digitized as grids and a flow is routed as a movement of water among grids. The rainfall spatial distribution can be taken into account by generating the different rainfalls for different grids. The spatial characteristics of the basin can also be taken into account as the same way. One of the difficulties of this model is that the input rainfall must be a gridded rainfall. In the real simulation, the gridded rainfall measured by satellite or radar or interpolated rainfall measured by a network of raingauges can be used. In the ideal simulation, if the rainfall can be assigned for each grid, this type of model can also be used. However, for our study, we aim to simulate numerous rainfall events with different spatial distribution which can represent the general rainfall characteristics in the area. In this case, it is difficult to design the rainfall for each of numerous grids. Moreover, another difficulty is that since the basin characteristics should be defined for each grid, it is difficult get the data to represent the whole area.

Nevertheless, there are some studies [Tingsanchali and Karim, 2010, Kure and Tebakari, 2012] which used what is called a semi-distributed model which requires more simple data [Haghnegahdar et al., 2015]. This type of model is developed from a lumped model which transforms a lumped basin rainfall hyetograph into basin discharge hydrograph under a specified transformation method. Basin characteristics can be assigned as parameters for the transformation. Obviously, the rainfall spatial distribution cannot be taken into account in the lumped model. However, in the semi-distributed model, the area is separated into subbasins, and then, rainfall in each subbasin is transformed to discharge like in the lumped model. The total discharge from the area can be calculated by routing the discharges from all subbasins to the outlet of the area. The routing can be done by linear routing or by a river network model where the discharge from each subbasin is input as a lateral flow to the river. Regardless of how the discharge is routed, the spatial distribution of rainfall can be taken into account by generating different rainfalls to different subbasins. The spatial rainfall simulated in this type of model may not be as much in detail as the gridded rainfall simulated in the distributed model, but the simulated peak discharge is still acceptable if the area is not very large as Lee et al. [2009] suggested that the rainfall spatial distribution does not affect the peak discharge when the area is small.

In comparison between distributed model and semi-distributed model, the latter one seems to be more suitable for our work because of the fewer requirements of the data. However, as mentioned above, the assumption of small area size is required to ensure that the peak discharge simulated in the model is acceptable. Our study area seems not to meet this requirement since the area is as large as 19,000 km^2 and the lower part of the area is too flat to clearly define the subbasin boundary. In order to solve this problem, the area should be separated into subbasins, and in the flat area, the subbasin boundary may be defined by assuming that the water is drained to the nearest stream. This assumption is similar to Klongvessa and Chotpantarat [2014] where the storm water in the city was drained to the nearby drainage canal.

2.7.2 Calculation schemes in HEC-HMS and HEC-RAS models

The calculation schemes required for the simulation depend on the type of the model as well as the objective of the simulation. For our study which used the semi-distributed model to calculate the river discharge from of rainfalls in a basin with non-uniform characteristics, the required schemes include schemes for calculation of excess rainfall, transformation of excess rainfall hyetograph to discharge hydrograph, calculation of baseflow, and channel flow routing. In our study, we used the Hydrologic Engineering Center's Hydrologic Modeling System (HEC-HMS) to calculate discharge from rainfall and used Hydrologic Engineering Center's River Analysis System (HEC-RAS) to route the channel flow [Feldman, 2000, Brunner, 2010]. This couple of models has been developed for flood simulation in a basin scale and has been used in many studies [Knebl et al., 2005, Suriya and Mudgal, 2012, Mandal and Chakrabarty, 2016]. There are a lot of widely used calculation schemes available. In this section, only concepts of these schemes are introduced. Details of the schemes selected in our study will be mentioned in the section 5.2.1.

2.7.2.1 Excess rainfall

In HEC-HMS model, the excess rainfall is the portion of rainfall remained from the canopy model which determines an interception, loss model which determines various process such as an infiltration, and surface storage. However, in our study, the interception is insignificant. Therefore, the excess rainfall is determined by the loss model and surface storage.

Loss model

In HEC-HMS model, without the canopy model, the rainfall is first interacted by the loss model. The loss model can be chosen among initial and constant loss model, deficit and constant loss model, Soil Conservation Service (SCS) curve number loss model, Green and Ampt loss model, and soil moisture accounting loss model.

In the initial and constant loss model, the rainfall becomes loss until the soil is saturated. After that, the loss rate will be at the lowest value among precipitation intensity and a specified constant rate. The water stored in the soil cannot be taken out in this model.

The deficit and constant loss model is similar to the initial and constant loss model. The difference is that the water stored in the soil can be taken out by evapotranspiration and percolation in this model.

In the SCS curve number loss model, the accumulated rainfall amount remained from the loss is calculated by a function of accumulated rainfall. This function is characterized by a maximum potential retention and an initial abstraction. The maximum potential retention indicates the ability of the basin to retain the precipitation. The higher value of the maximum potential retention leads to the higher loss. However, in HEC-HMS model, this value is determined from SCS curve number (CN). The maximum value of CN is 100 which gives no retention. The lower value of CN leads to the higher maximum potential retention. The initial abstraction is the amount of the rainfall required before the surface excess occurs. Usually, the initial abstraction is estimated as 0.2 times the potential retention.

The Green and Ampt loss model is the simplification of the Richard's equation for unsteady flow in soil. This equation is the result from solving the Darcy's law, the law describing the flow through a groundwater aquifer, with mass conservation. In this model, the loss is calculated by a function of volume moisture deficit and cumulative loss. Higher loss rate is

associated with the higher volume moisture deficit and lower cumulative loss. The function is characterized by a saturated hydraulic conductivity and wetting front suction.

In the soil moisture accounting loss model, the soil is divided into 3 layers, soil storage, upper groundwater storage, and lower groundwater storage. The soil storage is divided into tension storage and gravity storage. Among these layers, there are movements of water which are consisted of infiltration from surface to the soil storage, percolation from the gravity storage layer of the soil storage to the upper groundwater storage, percolation from the upper groundwater storage to the lower groundwater storage, and deep percolation from the groundwater storage downwards. These movements are determined by amounts of water stored in the layers. The higher rates of movements are associated with the lower amount of the stored water. The water stored in the soil storage, both gravity and tension storages, can be taken out by evapotranspiration.

It should be noted that the water stored in the soil can be taken out only in the deficit and constant loss model and the soil moisture accounting loss model. In the others model, the space in the storage cannot be cleared up, and therefore, the drying process during no rainfall periods cannot be simulated. With this reason, only the deficit and constant loss model and the soil moisture accounting loss model are capable of multiple rainfall events with dry periods in between. The others model are capable of only a single rainfall event or the case that the drying process can be ignored. In our study, we used the deficit and constant loss model because flood years in our study area have been found to coincide with a saturated soil condition [Kotsuki and Tanaka, 2013], and therefore, the soil can be assumed to be saturated throughout a flood-induced rainfall event.

Surface storage

After the loss model, the remaining portion of the rainfall fills up the surface storage, such as a reservoir, until the storage is full. After the storage is full the remaining portion of the rainfall is called excess rainfall and is subject to reach the channel as the direct runoff.

However, the water stored in the surface storage can be taken out by the evapotranspiration and infiltration, and therefore, in the simulation of multiple rainfall events, the surface storage can be recovered to store the water from the subsequent rainfalls.

2.7.2.2 Direct runoff

In HEC-HMS model, the methods to transform the excess rainfall to discharge can be chosen among unit hydrograph model and kinematic wave model.

The unit hydrograph model is based on the concept that a unit rainfall, a temporally uniform rainfall with unit intensity under a unit time, can generate a unit of direct runoff hydrograph. For each rainfall event, the excess rainfall intensity at each time step is considered as an expansion of the unit rainfall intensity, and therefore, the runoff hydrograph from each time step of rainfall is considered as the expansion of that unit hydrograph with the same scale. In the whole rainfall event, the different time step of rainfall leads to the different time step of runoff generation. The runoff hydrograph from the whole event is the summation of the runoff hydrographs from each time step of rainfall. There are several methods to determine the shape of the unit hydrograph, Snyder's unit hydrograph model, SCS unit hydrograph model, and Clark unit hydrograph model. The Snyder's model focuses on a lag and a peak flow. The SCS model is based on the observed data in the United States. The Clark model is based on a linear reservoir model, where the discharge directly varies

upon an amount of water stored in a soil. Apart of these unit hydrograph models, the unit hydrograph can also be manually defined.

In the kinematic wave model, the hydrograph is determined by considering the basin as an open channel with the excess precipitation as an inflow. The model is composed of overland flow planes, subcollector channels, collector channels, and a main channel. The overland flow planes contribute the water to the subcollector channels, the subcollector channels contribute the water to the collector channels, and the collector channels contribute the water to the main channel. The flow in each component is determined by the momentum equation and continuity equation with parameters based on the flow geometry and surface roughness of the component. In order to represent the heterogeneity of the basin, the overland flow planes can be divided into 2 planes with different characteristics. However, Ponce [1991] has suggested that a solution algorithm in this model is suitable for a small basin rather than a large basin.

In our study, due to the large size of the area, the kinematic wave model is not suitable. Therefore, we used the unit hydrograph model. The Snyder's unit hydrograph model was selected because this model focuses on a peak discharge, which is the objective of our study.

2.7.2.3 Baseflow

In each rainfall event, some portion of the rainfall is stored in the infiltration and surface storages. The stored water can slowly move to the channel and produce additional runoff called a baseflow. In HEC-HMS model, the baseflow can be set to be constant, set to be monthly dependent, or calculated by a baseflow model. For the calculation by the model, exponential recession model and linear reservoir model can be chosen.

In the exponential recession model, the flow exponentially decays when it recedes to a specified threshold value. At the beginning of the simulation, the initial flow can be specified. During the simulation, the flow exponentially decays until the rainfall generates a direct runoff. After that, the flow hydrograph will be determined as the summation of the currently decaying baseflow and the direct runoff from the rainfall. As the usual behavior of the runoff from the rainfall, the flow hydrograph reaches the peak and recedes. After the flow recedes to the threshold value, the flow exponentially decays again. If there is the next rainfall event, the direct runoff from the next rainfall will be included to the flow, and then, the flow will reach the peak, decay to the threshold value, and exponentially decay again. This loop continues until the simulation is over.

In the linear reservoir model, the baseflow directly varies upon the amount of water stored in the soil. This model is linked to the loss model which determines the infiltration as an inflow to the storage (see the detail of the loss model in the section 2.7.2.1). In the soil moisture accounting loss model, this baseflow model is linked to the upper and lower groundwater layers. The baseflows from these two layers can be calculated separately. In the others loss model, there is only one storage layer to produce the baseflow.

In our study, we used the exponential recession model to calculate the baseflow because the baseflow in the area appears to depend on rainfall. In some parts of the area where seasonal baseflow is dominant, a constant baseflow was also applied.

2.7.2.4 Channel flow

The runoff from rainfall calculated in the HEC-HMS model can be input to the HEC-RAS model, a river network model, as the lateral flow to a channel network. In the HEC-RAS model, the water is routed to the downstream area through the channel and flood plain which lies along the channel. The routing is based on the principle of conservation of mass

and principle of conservation of momentum. The principle of conservation of mass is used to control the water volume. The principle of conservation of momentum is used to determine the change of momentum due to external forces. The external forces include forces from pressure, gravity, and friction.

2.7.3 Concepts of rainfall design

Once the model is developed, we can simulate the discharge from rainfall. For the real event, the observed rainfall can be simply input to the model. However, for the designed event, it is important to ensure that the rainfall simulated in the model can represent the rainfall characteristics in the area. Therefore, the rainfall should be carefully designed. The characteristics to be designed include rainfall amount, duration, spatial distribution, and temporal distribution. In this section, only the concepts of rainfall design are mentioned. The methods of rainfall design used in this study will be mentioned in detail in the section 5.2.3.

2.7.3.1 Rainfall amount

The widely used method to consider a rainfall amount is a frequency analysis of extreme rainfall [Singh, 1992]. The concept of this method is finding the appropriate statistical distribution to show the relation between extreme rainfall amount and its occurrence probability. In this method, the observed maximum rainfall amount in each year was determined. Then, the probability of that observed rainfall amount is assigned using an equation of a probability distribution such as Weibull equation. After that, the series of observed rainfall amounts under the assign probabilities are fitted with a probability distribution such as log-normal distribution, Pearson type III distribution, or generalized extreme value (GEV) distribution. Once the observed data is fitted, the equation of the statistical distribution used to fit the data can be used to calculate extreme rainfall amount under each occurrence probability.

In our study, the probability of the extreme rainfall amount was assigned by the widely used Weibull equation and the data was fit by the GEV distribution which has been used in many studies [Crisci et al., 2002, Feng et al., 2007, Overeem et al., 2008]. The GEV distribution is derived from the combination of Fréchet, Gumbel, and Weibull distributions. According to the Fisher-Tippett-Gnedenko theorem (extreme value theorem), a probability distribution of an extreme value belongs to a family of one of these 3 distributions [de Haan and Ferreira, 2006].

2.7.3.2 Rainfall duration

In most of the extreme rainfall simulations, rainfall duration is usually assigned to be equal to the concentration time, the travel time of water from the most remote part of the basin to the outlet. The reason is that this duration of rainfall usually gives the critical flood, the highest flood in comparison to that simulated from others duration of rainfall [Fleig and Wilson, 2013].

If the constant intensity rainfall is simulated, the basin discharge will begin to rise after the excess rainfall begin to reach the outlet, and then, the rising will go on due to the incoming rainwater until the time of concentration is reached. At that time, the incoming rainwater and the outgoing discharge are balanced, and therefore, the total discharge is constant until the rain stops. In a case that the rainfall duration is shorter than the concentration time, the incoming rainwater will be cut before the balancing point, and as a result, the peak

discharge is not as high as when the rainfall duration is longer. On the other hand, when the rainfall duration is longer than the concentration time, the discharge will remain constant after the balancing point, and as a result, the peak discharge is still not different from when the rainfall duration is as the concentration time.

In reality, the rainfall intensity is higher for short duration rainfall and lower for long duration rainfall. With this reason, when the rainfall duration is longer than the concentration time, the intensity will be too low to generate the high peak discharge in comparison to when the rainfall duration is as the concentration time. However, when the rainfall duration is shorter than the concentration time, even though the incoming rainfall is cut before the concentration time, it is mathematically possible that the high peak discharge will be generated because of the high rainfall intensity. Nevertheless, as of the statistical rainfall data, the intensity is usually not high enough to generate the peak discharge higher than when the rainfall duration is as the concentration time. However, in our study, we simulated different durations of rainfalls, both equal to and shorter than the concentration time.

2.7.3.3 Rainfall spatial distribution

Recently, many methods to design rainfall spatial distribution are introduced. These methods include applications of latent variable, copulas, and max-stable models [Davison et al., 2012].

In the latent variable model, the rainfall is calculated from the probability distribution function, such as GEV distribution, with the parameters depending on latent (unobserved) variables. These latent variables may be assumed to follow the statistical distribution such as the normal distribution with a correlation function.

In the copulas model, the rainfall is calculated from a copula, the multivariate probability distribution with the marginal probability of each variable uniformly distributed. The copula is fit with a marginal distribution, such as GEV marginal distribution, and a correlation function.

For the max-stable model [de Haan, 1984], it is the multivariate model extended from the GEV distribution. This model is widely used to generate the distribution of extreme rainfall. There has been several max-stable models developed by researchers such as the models of Schlather [2002] and Brown-Resnick [Kabluchko and Schlather, 2010].

In studies on uncertainty of rainfall spatial distribution, Golian et al. [2010] interestingly applied Monte Carlo method to generate rainfalls with different spatial distributions. In that study, for each observed rainfall event, the rainfall amount at each location was converted dimensionless by dividing by mean areal rainfall. Then, the probability of those observed dimensionless rainfall amount was assigned by the Weibull equation. After that, for each location, the probability distribution function was used to fit the observed dimensionless rainfall under the assigned probability. Next, the Monte Carlo method was applied by a randomization the number between 0 and 1 for each location, and then, that random number is applied to the fit distribution function to calculate the dimensionless rainfall for each location. Finally, the dimensionless rainfall was converted to the dimensioned rainfall under the desired areal rainfall amount. However, in Golian et al. [2010], the rainfall spatial correlation was not taken into account. Therefore, Golian et al. [2011] applied copula method to random the correlated number to take the spatial correlation into account.

In our study, we also applied the Monte Carlo method to random the rainfall spatial distribution. The difference of our work from Golian et al. [2010] and Golian et al. [2011] is that we fit the dimensionless rainfall probability with the normal distribution and randomized the correlated numbers by a Cholesky randomization [Kreyszig, 1999]. With this

randomization, the random numbers are normally distributed and suitable for the normal distribution which is used to fit the rainfall data.

2.7.3.4 Rainfall temporal distribution

There have been many methods to design a rainfall temporal distribution. The widely used ones are SCS method [Cronshey, 1986], Huff method [Huff, 1967], triangular method, and alternating block method [Chow et al., 1988].

In the SCS method, SCS has adopted the rainfall temporal patterns according to the rainfall data in the United States. The rainfall pattern varies upon the location. Overall, there are 4 different patterns called SCS types I, IA, II, and III curves. The rainfall can be designed by choosing an appropriate type curve and rescaling the curve by the designated rainfall amount and duration.

In the Huff method, several hyetographs of observed rainfalls are converted dimensionless in both accumulated amounts and durations. Then, for each dimensionless time step, the dimensionless accumulated rainfall amounts are classified into 4 quartiles. Next, the appropriate quartile is chosen based on the statistical data. The temporal pattern of the designed rainfall is the 50th percentile of the dimensionless accumulated rainfall amount in the chosen quartile. However, for simulating a rare case, the 10th and 90th percentile can be used instead of the 50th percentile. Finally, similar to the SCS method, the temporal pattern of the designed rainfall is rescaled by the designated amount and duration to become the designed rainfall.

In the triangular method, the designed rainfall hyetograph is in a triangular shape with designated time of peak, peak intensity, and duration. After the rainfall begins, its intensity increases constantly until the peak intensity is reached, and after that, its intensity decreases constantly until the rainfall is over.

In the alternating block method, for each rainfall event, the highest intensity is put to the middle of the rainfall duration, and lower intensities are put to the points farther from the middle of the duration. The hyetograph generated from this method can give high flood peak because timesteps with high rainfall intensities in the hyetograph are close to one another.

Apart from these methods, in the section 2.7.3.3, the applications of latent variable, copulas, and max-stable models to generate spatial rainfall distribution are mentioned. In fact, these models can also be used to generate rainfall temporal distribution by applying the auto correlation of rainfall apart from the spatial correlation [Allcroft and Glasbey, 2003, Bárdossy and Pegram, 2009, Huser and Davison, 2014].

In our study, we decided to use the alternating block method because it can give high flood peak with the realistic rainfall intensity. This method is often used to design storms in the United States [Chow et al., 1988, Gong et al., 2016]. Moreover, this method appears to be capable of representing the large rainfalls in our study area (see the section 5.3.2.2).

Chapter 3

Study area

3.1 Location

Yom basin covers the area of approximately 24,000 km^2 in Thailand. It is one of the four upstream basins of Chao Phraya basin, the largest basin in Thailand covering the northern mountainous region and central plain of the country. The four upstream basins are Ping, Wang, Yom, and Nan basins which are named according to their main river as shown in Fig. 3.1. These 4 basins cover the area of approximately 100,000 km^2 from the northern region to the upper part of the central plain.

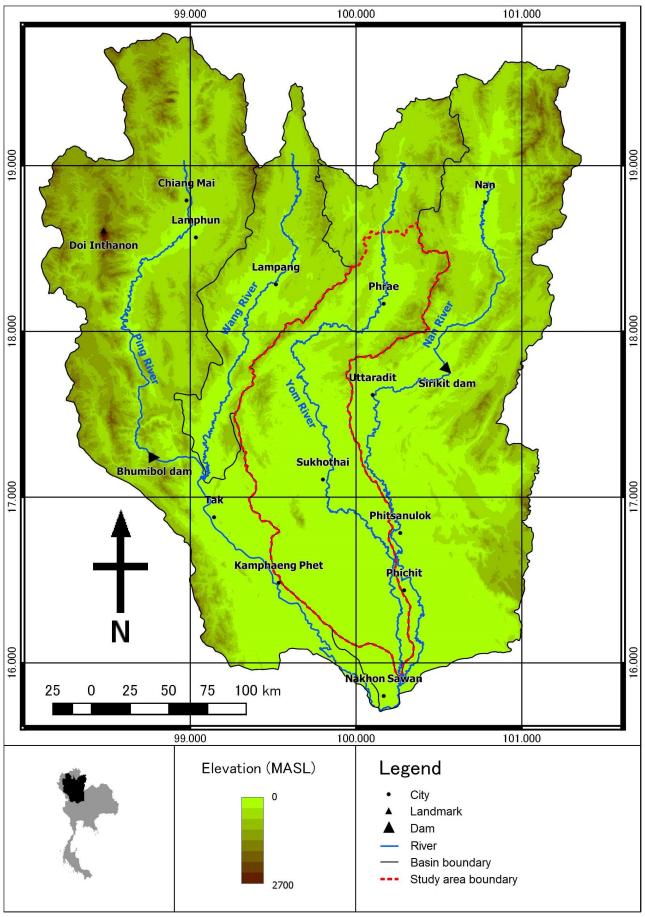

Figure 3.1: Location of the study area.

In the Chao Phraya basin, the Wang river merges with the Ping river in the northern part of Tak province, the Yom river merges with the Nan river in the northern part of Nakhon Sawan province, and then, the Ping river merges with the Nan river to form the Chao Phraya river in the middle part of the Nakhon Sawan province (see Fig. 3.1). After that, the Chao Phraya river drains the water to the outlet at the Gulf of Thailand (Figure not shown).

Among the four upstream basins, the water flow nearly naturally in the Wang and Yom basins. For the Ping and Nan basins, there are large scale dams to control the flow (see Fig. 3.1). In comparison between the Wang and Yom basins, the Yom basin is obviously larger with the size of approximately 24,000 km^2 and has longer river with the length of approximately 700 km. Because of the long river without a large scale control structure, the Yom basin is appropriate to study the natural river flow. With this reason, this study focuses on the Yom basin.

However, the Yom basin can be separated into 3 parts according to the group of subbasins, upper, middle, and lower parts. In our study, we exclude the upper part because of the different flow characteristics [Royal Irrigation Department, 2015]. From the upper part to the middle part, the larger flood seems to have shorter travel time, but from the middle part to the lower part, the larger flood seems to have longer travel time. Moreover, there is a weir (detail is in section 3.2.1) which can affect the natural flow between the upper and middle parts. Therefore, our study area covers the middle and lower parts of the Yom basin with the area of approximately 19,000 km^2 and river length of approximately 600 km (see Fig. 3.1).

3.2 Physical characteristics

3.2.1 Topography and river flow

Generally, the topography of the study area, middle and lower Yom basin, follows the characteristics of the upstream part of the Chao Phraya basin. It is composed of a mountainous region in the northern part and a plain area in the southern part as shown in Fig. 3.2. However, the height of the mountainous region in the study area is not as much as those in others basin, the Ping, Wang, and Nan basins. Considering the Ping, Wang, Yom, and Nan basins together, the elevation of the area ranges from less than 100 MASL over the plain area to approximately 2,600 MASL at Doi Inthanon in the mountainous region (see Fig. 3.1), but in the study area, the maximum elevation is approximately 1,400 MASL.

A river flow in the study area comes from the upper part of the Yom basin which enters the area at the Mae Yom weir (see Fig. 3.2). After the weir, the flow passes the Phrae city in the mountainous region and Sukhothai city in the plain area. Finally, it escapes the study area in the Nakhon Sawan province as mentioned in the section 3.1. There are small streams which contribute the water to the main river, the Yom river, along the area. The distances along the Yom river from the Mae Yom weir to the Phrae city, from the Phrae city to the Sukhothai city, and from the Sukhothai city to the outlet are 75 km, 272 km, and 257 km, respectively.

3.2.2 Soil texture

The importance of soil characteristics on flood is that the soil plays a role on an infiltration. Usually, the infiltration over clay, a fine texture soil, is more difficult than the infiltration over a coarser texture soil [Chow et al., 1988].

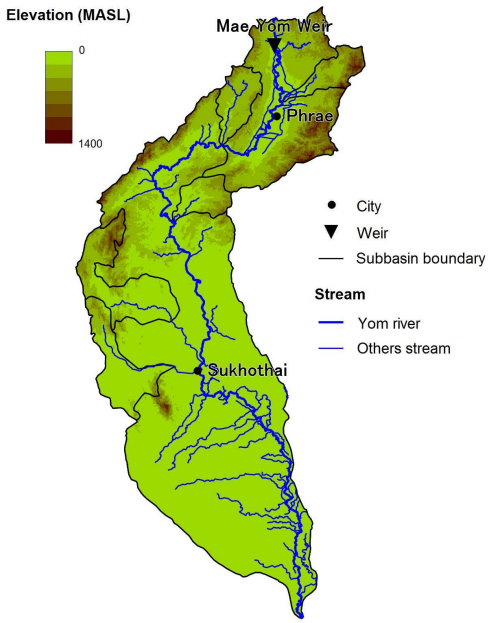

Figure 3.2: Topography, stream, and subbasin in the study area.

Fig. 3.3 shows the soil texture in the study area surveyed by the Land Development Department of Thailand. In our study area, the southern part, which is the plain area, is mostly covered by clay while the northern part, which is the mountainous region, is mostly covered by coarser texture soils. However, since the northern part has of a lot of high steep slope area which is difficult for the survey, the soil texture has not been identified for some zone.

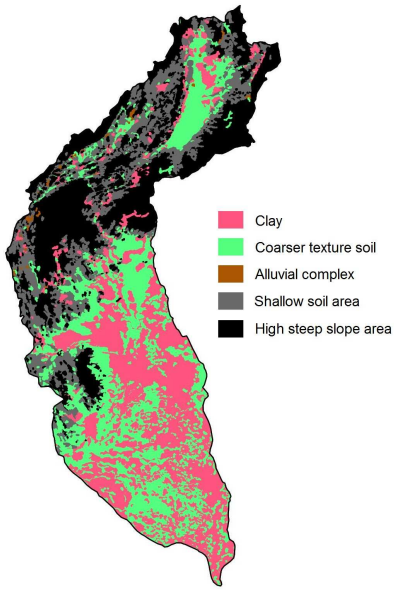

Figure 3.3: Soil texture in the study area.

3.2.3 Land use

Similar to the soil characteristics, land use also plays a role on flood. Usually among forest, agricultural area, and urban area, the forest is associated with the highest infiltration rate and lowest runoff flow velocity, followed by the agricultural area. The urban area is associated with the lowest infiltration rate and highest runoff flow velocity. Moreover, the land use also affects the vegetation which has an impact on a channel roughness [Chow et al., 1988].

Fig. 3.4 shows the land use in the study area surveyed by the Land Development Department of Thailand in 2009. The northern part is mostly covered by the forest while the southern part is mostly covered by the agricultural area with some storage of water. The urban area is not very dominant in the study area.

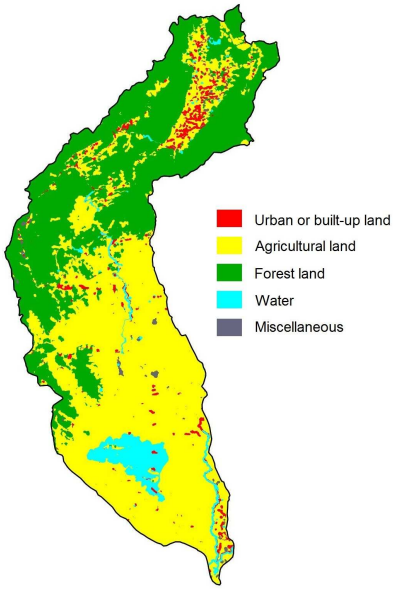

Figure 3.4: Land use in the study area.

3.3 Climate

Rainfall in the study area is influenced by monsoon [Thai Meteorological Department, 2015]. From mid-October to mid-February, the monsoon comes from the northeastern continental area. It brings cold and dry air to the study area. In this period the weather is dry and quite cold, and rainfall amount is small. The transitional period of monsoon from northeast to southwest is from mid-February to mid-May. During this period, there can be a confluence of the cold and warm air masses which causes a thunderstorm. Therefore, rainfall in this period is higher than that in the northeast monsoon period.

The remarkably high rainfall period is from mid-May to mid-October. During this period, the monsoon comes from the southwestern oceanic area, the Andaman sea. It brings warm and wet air to the study area. The rainfall amounts are extremely high during the beginning and the end of this period because a monsoon trough passes the study area. Moreover, at the end of the period, tropical cyclones can cause even more rainfall. Fig 3.5 shows the average monthly rainfall amount at the Sukhothai city during 1981-2010 observed by TMD.

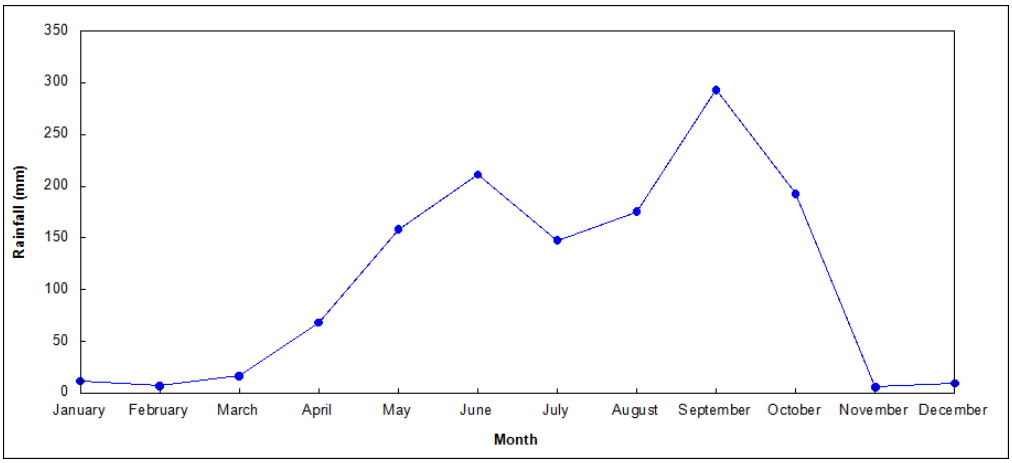

Figure 3.5: Average monthly rainfall during 1981-2010 at Sukhothai city.

Chapter 4

Study 1: Spatial rainfall

In this chapter, spatial characteristics of rainfall over the northern Thailand were established. Consecutiveness of rainfall days was determined by Markov chain probability model and chi-square test of independence and rainfall amount was determined by student-t test.

4.1 Data

The rainfall data used in this study was the daily rainfall data during the southwest monsoon period in the latest climatological period, May-October 1981-2010. The data are recorded by TMD raingauges which reach the standard of the World Meteorological Organization (WMO). Locations of these raingauges are shown in the Fig. 4.1. Note that the Fig. 4.1 does not show the raingauges that the records started later than 1981 or ended before 2010 because the data do not cover the study period and are not used in this study.

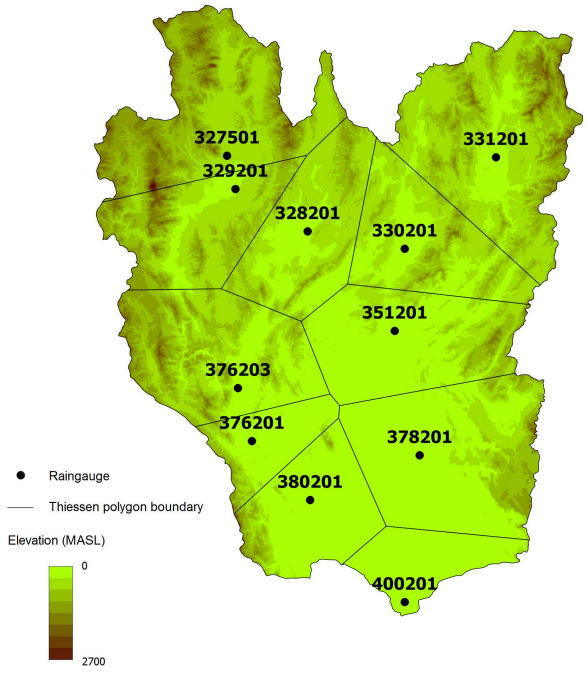

Figure 4.1: Locations of raingauges which record the data during 1981-2010.

The table 4.1 shows the locations of raingauges as well as elevations, coverage areas determined by Thiessen polygons, and the years the records started. The data was available at only 9 raingauges before 1981 while it was available at 11 raingauges afterwards.

Table 4.1: Information of raingauges shown in Fig 4.1.

Raingauge	Latitude	Longitude	Elevation[a] (MASL)	Coverage area (km^2)	Starting year
327501	18.7900	98.9769	316	13,031.9	1951
331201	18.7797	100.7778	204	14,912.1	1951
329201	18.5667	99.0333	298	8,153.8	1981
328201	18.2833	99.5167	257	8,549.7	1951
330201	18.1667	100.1667	163	8,451.6	1952
351201	17.6167	100.1000	67	10,262.8	1951
376203	17.2333	99.0500	162	11,011.8	1960
376201	16.8783	99.1433	124	3,965.8	1954
378201	16.7833	100.2667	47	13,555.2	1951
380201	16.4833	99.5333	78	7,381.4	1981
400201	15.8000	100.1667	25	4,388.2	1951

a Elevation data is from GMTED10 derived by United States Geological Surveys (USGS).

4.2 Methods

4.2.1 Markov chain probability model

The Markov chain probability model is a model used to determine probabilities of transitions among states. In this study, this model is used to investigate the transitions among the states of dry day and rainfall day similarly to Dahale et al. [1994], Moon et al. [1994], Dastidar et al. [2010], and Hossain and Anam [2012]. In the time series which is consisted of dry days and rainfall days, let n_0 be a count of dry days, n_1 be a count of rainfall days, n_{01} be a count of dry days followed by rainfall days, and n_{11} be a count of rainfall days followed by rainfall days. The transition probabilities from a dry day to a rainfall day (p_{01}) and from a rainfall day to a rainfall day (p_{11}) could be described by the equations 4.1 and 4.2, respectively.

$$p_{01} = \frac{n_{01}}{n_0} \tag{4.1}$$

$$p_{11} = \frac{n_{11}}{n_1} \tag{4.2}$$

Define the L consecutive rainfall days as the period of $L+1$ days the last day of which was a dry day and the others L day of which were rainfall days. The average length of consecutive rainfall days ($\bar{L}$) and the probability of consecutive rainfall days with the length of more than L days (p_L) could be calculated by equations 4.3 and 4.4, respectively [Sonnadara and Jayewardene, 2015]. The proofs of these 2 equations are shown in the appendix A.1.

$$\bar{L} = \frac{1}{1 - p_{11}} \tag{4.3}$$

$$p_L = \frac{p_{01}\,(1 - p_{11})\,p_{11}^L}{1 - p_{11} + p_{01}} \tag{4.4}$$

For each year, the count of consecutive rainfall days with the length of more than L days (N_L) could be calculated by multiplying p_L by the count of studied days in one year (s) as the equation 4.5.

$$N_L = sp_L \tag{4.5}$$

The return period (in years) of consecutive rainfall days with the length of more than L days (T_L) could be calculated by the equation 4.6.

$$T_L = \frac{1}{N_L} \tag{4.6}$$

About the definition of rainfall days, usually, a dry day is defined as a day with 0.0 mm rainfall and a rainfall day is defined as a day with >0.0 mm rainfall. However, different criteria for classifying dry and rainfall days may be applied. For example, Sonnadara and Jayewardene [2015] used 0.1, 1.0, and 3.0 mm rainfalls as threshold values to determine the rainfall days. In this study, the criteria to determine the rainfall days were >0.0, >10.0, and >35.0 mm rainfalls. These values are the criteria that TMD uses to classify the rainfall days. TMD classifies days with no rainfall, 0.1-10.0 mm rainfall, 10.1-35.0 mm rainfall, and >35.0 mm rainfall as dry, light rainfall, moderate rainfall, and heavy rainfall days, respectively.

4.2.2 Chi-square test of independence

The chi-square test of independence is a method to test that two variables are independent on each other [Sheskin, 1996]. In terms rainfall days, many studies applied this method to test the dependence between the state (dry or rainfall) of a day and the state of the previous day [Moon et al., 1994, Hossain and Anam, 2012]. In our study, we classified the states into no rainfall day (dry day), 0.1-10.0 mm rainfall day (light rainfall day), 10.1-35.0 mm rainfall day (moderate rainfall day), and >35.0 mm rainfall day (heavy rainfall day).

In the time series, let n_{ij} denote the count of 2 consecutive days the first days which were of state $i \in \{0, 1, 2, 3\}$ and the latter days of which were of the state $j \in \{0, 1, 2, 3\}$ where 0, 1, 2, and 3 denoted the states of dry day, light rainfall day, moderate rainfall day, and heavy rainfall day, respectively. Under the null hypothesis that whether the first day was a dry, light rainfall, moderate, rainfall, or heavy rainfall day did not affect whether the following day would be a dry, light rainfall, moderate, rainfall, or heavy rainfall day, the expected value of n_{ij} denoted by $E(n_{ij})$ followed the equation 4.7 [Sheskin, 1996],

$$E(n_{ij}) = \frac{n_i n_j}{n} \tag{4.7}$$

where n_i and n_j were the counts of days with the state i and j in the time series, respectively, and n was the total count of days in the time series.

The residual of the transitions from state i to state j denoted by (R_{ij}) was calculated by the equation 4.8.

$$R_{ij} = \frac{n_{ij} - E(n_{ij})}{\sqrt{E(n_{ij})}} \tag{4.8}$$

The larger positive value of R_{ij} meant the more likelihood that the state i on the first day led to the state j on the following day. The larger negative value of R_{ij} meant the more likelihood that the state i on the first day did not lead to the state j on the following day. The smaller value of R_{ij} meant the less likelihood that state i on the first day affected whether the following day would be of the state j.

The test value (χ^2) was the summation of the square residuals as the equation 4.9.

$$\chi^2 = \sum_i \sum_j R_{ij}^2 \tag{4.9}$$

A critical value was determined from the chi-square distribution with $(a-1)(b-1)$ degree of freedom where a and b were the counts of states of the previous days (i) and latter days (j) considered in the test, respectively. If χ^2 was less than the critical value, the null hypothesis of independence was true. Conversely, if χ^2 was more than the critical value, that null hypothesis was false, and therefore, the state of each day in the time series depended on the state of the previous day. In other words, there were dominant transitions between the states of the previous day and the states of the latter day. The dominant transitions could be seen from the residuals (R_{ij}) which were largely positive or largely negative. The significance of each residual could be determined by z-test where the critical values of R_{ij} were determined from the two-tailed standard normal distribution [Sheskin, 1996].

4.2.3 Student t-test

The student t-test is the method to test the difference of average values between two sets of data [Sheskin, 1996]. Some studies such as Raju et al. [2002] and Lee et al. [2014] applied this method to test whether rainfall amount at the specific location or duration is higher or lower than the average value. In our study, we used this method to compare the average rainfall amounts on >10.0 mm rainfall days among locations in the area.

For each year, average daily rainfall amounts on >10.0 mm rainfall day ($X_{10.0}$) was calculated at each station by the equation 4.10,

$$X_{10.0} = \frac{\sum p_{10.0}}{n_{10.0}} \tag{4.10}$$

where $\sum p_{10.0}$ was the summation of rainfall amount from >10.0 mm rainfall days in the year and $n_{10.0}$ was the count of >10.0 mm rainfall days in the year.

For each station, the test value (t) follows the equation 4.11,

$$t = \frac{\overline{X}_{10.0} - \mu_{10.0}}{\widetilde{s}_{X_{10.0}}/\sqrt{n_s}} \tag{4.11}$$

where $\overline{X}_{10.0}$ and $\widetilde{s}_{X_{10.0}}$ were average and standard deviation of $X_{10.0}$, respectively, $\mu_{10.0}$ was the areal average rainfall amount on >10.0 mm rainfall days throughout the study period, and n_s was the count of study years.

Critical values were determined from two-tailed t-distribution with $n_s - 1$ degree of freedom. If t was between the lower and higher critical values, the rainfall amount on >10.0 mm rainfall day was close to the average. The lower value of t than the negative critical value and the higher value of t than the positive critical value meant the lower and higher rainfall amounts on >10.0 mm rainfall day than the areal average, respectively.

4.3 Results and discussion

4.3.1 Accuracy of Markov chain model

Denote the count of isolated rainfall days by N_1^* and the count of consecutive rainfall days with durations of L days by N_L^*. The value of N_L^* with $L \in \{1, 2, 3, ...\}$ can be calculated as the equation 4.12,

$$N_L^* = N_{L-1} - N_L \tag{4.12}$$

where N_{L-1} and N_L can be calculated by the equation 4.5.

The Fig. 4.2 shows the comparison between observed and expected N_L^* and the table 4.2 shows the comparison between the observed and expected average consecutive lengths ($\bar{L}$ in the equation 4.3, section 4.2.1). The expected values show a good agreement with the observed values for all of >0.0, >10.0, and >35.0 mm rainfall days. Therefore, the Markov chain model successfully describes the probability of consecutive rainfall days.

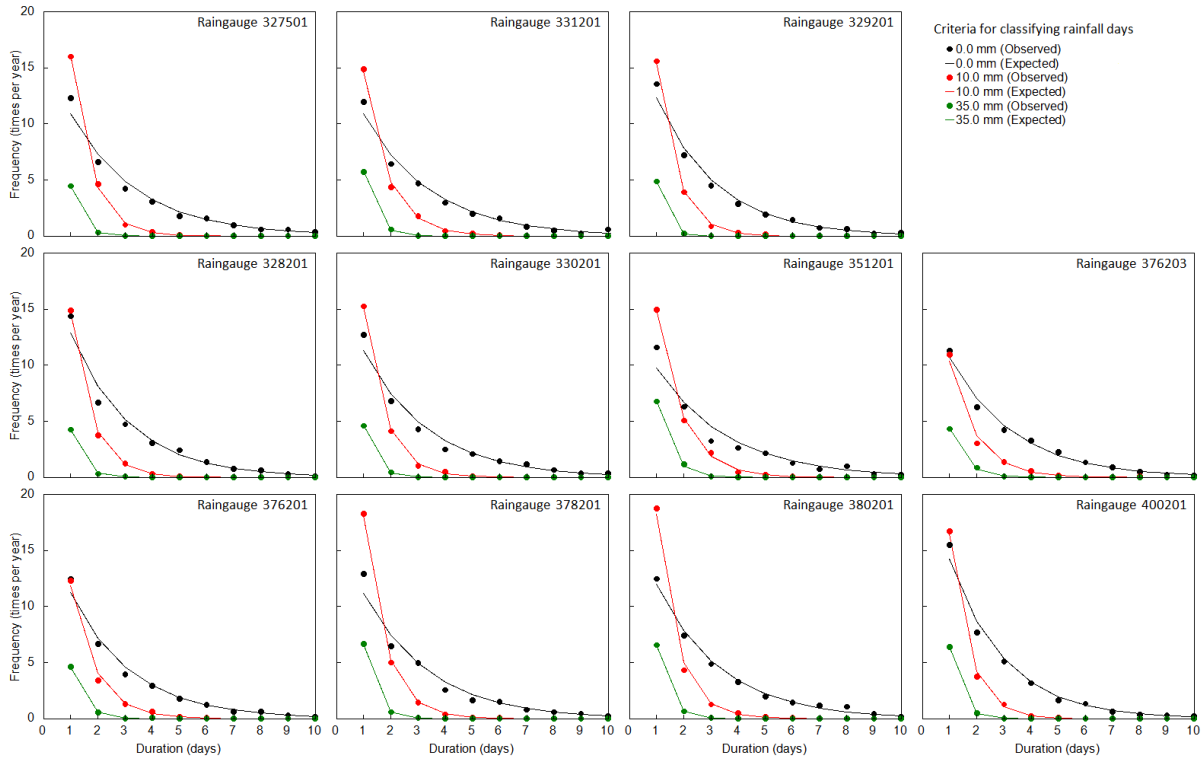

Figure 4.2: Observed and expected counts of consecutive rainfall days.

Table 4.2: Observed and expected average lengths of consecutive rainfall days.

Raingauge	>0.0 mm criteria		>10.0 mm criteria		>35.0 mm criteria	
	Observed	Expected	Observed	Expected	Observed	Expected
327501	3.040	3.025	1.370	1.368	1.083	1.083
331201	3.011	3.001	1.494	1.492	1.095	1.094
329201	2.741	2.739	1.351	1.352	1.046	1.046
328201	2.717	2.713	1.378	1.378	1.100	1.099
330201	2.943	2.931	1.391	1.390	1.092	1.092
351201	3.185	3.164	1.548	1.547	1.174	1.172
376203	2.903	2.901	1.564	1.565	1.208	1.208
376201	2.778	2.784	1.516	1.518	1.157	1.158
378201	2.966	2.966	1.404	1.405	1.100	1.100
380201	2.921	2.910	1.380	1.378	1.118	1.118
400201	2.576	2.573	1.346	1.345	1.082	1.081

4.3.2 Probability of consecutive rainfall days

The return periods of consecutive >0.0, >10.0, and >35.0 mm rainfalls days with different lengths (T_L in the equation 4.6, section 4.2.1) are calculated. It appears that the return periods of the consecutive >0.0 mm rainfall days in all parts of the area are similar. Conversely, for the consecutive >35.0 mm rainfall days, the shorter return periods are found over the joint between the mountainous region and plain area than the others part. The return periods of the consecutive >10.0 mm rainfall days are also shorter over the joint area than the others part but not as much obviously as that of the consecutive >35.0 mm rainfall days. The Fig. 4.3 shows the return periods of consecutive rainfall days with the length of more than 2 days (T_2). For others consecutive length, the patterns are similar. Therefore, quantitatively, the joint area has high probability of consecutive heavy rainfall days.

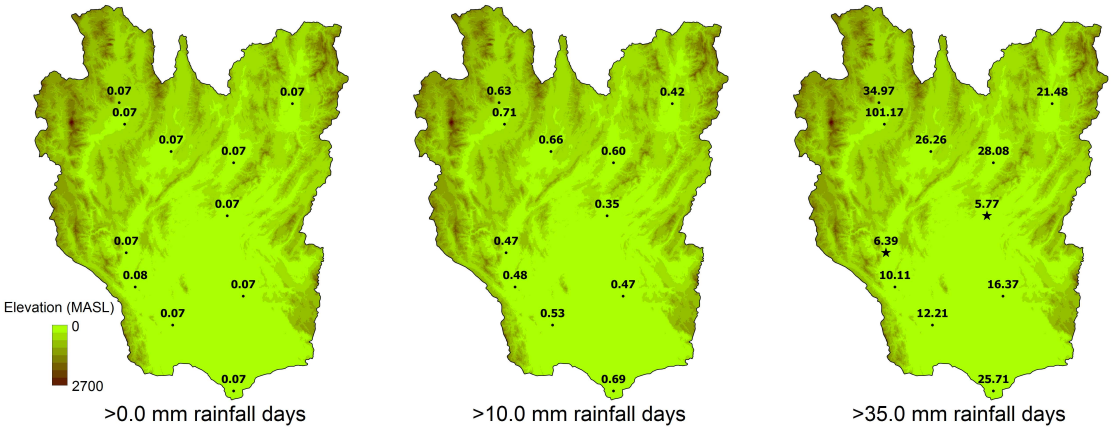

Return period is indicated in years.
Stars indicate locations with obvious consecutiveness of >35.0 mm rainfall days at 0.05 significance level.

Figure 4.3: Expected return period of more than 2 consecutive rainfall days.

The results are justified qualitatively by the chi-square test of independence (see the section 4.2.2) with a significance level of 0.05. The table 4.3 shows counts of transitions among 0.0, 0.1-10.0, 10.1- 35.0, and >35.0 mm rainfall days and the result of the test. At all raingauges, the 0.0 mm rainfall day tends to be followed by 0.0 mm rainfall day, and >0.0 mm rainfall day tends to be followed by >0.0 mm rainfall day. In other words, the rainfall days tend to be consecutive, and so do the dry days. This finding of consecutiveness of rainfall days is similar to results from many studies over others area [Moon et al., 1994, Hossain and Anam, 2012, Szyniszewska and Waylen, 2012].

However, the table 4.3 can show only the difference of characteristics between 0.0 mm rainfall day, which tends be followed by another 0.0 mm rainfall days, and >0.0 mm rainfall days, which tends be followed by another >0.0 mm rainfall days. The >0.0 mm rainfall days, all of 0.1-10.0, 10.1-35.0, and >35.0 mm rainfall days, have similar characteristics since all of 0.1-10.0, 10.1-35.0, and >35.0 mm rainfall days can be followed by any of 0.1-10.0, 10.1-35.0, and >35.0 mm rainfall days. We tried to distinguish the characteristics among 0.1-10.0, 10.1-35.0, and >35.0 mm rainfall days by applying the chi-square test of independence to only the transitions from 0.1-10.0, 10.1-35.0, and >35.0 mm rainfall days (the transition from 0.0 mm rainfall day was excluded). The result is shown in the table 4.4.

The difference between the characteristics of 0.1-10.0 and >10.0 mm rainfall days can be seen at all raingauges. The 0.1-10.0 mm rainfall day tends to be followed by the 0.0 mm rainfall day while the >10.0 mm rainfall day tends to be followed by another >10.0 mm

Table 4.3: Counts of transitions among 0.0, 0.1-10.0, 10.1-35.0, and >35.0 mm rainfall days and results of chi-square test of independence.

Raingauge	Previous	Latter day rainfall			
(χ^2 value)	day rainfall	0.0 mm	0.1-10.0 mm	10.1-35.0 mm	>35.0 mm
327501	0.0 mm	1,529 (1,149)$^+$	723 (952)$^-$	216 (342)$^-$	47 (72)$^-$
(479.68*)	0.1-10.0 mm	749 (956)$^-$	944 (792)$^+$	333 (285)$^+$	67 (60)
	10.1-35.0 mm	202 (345)$^-$	362 (286)$^+$	160 (103)$^+$	31 (21)$^+$
	>35.0 mm	42 (71)$^-$	60 (59)	42 (21)$^+$	12 (4)$^+$
331201	0.0 mm	1,596 (1,202)$^+$	707 (916)$^-$	215 (358)$^-$	55 (97)$^-$
(587.62*)	0.1-10.0 mm	764 (919)$^-$	819 (700)$^+$	305 (274)	79 (74)
	10.1-35.0 mm	182 (360)$^-$	346 (274)$^+$	186 (107)$^+$	56 (29)$^+$
	>35.0 mm	36 (98)$^-$	93 (75)$^+$	63 (29)$^+$	18 (8)$^+$
329201	0.0 mm	1,718 (1,354)$^+$	780 (959)$^-$	182 (340)$^-$	53 (79)$^-$
(462.70*)	0.1-10.0 mm	772 (962)$^-$	777 (681)$^+$	325 (242)$^+$	67 (56)
	10.1-35.0 mm	203 (340)$^-$	315 (241)$^+$	135 (85)$^+$	33 (20)$^+$
	>35.0 mm	42 (79)$^-$	65 (56)	45 (20)$^+$	7 (5)
328201	0.0 mm	1,623 (1,293)$^+$	773 (972)$^-$	228 (331)$^-$	47 (75)$^-$
(391.43*)	0.1-10.0 mm	799 (973)$^-$	877 (731)$^+$	275 (249)	59 (56)
	10.1-35.0 mm	212 (331)$^-$	292 (249)$^+$	146 (85)$^+$	34 (19)$^+$
	>35.0 mm	39 (75)$^-$	66 (56)	36 (19)$^+$	14 (4)$^+$
330201	0.0 mm	1,603 (1,223)$^+$	738 (959)$^-$	207 (335)$^-$	47 (78)$^-$
(499.32*)	0.1-10.0 mm	771 (963)$^-$	895 (755)$^+$	308 (264)$^+$	70 (61)
	10.1-35.0 mm	195 (336)$^-$	329 (264)$^+$	155 (92)$^+$	35 (21)$^+$
	>35.0 mm	32 (79)$^-$	78 (62)$^+$	43 (22)$^+$	14 (5)$^+$
351201	0.0 mm	1,652 (1,204)$^+$	654 (870)$^-$	202 (367)$^-$	66 (132)$^-$
(716.31*)	0.1-10.0 mm	675 (877)$^-$	775 (633)$^+$	321 (268)$^+$	103 (96)
	10.1-35.0 mm	209 (368)$^-$	317 (266)$^+$	188 (112)$^+$	72 (40)$^+$
	>35.0 mm	47 (134)$^-$	120 (97)$^+$	77 (41)$^+$	42 (15)$^+$
376203	0.0 mm	1,884 (1,436)$^+$	731 (990)$^-$	158 (291)$^-$	42 (98)$^-$
(873.87*)	0.1-10.0 mm	750 (991)$^-$	904 (683)$^+$	228 (201)	60 (68)
	10.1-35.0 mm	153 (291)$^-$	229 (200)$^+$	131 (59)$^+$	57 (20)$^+$
	>35.0 mm	29 (98)$^-$	76 (67)	54 (20)$^+$	33 (7)$^+$
376201	0.0 mm	1,967 (1,531)$^+$	714 (947)$^-$	188 (334)$^-$	39 (97)$^-$
(752.13*)	0.1-10.0 mm	727 (945)$^-$	757 (585)$^+$	247 (206)$^+$	65 (60)
	10.1-35.0 mm	175 (333)$^-$	258 (206)$^+$	144 (72)$^+$	55 (21)$^+$
	>35.0 mm	36 (96)$^-$	68 (60)	54 (21)$^+$	25 (6)$^+$
378201	0.0 mm	1,566 (1,190)$^+$	646 (876)$^-$	276 (384)$^-$	75 (112)$^-$
(457.47*)	0.1-10.0 mm	698 (877)$^-$	779 (645)$^+$	325 (283)$^+$	86 (83)
	10.1-35.0 mm	240 (384)$^-$	365 (283)$^+$	164 (124)$^+$	59 (36)$^+$
	>35.0 mm	59 (112)$^-$	97 (82)	63 (36)$^+$	22 (11)$^+$
380201	0.0 mm	1,424 (1,105)$^+$	691 (897)$^-$	277 (354)$^-$	75 (110)$^-$
(347.13*)	0.1-10.0 mm	720 (901)$^-$	890 (732)$^+$	312 (289)	89 (90)
	10.1-35.0 mm	267 (357)$^-$	329 (290)$^+$	144 (114)$^+$	56 (35)$^+$
	>35.0 mm	62 (110)$^-$	98 (89)	60 (35)$^+$	26 (11)$^+$
400201	0.0 mm	1,596 (1,314)$^+$	780 (943)$^-$	238 (326)$^-$	79 (110)$^-$
(269.50*)	0.1-10.0 mm	799 (942)$^-$	784 (676)$^+$	264 (234)$^+$	83 (79)
	10.1-35.0 mm	229 (327)$^-$	275 (235)$^+$	120 (81)$^+$	46 (27)$^+$
	>35.0 mm	70 (111)$^-$	93 (79)	47 (28)$^+$	17 (9)$^+$

Observed counts are indicated outside the parenthesis and expected counts are indicated inside the parenthesis.
The mark * indicates that the test value suggests the rejection of the null hypothesis at 0.05 significance level.
The mark + indicates the higher count than the expected count at 0.05 significance level.
The mark - indicates the lower count than the expected count at 0.05 significance level.

Table 4.4: Counts of transitions from 0.1-10.0, 10.1-35.0, and >35.0 mm rainfall days to 0.0, 0.1-10.0, 10.1-35.0, and >35.0 mm rainfall days and results of chi-square test of independence.

Raingauge	Previous	Latter day rainfall			
(χ^2 value)	day rainfall	0.0 mm	0.1-10.0 mm	10.1-35.0 mm	>35.0 mm
327501	0.1-10.0 mm	749 (692)$^+$	944 (952)	333 (373)$^-$	67 (77)
(43.23*)	10.1-35.0 mm	202 (250)$^-$	362 (343)	160 (134)$^+$	31 (28)
	>35.0 mm	42 (52)	60 (71)	42 (28)$^+$	12 (6)$^+$
331201	0.1-10.0 mm	764 (655)$^+$	819 (840)	305 (370)$^-$	79 (102)$^-$
(111.09*)	10.1-35.0 mm	182 (257)$^-$	346 (329)	186 (145)$^+$	56 (40)$^+$
	>35.0 mm	36 (70)$^-$	93 (90)	63 (39)$^+$	18 (11)$^+$
329201	0.1-10.0 mm	772 (709)$^+$	777 (806)	325 (352)	67 (75)
(37.96*)	10.1-35.0 mm	203 (250)$^-$	315 (285)	135 (124)	33 (26)
	>35.0 mm	42 (58)$^-$	65 (66)	45 (29)$^+$	7 (6)
328201	0.1-10.0 mm	799 (741)$^+$	877 (871)	275 (322)$^-$	59 (75)
(58.57*)	10.1-35.0 mm	212 (252)$^-$	292 (297)	146 (110)$^+$	34 (26)
	>35.0 mm	39 (57)$^-$	66 (67)	36 (25)$^+$	14 (6)$^+$
330201	0.1-10.0 mm	771 (697)$^+$	895 (910)	308 (354)$^-$	70 (83)
(60.97*)	10.1-35.0 mm	195 (244)$^-$	329 (318)	155 (124)$^+$	35 (29)
	>35.0 mm	32 (57)$^-$	78 (74)	43 (29)$^+$	14 (7)$^+$
351201	0.1-10.0 mm	675 (592)$^+$	775 (771)	321 (373)$^-$	103 (138)$^-$
(92.67*)	10.1-35.0 mm	209 (248)$^-$	317 (323)	188 (156)$^+$	72 (58)
	>35.0 mm	47 (90)$^-$	120 (118)	77 (57)$^+$	42 (21)$^+$
376203	0.1-10.0 mm	750 (669)$^+$	904 (868)	228 (297)$^-$	60 (108)$^-$
(192.66*)	10.1-35.0 mm	153 (196)$^-$	229 (255)	131 (87)$^+$	57 (32)$^+$
	>35.0 mm	29 (66)$^-$	76 (86)	54 (29)$^+$	33 (11)$^+$
376201	0.1-10.0 mm	727 (645)$^+$	757 (745)	247 (306)$^-$	65 (100)$^-$
(122.20*)	10.1-35.0 mm	175 (227)$^-$	258 (262)	144 (108)$^+$	55 (35)$^+$
	>35.0 mm	36 (66)$^-$	68 (76)	54 (31)$^+$	25 (10)$^+$
378201	0.1-10.0 mm	698 (637)$^+$	779 (792)	325 (352)	86 (107)$^-$
(41.09*)	10.1-35.0 mm	240 (279)$^-$	365 (347)	164 (155)	59 (47)
	>35.0 mm	59 (81)$^-$	97 (101)	63 (45)$^+$	22 (14)$^+$
380201	0.1-10.0 mm	720 (691)	890 (868)	312 (340)	89 (113)$^-$
(39.02*)	10.1-35.0 mm	267 (274)	329 (343)	144 (135)	56 (45)
	>35.0 mm	62 (85)$^-$	98 (106)	60 (42)$^+$	26 (14)$^+$
400201	0.1-10.0 mm	799 (750)	784 (786)	264 (294)	83 (100)
(30.35*)	10.1-35.0 mm	229 (260)	275 (273)	120 (102)	46 (35)
	>35.0 mm	70 (88)	93 (93)	47 (35)$^+$	17 (12)

Observed counts are indicated outside the parenthesis and expected counts are indicated inside the parenthesis.
The mark * indicates that the test value suggests the rejection of the null hypothesis at 0.05 significance level.
The mark + indicates the higher count than the expected count at 0.05 significance level.
The mark - indicates the lower count than the expected count at 0.05 significance level.

rainfall day. Therefore, the results at this step suggest that >10.0 mm rainfall days tend to be consecutive while 0.1-10.0 mm rainfall days do not lead to the following rainfall day as much as >10.0 mm rainfall days do. However, the characteristics of 10.1-35.0 and >35.0 mm rainfall days cannot be distinguished at this step still.

Similar to the previous step, we tried to distinguish the characteristics between 10.1-35.0 and >35.0 mm rainfall days by applying the chi-square test of independence to only the transitions from 10.1-35.0 and >35.0 mm rainfall days. The result is shown in the table 4.5.

Interestingly, there are different patterns between over the joint area (raingauges 351201 and 376203) and over the others part. Over the joint area, >35.0 mm rainfall day tends to be followed by another >35.0 mm rainfall day more obviously than 10.1-35.0 rainfall day does. Over the others part, the characteristics of 10.1-35.0 and >35 mm rainfall days are similar. Therefore, it can be concluded that >35.0 mm rainfall days tend to be consecutive over the joint area more obviously than others part.

Table 4.5: Counts of transitions from 10.1-35.0 and >35.0 mm rainfall days to 0.0, 0.1-10.0, 10.1-35.0, and >35.0 mm rainfall days and results of chi-square test of independence.

Raingauge	Previous	Latter day rainfall			
(χ^2 value)	day rainfall	0.0 mm	0.1-10.0 mm	10.1-35.0 mm	>35.0 mm
327501	10.1-35.0 mm	202 (202)	362 (350)	160 (167)	31 (36)
(7.95*)	>35.0 mm	42 (42)	60 (72)	42 (35)	12 (7)
331201	10.1-35.0 mm	182 (171)	346 (345)	186 (196)	56 (58)
(5.73)	>35.0 mm	36 (47)	93 (94)	63 (53)	18 (16)
329201	10.1-35.0 mm	203 (199)	315 (308)	135 (146)	33 (32)
(5.73)	>35.0 mm	42 (46)	65 (72)	45 (34)	7 (8)
328201	10.1-35.0 mm	212 (205)	292 (292)	146 (148)	34 (39)
(5.29)	>35.0 mm	39 (46)	66 (66)	36 (34)	14 (9)
330201	10.1-35.0 mm	195 (184)	329 (330)	155 (160)	35 (40)
(7.43)	>35.0 mm	32 (43)	78 (77)	43 (38)	14 (9)
351201	10.1-35.0 mm	209 (188)	317 (320)	188 (194)	72 (84)
(15.98*)	>35.0 mm	47 $(68)^-$	120 (117)	77 (71)	42 $(30)^+$
376203	10.1-35.0 mm	153 (136)	229 (228)	131 (138)	57 (67)
(16.14*)	>35.0 mm	29 $(46)^-$	76 (77)	54 (47)	33 $(23)^+$
376201	10.1-35.0 mm	175 (164)	258 (253)	144 (154)	55 (62)
(10.20*)	>35.0 mm	36 (47)	68 (73)	54 (44)	25 (18)
378201	10.1-35.0 mm	240 (232)	365 (358)	164 (176)	59 (63)
(6.50)	>35.0 mm	59 (67)	97 (104)	63 (51)	22 (18)
380201	10.1-35.0 mm	267 (251)	329 (326)	144 (156)	56 (63)
(11.03*)	>35.0 mm	62 (78)	98 (101)	60 (48)	26 (19)
400201	10.1-35.0 mm	229 (223)	275 (275)	120 (125)	46 (47)
(1.37)	>35.0 mm	70 (76)	93 (93)	47 (42)	17 (16)

Observed counts are indicated outside the parenthesis and expected counts are indicated inside the parenthesis.
The mark * indicates that the test value suggests the rejection of the null hypothesis at 0.05 significance level.
The mark + indicates the higher count than the expected count at 0.05 significance level.
The mark - indicates the lower count than the expected count at 0.05 significance level.

4.3.3 Rainfall amount on consecutive rainfall days

In the section 4.3.2, we have found that the >10.0 mm rainfall days tend to be consecutive over all parts of the area while the consecutiveness of 0.0-10.0 mm rainfall days is not obvious. In this section, we investigated the amount of rainfall in those >10.0 mm rainfall days, which have been found to be consecutive.

At all raingauges, average daily rainfall amounts on days with >10.0 mm rainfall were calculated and the student-t test (see the section 4.2.3) with 0.05 significance level was applied to determine if the rainfall amount was higher or lower than the areal average. The result is shown in the Fig. 4.4. Over the mountainous region, the average rainfall amount on >10.0 mm rainfall days is below 27.0 mm and the student t-test suggests that the amounts are significantly lower than the areal average at 3 stations, 327501, 329201, and 328201.

Conversely, over the plain area, the average rainfall amount on >10.0 mm rainfall days is above 27.0 mm and appears to be highest over the joint area. The student t-test suggests the higher rainfall amount than the areal average at the station 351201. Therefore, it is obvious that the mountainous region has lower rainfall amount on the consecutive rainfall days than the others part of the area.

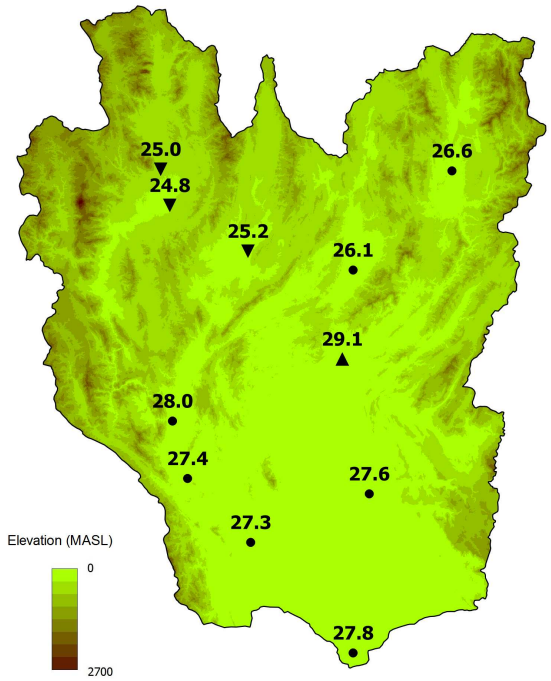

Rainfall amount is indicated in mm.
An upwards arrow indicates a high rainfall amount at the significance level is 0.05.
A downwards arrow indicates a low rainfall amount at the significance level is 0.05.

Figure 4.4: Average rainfall amount on >10.0 mm rainfall day.

4.4 Conclusions

In the southwest monsoon period, according to the Markov chain model and results of chi-square test of independence, consecutiveness of >10.0 mm rainfall days is common for all parts of the northern Thailand but the consecutiveness of >35.0 mm rainfall days is obvious only over the joint between the mountainous region and plain area. According to the result of the student t-test on rainfall amount on >10.0 mm rainfall days, the rainfall amounts on those days are lower over the mountainous region than over the plain area.

Therefore, the characteristics of consecutive rainfall days over the mountainous region, plain area, and joint area are different. Over the mountainous region, the rainfall amount on the consecutive rainfall days is lower than the plain area. Over the joint area, the consecutiveness of >35.0 mm rainfall days (heavy rainfall days) is most obvious. However, the common characteristic over all parts is the consecutiveness of >10.0 mm rainfall days.

Chapter 5

Study 2: Variability of flood peak

This part includes simulations of floods in Sukhothai city from spatially distributed rainfall over middle and lower Yom basin. First, the conceptual model was developed. Next, the rainfall was designed. After that, flood from uniform rainfall was simulated. Finally, floods from 1,000 spatial rainfalls were simulated and the peak discharges were compared.

5.1 Data

Data used for model development were cross sections, hourly water level, hourly discharge, 3-hour rainfall, and monthly pan evaporation during April-October 2011-2014. The data before 2011 were not used because there was a big flood which affected the cross section in 2011. The cross sections, water level, and discharge were obtained from RID. The cross sections were surveyed during 2013-2014 at locations of streamgauges shown in the Fig. 5.1 and table 5.1. The water level and discharge have been recorded hourly at the streamgauges Y1C, Y43, and Y37 and 5 times a day at the others streamgauges. The rainfall and pan evaporation have been collected by TMD at raingauges shown in the Fig. 5.1 and table 5.2.

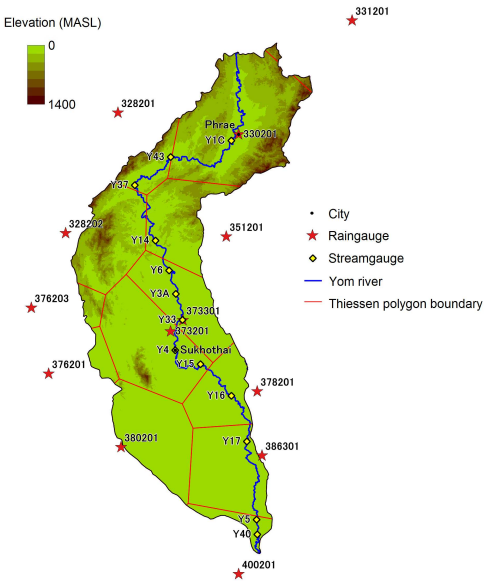

Figure 5.1: Locations of raingauges and streamgauges which record the data during 2011-2014.

Table 5.1: Information of streamgauges shown in Fig. 5.1.

Streamgauge	Latitude	Longitude	Elevation[a] (MASL)	Upstream distance (km)	Cross section area[b] (m^2)
Y1C	18.1331	100.1275	159	490.5	977.1
Y43	18.0447	99.8008	118	433.9	-[c]
Y37	17.8933	99.6074	107	384.5	1,102.4
Y14	17.5950	99.7189	79	322.7	1,344.0
Y6	17.4342	99.7922	72	297.5	1,177.6
Y3A	17.3081	99.8286	63	275.8	944.5
Y33	17.1681	99.8644	60	251.9	511.9
Y4	17.0050	99.8253	54	219.0	370.0
Y15	16.9297	99.9614	44	175.0	694.4
Y16	16.7597	100.1278	41	129.4	339.1
Y17	16.5139	100.2111	38	84.4	453.6
Y5	16.0931	100.2633	32	13.5	835.3
Y40	16.0135	100.2673	31	0.0	483.2

a Elevation data is from GMTED10 derived by USGS.
b Cross section areas were surveyed by RID between the end of 2013 and the beginning of 2014.
c The cross section areas at the streamgauge Y43 is not shown because the mistake of the data is suspected.

Table 5.2: Information of raingauges shown in Fig. 5.1.

Raingauge	Latitude	Longitude	Elevation[a] (MASL)	Coverage area (km^2)
331201	18.7797	100.7778	204	87.0
328201	18.2833	99.5167	257	696.1
330201	18.1667	100.1667	163	4,186.8
328202	17.6350	99.2347	173	1,940.1
351201	17.6167	100.1000	67	1,623.0
376203	17.2333	99.0500	162	254.1
373301	17.1667	99.8667	59	1,720.0
373201	17.1061	99.8000	51	2,724.0
376201	16.8783	99.1433	124	284.6
378201	16.7833	100.2667	47	1,274.5
380201	16.4833	99.5333	78	2,084.5
386301	16.4381	100.2925	39	2,062.5
400201	15.8000	100.1667	25	360.2

a Elevation data is from GMTED10 derived by USGS.

For the rainfall design, we used the rainfall data during the southwest monsoon season during the latest climatological period, May-October 1981-2010. The raingauges which recorded rainfall during that period were only the raingauges 331201, 328201, 330201, 351201, 379203, 376201, 378201, 380201, and 400201.

5.2 Methods

5.2.1 Model description

In this study, there were 2 models used for the simulation, rainfall-runoff model and river network model. The rainfall-runoff model calculated basin discharge to the river from rainfall while the river network model calculated the flow in the river.

5.2.1.1 HEC-HMS: Rainfall-runoff model

The rainfall-runoff model used in this study was HEC-HMS model [Feldman, 2000]. In this model, the rainwater filled the interception storage first. After the infiltration storage was full, the remaining water filled up the infiltration storage. After the infiltration storage was full, the remaining water filled up the surface storage. Finally, after the surface storage was full, the remaining water was called excess rainfall and was transformed to direct runoff of the basin. However, the interception was insignificant for our study, and therefore, it was not included in our model. Furthermore, apart from the direct runoff, the basin discharge was contributed by a baseflow.

The infiltration was calculated by the deficit and constant loss model. In this model, the rainwater filled up the infiltration storage and did not become runoff until the storage was full. The water in the infiltration storage could be removed by a percolation and evapotranspiration. The parameters specified in this model were the infiltration storage capacity (max $S_{infiltration}$) and percolation rate (f_c). The value of f_c was associated with a soil texture. The coarse-textured soil usually had high value of f_c [Haan et al., 1982, Cronshey, 1986].

The surface storage was the next storage the rainwater filled after the infiltration storage was full. The rainwater could become runoff after this storage was full. However, the water stored in this storage could be removed by infiltration and evapotranspiration. The parameter specified for the surface storage was the storage capacity (max $S_{surface}$).

The remaining water from the infiltration and surface storages were transformed to direct runoff hydrograph by Snyder's model. This model was a unit hydrograph model where the discharge was determined by a unit hydrograph (see the detail of unit hydrograph model in the section 2.7.2.1). The standard hydrograph for the Snyder's model was the hydrograph which satisfies the equation 5.1,

$$t_p = 5.5 t_r \tag{5.1}$$

where t_p was the lag time (or standard lag time) and t_r was the rainfall duration.

For the desired rainfall duration t_R, which was controlled by the timestep in the model, the desired time to peak t_{pR} could be calculated by the equation 5.2.

$$t_{pR} = t_p - \frac{t_r - t_R}{4} \tag{5.2}$$

The peak discharge of the unit hydrograph (U_{pR}) was determined by the equation 5.3,

$$\frac{U_{pR}}{A} = 2.75 \frac{C_p}{t_{pR}} \tag{5.3}$$

where C_p was a peak coefficient, A was a basin area in square kilometers, and U_{pR} was in cubic meters per second, and t_{pR} was in hours.

The value of t_p could be estimated by the equation 5.4,

$$t_p = 0.75 C_t \left(L_b L_c\right)^{0.3} \tag{5.4}$$

where C_t was the basin coefficient, L_b was the distance from the outlet to the furthest boundary of the basin in kilometers, L_c was the distance from the outlet to the centroid of the basin in kilometers, and t_p was in hours. The C_t was not a physically-based parameter. However, it was affected by steepness. A steep slope area was found to be associated with the low value of C_t [Snyder, 1938, Bedient and Huber, 1992].

The baseflow in our model was determined by the exponential recession model. The baseflow began at the specified point in the recession limb of the hydrograph. That point

was specified by a ratio to peak ($Q_{baseflow,0}/Q_p$ where $Q_{baseflow,0}$ was initial baseflow and Q_p was the peak discharge of the hydrograph). The base flow at the time t was determined by the equation 5.5,

$$Q_{baseflow,t} = Q_{baseflow,0} k_{baseflow}^{t} \tag{5.5}$$

where $Q_{baseflow,t}$ was the baseflow at the time t, and $k_{baseflow}$ was the recession constant.

5.2.1.2 HEC-RAS: River network model

The river network model used in this study was HEC-RAS model [Brunner, 2010]. This model determined the flow by the principles of conservation of mass and conservation of momentum. These equations were discretized and solved by a 4-point implicit scheme.

The principle of conservation of mass was described by the 5.6 and the principle of conservation of momentum was described by the equation 5.7,

$$\frac{\partial A}{\partial t} + \frac{\partial S}{\partial t} + \frac{\partial Q}{\partial x} - q_l = 0 \tag{5.6}$$

$$\frac{\partial Q}{\partial t} + \frac{\partial (VQ)}{\partial x} + gA\left(\frac{\partial z}{\partial x} + S_f\right) = 0 \tag{5.7}$$

where t was a time, x was a spatial location, A was a flow area, S was a storage from non-conveying portions, Q was a discharge, q_l was a lateral flow, V was a flow velocity, g was an acceleration due to the gravity, z was a water surface elevation, and S_f was a friction slope estimated by Manning's equation, the equations 5.8,

$$S_f = \frac{Q|Q|}{K^2} \tag{5.8}$$

$$K = \frac{AR^{2/3}}{n} \tag{5.9}$$

where R was a hydraulic radius, n was a Manning's coefficient and units of S_f, n, Q, A, and R were in the SI system. Note that the unit of n was $\mathrm{m}^{1/3}/\mathrm{s}$ but usually not written. The variable K was called a conveyance.

In the 4-point implicit scheme, given the time from t to $t + \Delta t$ and the spatial location from x to $x + \Delta x$, at an interior point with the time $t + \theta\Delta t$ for a specified $\theta \in (0, 1]$ and spatial location $x + 0.5\Delta x$, this scheme estimated the function value (f), time derivative ($\frac{\partial f}{\partial t}$), and space derivative ($\frac{\partial f}{\partial x}$) by the equations 5.10, 5.11, and 5.12, respectively,

$$f \approx \bar{f} = 0.5\left(f_{x+\Delta x}^{t} + f_{x}^{t}\right) + 0.5\theta\left(\left(f_{x+\Delta x}^{t+\Delta t} - f_{x+\Delta x}^{t}\right) + \left(f_{x}^{t+\Delta t} - f_{x}^{t}\right)\right) \tag{5.10}$$

$$\frac{\partial f}{\partial t} \approx \frac{\Delta f}{\Delta t} = \frac{0.5\left(\left((f_{x+\Delta x}^{t+\Delta t} - f_{x+\Delta x}^{t}\right) + \left(f_{x}^{t+\Delta t} - f_{x}^{t}\right)\right)}{\Delta t} \tag{5.11}$$

$$\frac{\partial f}{\partial x} \approx \frac{\Delta f}{\Delta x} = \frac{\left(f_{x+\Delta x}^{t} - f_{x}^{t}\right) + \theta\left(\left(f_{x+\Delta x}^{t+\Delta t} - f_{x+\Delta x}^{t}\right) - \left(f_{x}^{t+\Delta t} - f_{x}^{t}\right)\right)}{\Delta x} \tag{5.12}$$

where f_j^n was the function value at time $n \in \{t, x+\Delta t\}$ and spatial location $j \in \{x, x+\Delta x\}$.

The model discretized the equations of the principles of conservation of mass (equation 5.6) and conservation of momentum (equation 5.7) by the equations 5.10, 5.11, and 5.12. The discretization was done separately for the flows in a channel and over the floodplain. In the channel, the flow followed the path of the channel and there was no storage from

non-conveying portions (S). Over the flood plain, the flow did not follow the path of the channel and there were storages from non-conveying portions (S).

In the momentum equation, a term gAS_h was also added to represent the force from structures which opposed the flow and caused the rising of a local water level with the slope of S_h. The local slope S_h was calculated by the equations 5.13 and 5.14,

$$S_h = \frac{dh_l}{dx} \tag{5.13}$$

$$h_l = \frac{CV^2}{2g} \tag{5.14}$$

where C was a function of velocity, depth, and geometric properties of the channel but was assumed to be constant. The variable h_l was a head loss.

The results of the discretization were as the equation 5.15 for the principle of conservation of mass and the equations 5.16-5.18 for the principle of conservation of momentum,

$$\left(\frac{\Delta A_C}{\Delta t}\Delta x_C + \frac{\Delta A_F}{\Delta t}\Delta x_F\right) + \frac{\Delta S}{\Delta t}\Delta x_F + \Delta Q - \bar{Q_l} = 0 \tag{5.15}$$

$$\frac{\Delta\left(Q_C\Delta x_C + Q_F\Delta x_F\right)}{\Delta t\Delta x_e} + \frac{\Delta\left(\beta VQ\right)}{\Delta x_e} + g\bar{A}\left(\frac{\Delta z}{\Delta x_e} + \bar{S}_f + \bar{S}_h\right) = 0 \tag{5.16}$$

$$\beta = \frac{V_C^2 A_C + V_F^2 A_F}{V^2 A} \tag{5.17}$$

$$\Delta x_e = \frac{\bar{A_C}\bar{S_{fC}}\Delta x_C + \bar{A_F}\bar{S_{fF}}\Delta x_F}{\bar{A}\bar{S_f}} \tag{5.18}$$

where subscripts C and F (below the variables A, x, Q, V, and S_f) represented the values of the variables in a channel and on a floodplain, respectively, $\bar{Q_l}$ was an average lateral flow, and $\bar{S}_h$ was an average local slope over the distance Δx_e.

The variable β was defined as a velocity distribution factor. The distance Δx_e was defined as an equivalent flow path. In the model, the friction slopes of channel and floodplain were assumed to be the same, and therefore, the equation 5.18 could be reduced to the equation 5.19.

$$\Delta x_e = \frac{\bar{A_C}\Delta x_C + \bar{A_F}\Delta x_F}{\bar{A}} \tag{5.19}$$

The finite differential equations 5.16-5.19 were linearized under the following assumptions,

1. The finite differences of the flow area ($A(z)$), storage from non-conveying portions ($S(z)$), friction slope ($S_f(z,Q)$), and local slope ($S_h(z,Q)$) over the time from t to $t+\Delta t$ could be approximated by the first term of the Taylor series as the equations 5.20-5.23.

$$A_j^{t+\Delta t} - A_j^t \approx \left(\frac{dA}{dz}\right)_{z_j^t}\left(z_j^{t+\Delta t} - z_j^t\right) \tag{5.20}$$

$$S_j^{t+\Delta t} - S_j^t \approx \left(\frac{dS}{dz}\right)_{z_j^t}\left(z_j^{t+\Delta t} - z_j^t\right) \tag{5.21}$$

$$S_{fj}^{t+\Delta t} - S_{fj}^t \approx \left(\frac{\partial S_f}{\partial z}\right)_{z_j^t,Q_j^t}\left(z_j^{t+\Delta t} - z_j^t\right) + \left(\frac{\partial S_f}{\partial Q}\right)_{z_j^t,Q_j^t}\left(Q_j^{t+\Delta t} - Q_j^t\right) \tag{5.22}$$

$$S_{hj}^{t+\Delta t} - S_{hj}^{t} \approx \left(\frac{\partial S_h}{\partial z}\right)_{z_j^t, Q_j^t} \left(z_j^{t+\Delta t} - z_j^t\right) + \left(\frac{\partial S_h}{\partial Q}\right)_{z_j^t, Q_j^t} \left(Q_j^{t+\Delta t} - Q_j^t\right) \tag{5.23}$$

The equation 5.20 was also applied to A_F and A_C.

2. When Δt was small, the equivalent flow path (Δx_e), flow distribution factor ($\phi = \frac{Q_C}{Q_C+Q_F}$), velocity distribution factor (β), and velocity (V) over the time from t to $t + \Delta t$ could be assumed to be constant as the equations 5.24-5.27.

$$\Delta x_e^{t+\Delta t} \approx \Delta x_e^t \tag{5.24}$$

$$\phi_j^{t+\Delta t} \approx \phi_j^t \tag{5.25}$$

$$\beta_j^{t+\Delta t} \approx \beta_j^t \tag{5.26}$$

$$V_j^{t+\Delta t} \approx V_j^t \tag{5.27}$$

3. For each variable (f), at the locations $j_1, j_2 \in \{x, x + \Delta x\}$ over the time from t to $t + \Delta t$, when the product of the finite differences of the variable ($\Delta f \times \Delta f$) was very small in comparison to the product of the values of the variable ($f \times f$), the product of finite differences could be approximated 0 as the equation 5.28.

$$\left(f_{j_1}^{t+\Delta t} - f_{j_1}^t\right)\left(f_{j_2}^{t+\Delta t} - f_{j_2}^t\right) \approx 0 \tag{5.28}$$

The algorithm and results of the linearization can be seen in the appendix B.1.

5.2.2 Model development

5.2.2.1 Model digitization

The figure 5.2 shows the boundaries of the modelled river and basins as well as locations of data input to the model. This study simulated floods at the Sukhothai city, streamgauge Y4, by routing the channel flow along the Yom river from the streamgauge Y1C to the streamgauge Y40 using HEC-RAS model. At the station Y1C, a discharge was used as an upstream boundary condition, and at the streamgauge Y40, a water level was used as a downstream boundary condition. The cross section data were input at all streamgauges shown in figure 5.2 except at the streamgauge Y43 because the error was suspected. The spatial resolution was set to be approximately 5 km and the temporal resolution was set to 15 minutes. Note that the spatial resolution may not be exactly 5 km because the model specified calculation points by divided the distance between the cross sections equally and that equally divided distance depended on the distance between the cross sections.

The runoff from rainfall was input to the river as a lateral flow to each of 13 steamgauges. The basin was divided into 13 sub-areas which drained the water to corresponding 13 streamgauges. The division used subbasin boundary. In the flat area where the subbasin boundary could not be defined, the water was assumed to be drained to the nearest stream. Boundaries and information of these sub-areas are shown in figure 5.2 and table 5.3, respectively. For each sub-area, the rainfall and evaporation was calculated by Thiessen polygon. Locations of raingauges and Thiessen polygon boundaries are shown in figure 5.2.

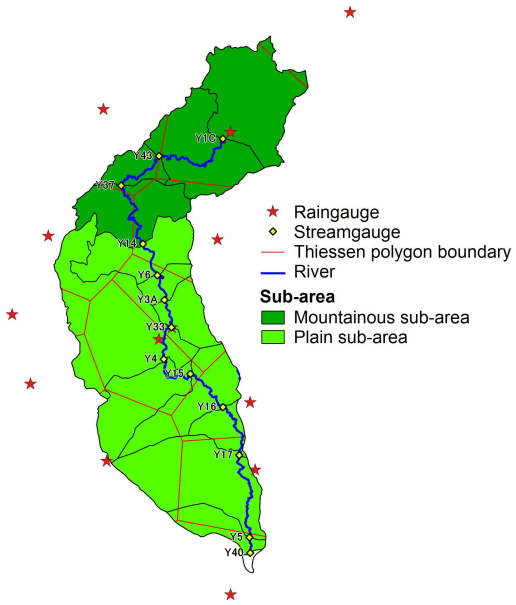

Figure 5.2: Modelling stream and sub-areas.

Apart from lateral flow from rainfall, there were also lateral flow from branches and the water diversion for an irrigation. There were many small streams which contributed the water to the river between the streamgauges Y1C and Y6. The lateral flows from these streams were included to the model as a uniform lateral inflow. This flow was estimated as 90 cms. Between the streamgauges Y6 and Y3A, there was a floodgate which diverted the water from the Yom river for an irrigation. This floodgate was included as a lateral diversion structure in the model. The diversion rate was 75 cms. Between the streamgauges Y33 and Y4, there were large contributions of flows from the river branches, and therefore, another lateral inflow was included in that part. This flow was estimated as 75 cms. Between the streamgauges Y4 to Y40, eventhough there were many small streams, the channel flow over that part appeared not to affect the simulation result at the Sukhothai city, and therefore, it was not necessary to include the lateral flow to that part in the model.

5.2.2.2 Model calibration

After the model was digitized, the calibration was done to assign model parameters. In the calibration, the parameters were determined by trial and error. For each observed rainfall, numerous simulations with different values of model parameters were carried out and the value which gives the most accurate simulated water level were selected.

First, the water level was simulated with randomly assigned parameters. Then, for each parameter, the value was adjusted, the subsequent simulation was done, and the value which gives the most accurate water level was selected. The adjustment was done until an optimum value which gives the most accurate water level was reached. However, when the value of one parameter changed, the optimum values of the others parameter might not be the same. Therefore, the previously optimized parameters should be optimized again after another parameter was optimized. The calibration was finished when all parameters reached the optimum values together.

For our study, the parameters to calibrate in the model included the followings,

1. Parameters for loss model which were infiltration storage capacity (max $S_{infiltration}$)

Table 5.3: Information of sub-areas shown in Fig. 5.1.

Outlet streamgauge	area (km^2)	centroid distance (km)	Length[a] (km)	Average slope[b] (%)
Y1C	2,457.0	27.9	63.7	15
Y43	2,075.6	22.6	57.3	14
Y37	544.1	12.2	27.2	16
Y14	1,544.9	20.6	43.8	14
Y6	1,364.1	16.2	48.0	12
Y3A	370.3	9.6	24.9	1
Y33	702.1	10.7	31.1	1
Y4	3,410.7	35.2	106.9	8
Y15	1,465.3	32.9	66.7	4
Y16	1,505.8	17.8	64.5	0
Y17	528.1	17.7	32.7	0
Y5	2,637.2	43.9	88.3	0
Y40	632.5	24.7	51.4	0

a Length is the distance from the outlet streamgauge to the furthest point in the boundary.
b Slope was as of a 90 m digital elevation map created from a 1:50,000 topographic map from Royal Thai Survey Department.

and percolation rate (f_c).

2. Surface storage capacity (max $S_{surface}$).

3. Parameters for hydrograph transformation which were basin coefficient (C_t) for the equation 5.4 and peak coefficient (C_p) for the equation 5.3.

4. Parameters for basefow model which were ratio to peak ($Q_{baseflow,0}/Q_p$) and recession constant ($k_{baseflow}$) for the equation 5.5.

5. Parameter for channel flow routing which was a Manning's coefficient (n) for the equation 5.8.

The calibration was done from May to October in 2013 and 2014. The simulation began from April to eliminate the influence of initial conditions before the calibration period. The rainfall was input every 3 hour, the evaporation was input as a monthly average, and the upstream water level was input every hour while the downstream water level was input 5 times according to the availability. Since the upstream and downstream areas had different characteristics, the calibration was done separately between these 2 parts. The boundary between these 2 parts was the streamgauge Y14 (see figure 5.2). The objective functions of the calibration were the root-mean-square errors (RMSE) of the water level at the streamgauge Y4, Sukhothai city, and the streamgauge Y14, the boundary between plain area and mountainous region where the water level was not influenced by the flow in the plain area.

The parameter values used for an experimental simulation were average optimum values from the calibrations in 2013 and 2014.

5.2.2.3 Model verification

After the model was parameterized, the verification was done to test the model accuracy. For each observed rainfall which was not used for the calibration, the simulation was carried out and an accuracy of simulated water level was assessed.

The verification was done from May to October in 2011 and 2012. Similarly to the calibration, the simulation began from April to eliminate the influence of initial conditions. The data before 2011 was not used because there was a big flood in 2011 which affected the cross sections.

5.2.2.4 Model simplification

With 13 sub-areas in the model, there was a requirement of 13 rainfall hyetographs. However, Kotsuki and Tanaka [2013] suggested that the spatial distribution of rainfall does not affect the peak discharge of the basin if the basin is small. As a result, averaging the rainfall data among some sub-areas could be done if the total size of the sub-areas for averaging was small. In order to make the model most simple, we tried to average the rainfall among as large area as possible. However, if the area for averaging was too large, the simulated water level could be inaccurate.

We tried numerous ways of choosing the sub-areas to average the rainfall and compared the simulated water level with the one simulated from the typical case, when 13 rainfall hyetographs were used. The comparison was done during May-October 2011-2014. If the simulated water levels were too much different, the averaging could not be done and another way of choosing the sub-areas must be tried. Conversely, if the simulated water levels were similar, the averaging could be done and expanding the area for averaging could be tried. By this way, the number of rainfall hyetographs required for the simulation could be reduced.

5.2.3 Experimental simulation

5.2.3.1 Rainfall frequency analysis

We determined the rainfall amount by frequency analysis of extreme rainfall. The data used for the frequency analysis were annual maximum areal average 24-, 48-, and 72-h rainfalls for the design 24-, 48-, and 72-h rainfalls, respectively. For each duration, the annual maximum rainfalls were sorted descending and the Weibull equation was used to assign the exceedance probabilities of the rainfall amounts as the equation 5.29 [Singh, 1992],

$$P = \frac{m}{N+1} \tag{5.29}$$

where P was an exceedance probability, m was an order of the data, and N was a count of data.

After the probability was assigned, the GEV distribution was used to fit the data. The objective function was the RMSE of the rainfall amount. As mentioned in the section 2.7.3.1, the GEV distribution was derived from the combination of the Fréchet, Gumbel, and Weibull distributions. The cumulative distribution function of the GEV distribution (F) was the equation 5.30 [Martins and Stedinger, 2000],

$$F(X) = \begin{cases} e^{-\left(1-\kappa\left(\frac{X-\xi}{\alpha}\right)\right)^{\frac{1}{\kappa}}} & \text{for } \kappa \neq 0 \\ e^{-e^{\left(-\frac{X-\xi}{\alpha}\right)}} & \text{for } \kappa = 0 \end{cases} \tag{5.30}$$

where $\xi + \alpha/\kappa \leq X < +\infty$ for $\kappa < 0$, $-\infty \leq X < +\infty$ for $\kappa = 0$, and $-\infty \leq X < +\alpha/\kappa$ for $\kappa > 0$. The constants ξ, α, and κ were location, scale, and shape parameters, respectively. The function F belonged to Fréchet, Gumbel, and Weibull distributions when $\kappa < 0$, $\kappa = 0$, and $\kappa > 0$, respectively.

From the equation 5.30, the expected rainfall amount (X) could be calculated as the equation 5.31. Note that the expected value of P was equal to $1 - F(X)$.

$$X = \begin{cases} \xi + \frac{\alpha}{\kappa}\left(1 - \left(-\ln\left(1-P\right)\right)^{\kappa}\right) & \text{for } \kappa \neq 0 \\ \xi - \alpha \ln\left(-\ln\left(1-P\right)\right) & \text{for } \kappa = 0 \end{cases} \tag{5.31}$$

In our study, the extreme rainfall used for the simulation were 2-, 5- and 10-y rainfalls the amounts of which were coincide with the exceedance probabilities of 0.50, 0.20, and 0.10, respectively.

5.2.3.2 Rainfall hyetograph design

Hyetographs were designed by an alternating block method. The concept of this method was putting the high intensity in the middle of the duration and putting the lower intensity farther from the middle of the duration. The data used for the hyetograph design were hyetographs of events which contained 24-h periods with >35.0 mm rainfalls.

In these hyetographs, rainfall durations and magnitudes were converted dimensionless. Then, the alternating block method was applied. For each dimensionless hyetograph, the highest intensity was put to the middle of the duration. The second highest intensity was put to the right of the highest intensity. For smaller k-th intensities where $k > 2$, they were put to the left and right of the $k-2$-th intensities when k's were odd and event, respectively. After that, the dimensionless hyetographs of all events which were results of the alternating block method were averaged. This average dimensionless hyetograph was the dimensionless hyetograph of the design rainfall.

The dimensionless hyetograph was converted to a dimensioned hyetograph by multiplying the dimensionless rainfall amount with desired rainfall amounts (2-, 5-, and 10-y rainfall amounts) and multiplying the dimensionless duration with desired durations (24-, 48-, and 72-h).

5.2.3.3 Rainfall spatial distribution randomization

Data used to design rainfall spatial distributions were the rainfall events which contains >35.0 mm rainfall day, 2 consecutive >35.0 mm rainfall days, and 3 consecutive >35.0 mm rainfall days for the simulated 24-, 48-, and 72-h rainfalls, respectively. For each event, the rainfall amount in each zone of the area was converted dimensionless by dividing with areal average rainfall amount as the equation 5.32,

$$X^*_{zone} = \frac{X_{zone}}{X} \tag{5.32}$$

where X^*_{zone} was a dimensionless zonal rainfall amount, X_{zone} was an actual zonal rainfall amount, and X was an actual areal rainfall amount. It should be noted that the areal average dimensionless rainfall amount among all zones was equal to 1.

The Monte Carlo analysis [Golian et al., 2010] and Cholesky randomization [Kreyszig, 1999] were used to generate random 1,000 dimensionless rainfalls for the simulation according to characteristics of the observed dimensionless rainfall (detail will be discussed later in this section). Finally, these generated dimensionless rainfalls were converted to the design rainfall by multiplying dimensionless zonal rainfalls with desired rainfall amounts (2-, 5-, and 10-y rainfall amounts).

Monte Carlo analysis

The Monte Carlo analysis included fitting the dimensionless zonal rainfall with a statistical distribution and randomization of dimensionless rainfalls for the simulation according to that statistical distribution [Golian et al., 2010]. For each zone, the dimensionless rainfalls were sorted descending and the Weibull equation was applied to assign the exceedance probability

of those dimensionless rainfall amounts as the equation 5.29. After that, the normal distribution was used to fit the dimensionless zonal rainfall data. The objective function was the RMSE of the dimensionless zonal rainfall. The expected value of the dimensionless zonal rainfall can be calculated as the equation 5.33,

$$X^*_{zone} = \begin{cases} \mu + \sigma\sqrt{2}\text{erf}^{-1}(1-2P) & \text{for } \mu + \sigma\sqrt{2}\text{erf}^{-1}(1-2P) \geq 0 \\ 0 & \text{for } \mu + \sigma\sqrt{2}\text{erf}^{-1}(1-2P) < 0 \end{cases} \tag{5.33}$$

where μ was a location parameter, σ was a scale parameter, P was an exceedance probability, and erf was an error function defined as the equation 5.34.

$$\text{erf}(x) = \int_{-x}^{x} e^{-t^2} dt \tag{5.34}$$

It should be noted that since the rainfall amount could not be negative, the dimensionless zonal rainfall should be set to 0 when the expected value from the distribution is negative.

The chi-square goodness of fit test [Sheskin, 1996] was used to test if the equation 5.33 could fit the dimensionless zonal rainfall data. The test value (χ^2) was calculated as the equation 5.35,

$$\chi^2 = \sum \frac{\left(O\left(X^*_{zone}\right) - E\left(X^*_{zone}\right)\right)^2}{E\left(X^*_{zone}\right)} \tag{5.35}$$

where $O\left(X^*_{zone}\right)$ and $E\left(X^*_{zone}\right)$ were an observed and expected values of X^*_{zone}, respectively.

The critical value of the chi-square test was determined from the chi-square distribution with $n_{events} - 3$ degree of freedom where n_{events} was a count of observed data.

After the data was fit and the goodness of fit was tested, a thousand of dimensionless zonal rainfall was randomly generated. A Cholesky randomization [Kreyszig, 1999] was applied to random normally distributed numbers under specified correlations (detail will be discussed later in this section). The number from the randomization could be converted to the zonal dimensionless rainfall by the equation 5.36,

$$X^*_{zone} = \begin{cases} \mu + n_{random}\sigma & \text{for } \mu + n_{random}\sigma \geq 0 \\ 0 & \text{for } \mu + n_{random}\sigma < 0 \end{cases} \tag{5.36}$$

where n_{random} was the random number, and μ and σ were those in the equation 5.33.

It should be noted that for each simulated events, the areal average amount of generated dimensionless rainfall among all zones might not be 1 because it depended on the random number for each zone. Therefore, the generated zonal dimensionless rainfalls should be reweighted to make the areal average amount of dimensionless rainfall become 1.

Cholesky randomization

The Cholesky randomization [Kreyszig, 1999] is the method to random normally distributed numbers under specified correlations. For a simulation of r rainfall events in c zones, given uncorrelated random vectors $v_1 = [\ v_{11}\ \ v_{21}\ \ \cdots\ \ v_{r1}\ ]$, $v_2 = [\ v_{12}\ \ v_{22}\ \ \cdots\ \ v_{r2}\ ]$, ..., $v_c = [\ v_{1c}\ \ v_{2c}\ \ \cdots\ \ v_{rc}\ ]$ where all elements of these vectors were randomly generated under the standard normal distribution, the matrix of uncorrelated random number ($V_{uncorrelated}$) was written as the equation 5.37.

$$V_{uncorrelated} = \begin{bmatrix} v_{11} & v_{12} & \cdots & v_{1c} \\ v_{21} & v_{22} & \cdots & v_{2c} \\ \vdots & \vdots & \ddots & \vdots \\ v_{r1} & v_{r2} & \cdots & v_{rc} \end{bmatrix} \tag{5.37}$$

Let $c_{i_1 i_2}$ denote a correlation coefficient between dimensionless rainfalls in the zones $i_1 \in \{1, 2, ..., c\}$ and $i_2 \in \{1, 2, ..., c\}$. The correlation matrix (C) was written as the equation 5.38.

$$C = \begin{bmatrix} 1 & c_{12} & \cdots & c_{1c} \\ c_{12} & 1 & \cdots & c_{2c} \\ \vdots & \vdots & \ddots & \vdots \\ c_{1c} & c_{2c} & \cdots & 1 \end{bmatrix} \tag{5.38}$$

It should be noted that our study assumed the fixed spatial correlation of dimensionless zonal rainfall for each of 24-, 48-, and 72-h rainfalls which was determined from the observed data.

Let Z be a triangular matrix which satisfied the equation 5.39. The matrix of correlated random numbers ($V_{correlated}$) could be calculated as the equation 5.40.

$$C = Z^T Z \tag{5.39}$$

$$V_{correlated} = V_{uncorrelated} Z = \begin{bmatrix} v^*_{11} & v^*_{12} & \cdots & v^*_{1c} \\ v^*_{21} & v^*_{22} & \cdots & v^*_{2c} \\ \vdots & \vdots & \ddots & \vdots \\ v^*_{r1} & v^*_{r2} & \cdots & v^*_{rc} \end{bmatrix} \tag{5.40}$$

For some matrix C, there was no matrix Z which satisfied the equation 5.39. In that case, some values of $c_{i_1 i_2}$ could be slightly adjusted [Higham, 2002].

The correlation coefficient between the elements of the vectors $[\ v^*_{1i_1} \quad v^*_{2i_1} \quad \cdots \quad v^*_{ri_1}\ ]$ and $[\ v^*_{1i_2} \quad v^*_{2i_2} \quad \cdots \quad v^*_{ri_2}\ ]$ was $c_{i_1 i_2}$. Therefore, for the event $r^* \in \{1, 2, ..., r\}$, n_{random} in the equation 5.36 at the zone $c^* \in \{1, 2, ..., c\}$ was $v^*_{r^* c^*}$. The proof of the Cholesky randomization and the method to find the matrix Z are shown in the appendices A.2 and B.2, respectively.

5.2.3.4 Modelling conditions

In this study, the initial infiltration storage was assumed to be full because Kotsuki and Tanaka [2013] suggested that the condition of flood years in the area is that rainfalls in the mid-rainy season cause the soil to be saturated. The removal of water stored in the soil and on the surface by an evapotranspiration was not included in the experimental simulation because the evapotranspiration has very low influence in a short term simulation. However, there was a removal of the water stored in the soil by a percolation, and consequently, there was a removal of the water stored on the surface by an infiltration.

5.2.4 Analysis of simulation results

After the simulation, the flood peak in the Sukhothai city was determined. For each rainfall duration and return period, average and standard deviation of flood peak were calculated.

The average indicated the expected flood peak while the standard deviation indicated the uncertainty of flood peak due to the uncertainty of rainfall spatial distribution.

After that, we investigated which rainfall spatial distribution caused the high flood peak. The investigation was done by a determination of a correlation between the flood peak in the Sukhothai city and the rainfall intensity in each zone. The zone where the correlation was strong is the zone where the concentration of rainfall caused the high flood peak.

Finally, we investigated which basin characteristics caused a strong response of the flood peak to the rainfall. For each characteristic, its influence on the response of the flood peak was assessed by a difference between the simulated flood peaks when the characteristic of the mountainous region were applied over the whole basin and when the characteristic of the plain area were applied over the whole basin. The comparison among influences of those basin characteristics revealed which basin characteristics caused the strong response of the flood peak to the rainfall.

5.3 Results and discussion

5.3.1 Developed model

5.3.1.1 Calibrated parameter

The calibrated parameters are shown in table 5.4. It can be seen that the mountainous region and plain area were characterized by different Manning's coefficient (n), percolation rate (f_c), basin coefficient (C_t), and surface storage capacity (max $S_{surface}$). Over the mountainous region, the value of n is high due to the vegetation in the forest which is the major land cover and the value of f_c is high due to a coarser soil texture than the plain area (see the section 3.2). Over the plain area, the value of C_t and max $S_{surface}$ is high due to a flatness of the area (see table 5.3).

Table 5.4: Calibrated parameters.

Parameter	Mountainous region	Plain area
n	0.047	0.019
max $S_{surface}$	0 mm	30 mm
C_t	2.9	5.8
C_p	0.16	0.18
$Q_{baseflow,0}/Q_p$	0.25	0.20
$k_{baseflow}$	0.87	0.89
max $S_{infiltration}$	285 mm	320 mm
f_c	2.95 mm/h	0.45 mm/h

5.3.1.2 Model accuracy

Observed and simulated water levels are shown in the figure 5.3 and table 5.5. The comparison was done only at the streamgauges Y37, Y14, Y6, Y3A, Y33, and Y4. For the streamgauge Y43, the data was not of a very good quality. For the streamgauges Y15, Y16, Y17, and Y5, the flows at these streamgauges were affected by the downstream boundary condition. Moreover, the flow at the streamgauge Y4 was not influenced by the flows at these downstream gauges. At the 6 streamgauges where the water levels were compared, the model appears to simulate the water level accurately. Without the year 2011, the year of

big flood, RMSEs are at most 1.0 m. The RMSE is higher over the plain area because there is a diversion of the flow to the nearby basin, Nan basin.

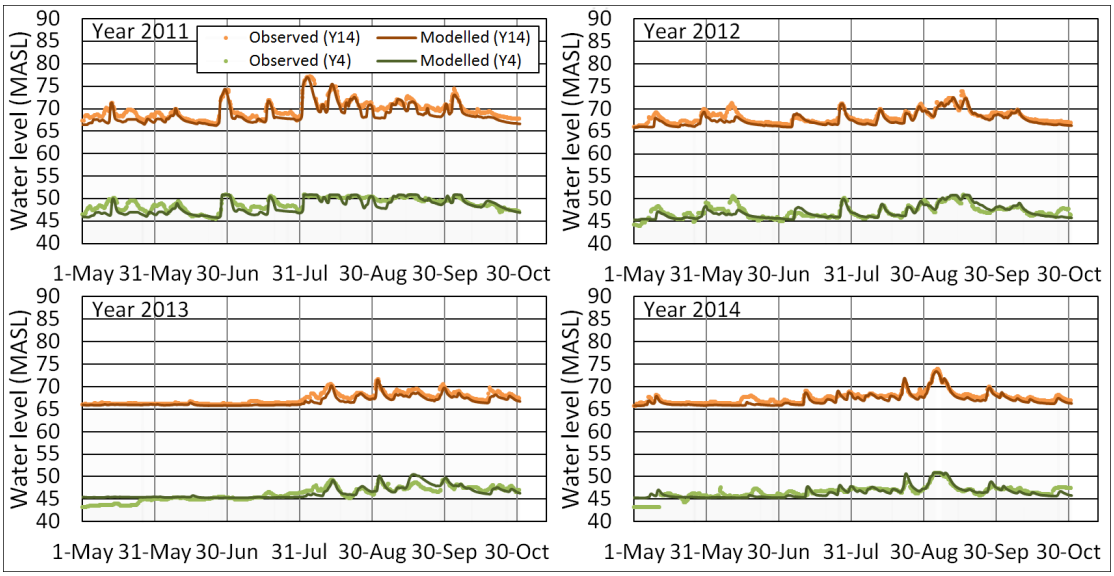

Figure 5.3: Observed and modeled water levels.

Table 5.5: RMSE values of the simulated water levels.

Streamgauge	Year 2011	Year 2012	Year 2013	Year 2014
Y37	0.83	0.55	0.33	0.30
Y14	1.04	0.79	0.66	0.59
Y6	0.99	0.82	0.70	0.78
Y3A	1.48	1.02	0.80	0.58
Y33	1.51	1.01	0.60	0.62
Y4	0.90	0.82	0.89	0.74

The RMSE is indicated in m.

5.3.1.3 Simplified model

Rainfalls in some sub-areas were averaged to make the model simpler. After the numerous ways of choosing the sub-areas to average the rainfall were tried, we have found that the rainfall can be averaged among the sub-areas Y1C and Y43, among the sub-areas Y37 and Y14, and among the sub-areas Y6, Y3A, and Y33. For the sub-area Y4, the rainfall cannot be averaged with rainfall in any of others sub-area. For the sub-areas Y15, Y16, Y17, Y5, and Y40, the rainfalls do not affect the flow at the Sukhothai city, and therefore, these sub-areas can be excluded. Hence, the number of rainfall hyetographs required in our model can be reduced from 13 to 4. The first hyetograph is applied to the sub-areas Y1 and Y43 which will be referred as "zone 1", the second hyetograph is applied the sub-areas Y37 and Y14 which will be referred as "zone 2", the third hyetograph is applied to the sub-areas Y6, Y3A, and Y33 which will be referred as "zone 3", and the fourth hyetograph is applied to the sub-area Y4 which will be referred as "zone 4". The locations of these 4 zones are shown in figure 5.4. The zones 1-2 are in the mountainous region while the zones 3-4 are in the plain area.

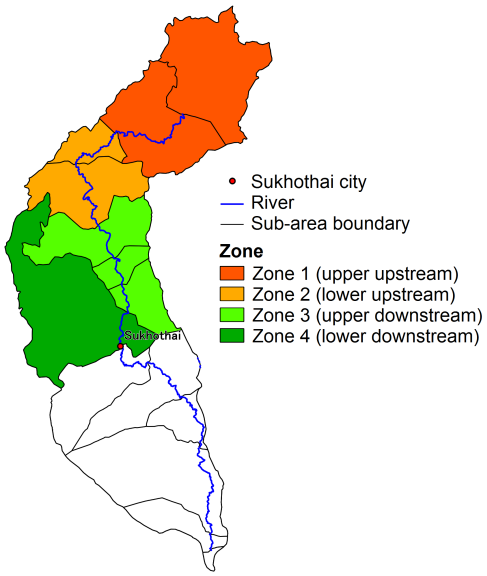

Figure 5.4: Zones where rainfalls can be averaged.

The water levels simulated before averaging the rainfall, which is called "control case", after averaging the rainfall within 4 zones, which is called "optimum case", and when the rainfall is averaged among all 13 sub-areas, which is called "lumped case", are shown in figure 5.5, and the maximum differences of water levels are shown in table 5.6. It can be seen that the water levels simulated from the control and optimum cases are similar. The maximum differences of water levels are mostly less than the model error (see RMSE in table 5.5). Conversely, the differences between water levels simulated from the control case and lumped case are different. The maximum differences of water levels are even more than the model error. Therefore, it is appropriate to use 4 rainfall hyetographs in the simulation but not appropriate to use only 1 rainfall hyetograph.

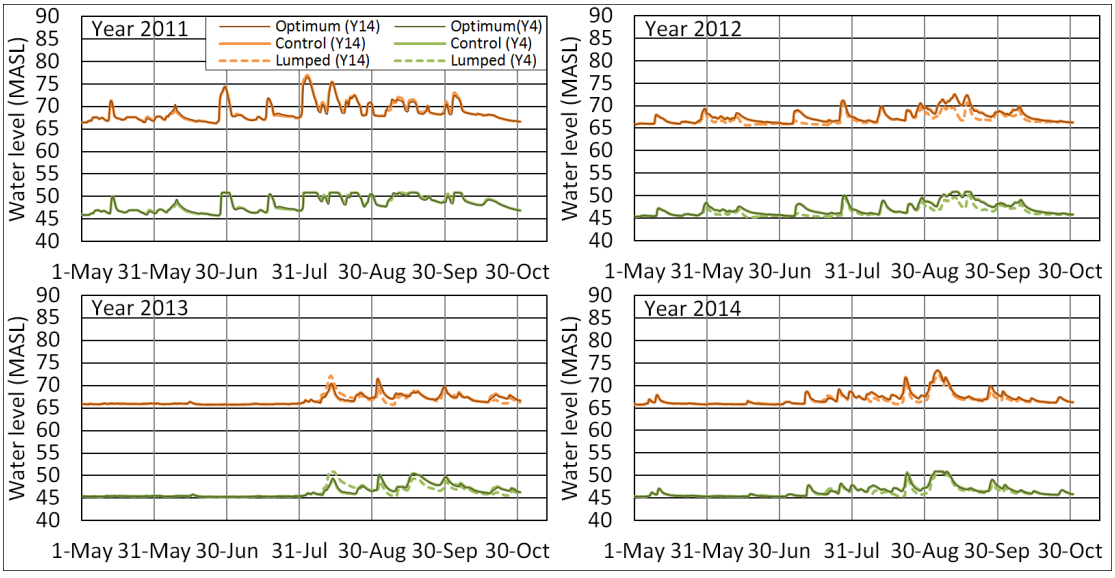

Figure 5.5: Simulated water levels from the control, optimum, and lumped cases.

Table 5.6: Maximum differences between simulated peak water levels from the control and optimum cases, and those between simulated peak water levels from the control and lumped cases.

Streamgauge	Year 2011	Year 2012	Year 2013	Year 2014
Y37	0.59 (-)	0.21 (2.88)	0.33 (1.75)	0.33 (1.16)
Y14	0.64 (-)	0.25 (2.59)	0.31 (1.97)	0.27 (1.14)
Y6	0.58 (-)	0.17 (2.34)	0.29 (2.10)	0.25 (1.22)
Y3A	0.64 (-)	0.27 (2.98)	0.35 (2.62)	0.30 (1.43)
Y33	0.70 (-)	0.28 (3.04)	0.33 (2.48)	0.28 (1.35)
Y4	0.54 (-)	0.22 (2.10)	0.27 (1.69)	0.23 (1.15)

Differences between the control and optimum cases are shown outside the parenthesis.
Differences between the control and lumped cases are shown inside the parenthesis.
The unit is m.

5.3.2 Design rainfall

5.3.2.1 Rainfall amount

The GEV distribution (equation 5.31) describes the extreme rainfall amount accurately with the RMSE of approximately 4.0 mm. The results of fitting are shown in Fig. 5.6 and table 5.7. The table 5.7 also shows amounts of expected 2-, 5-, and 10-y rainfalls.

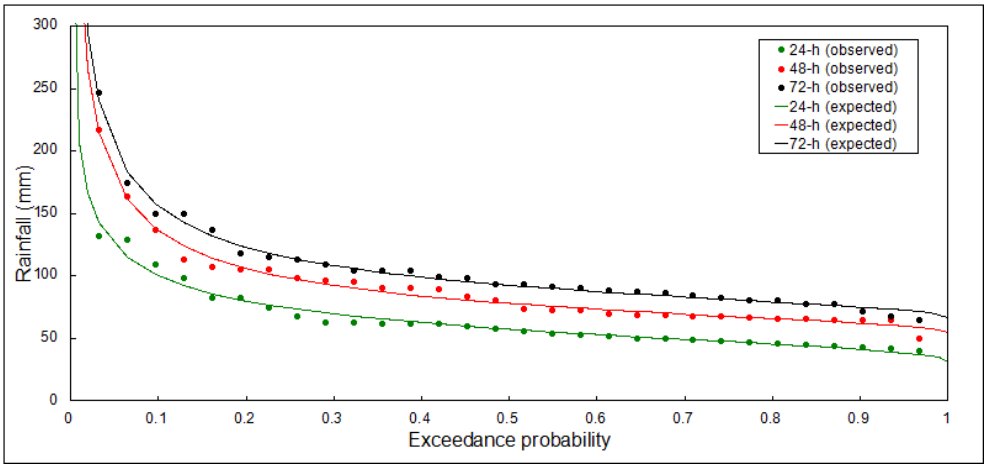

Figure 5.6: Observed and expected extreme rainfall magnitude.

Table 5.7: Parameters of the GEV probability distribution of 24-, 48-, and 72-h rainfall amount, RMSE between observed and expected values, and expected amounts of 2-, 5-, and 10-y rainfall.

Rainfall duration	ξ	α	κ	RMSE	rainfall amount		
					2-y	5-y	10-y
24-h	51.81070	14.38137	-0.33155	4.4	57.4	79.7	99.9
48-h	72.09355	14.66358	-0.53568	4.0	78.0	106.9	136.1
72-h	86.09529	16.19387	-0.52572	3.8	92.6	123.1	155.8

The unit is mm.

5.3.2.2 Rainfall hyetograph

The rainfall hyetograph designed by the alternating block method was compared with observed hyetographs. At each timestep, dimensionless cumulative magnitudes of the design

and observed rainfalls were calculated. The dimensionless cumulative magnitudes of the design rainfall and those of the observed rainfalls at 10th and 90th percentiles are shown in Fig. 5.7. Since the dimensionless cumulative magnitude of the design rainfall is between 10th and 90th percentiles of the dimensionless cumulative magnitudes of the observed rainfalls, the hyetograph of the design rainfall can represent the hyetographs of the observed rainfalls.

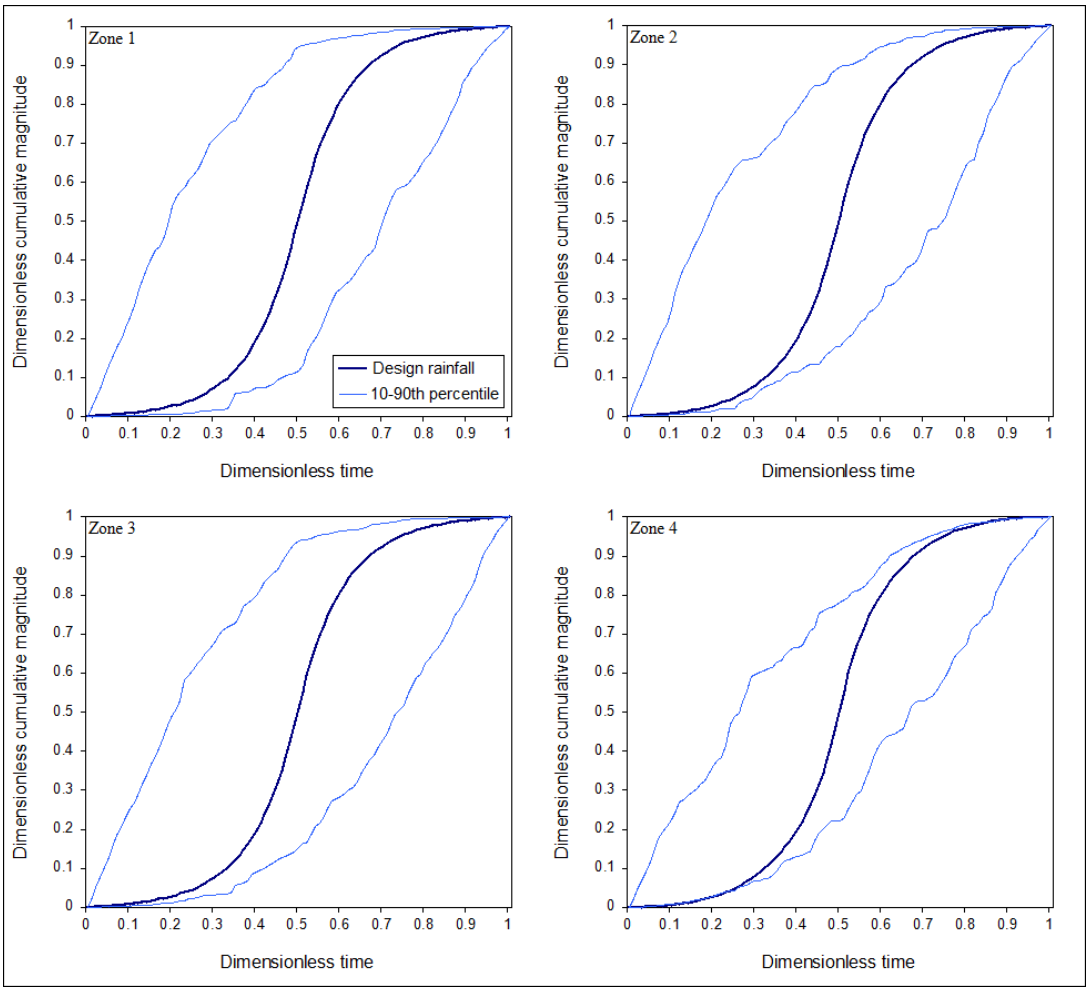

Figure 5.7: Dimensionless cumulative magnitudes of observed (10-90th percentile) and design rainfalls.

5.3.2.3 Rainfall spatial distribution

Results of fitting dimensionless zonal rainfall amounts by the equation 5.33 are shown Fig. 5.8 and table 5.8. The chi-square test suggests that the equation 5.33 can represent the observed dimensionless zonal rainfalls since all test values are lower than critical values.

Averages and standard deviations of 1,000 synthetic dimensionless zonal rainfalls are shown in table 5.9, and spatial correlations are shown in table 5.10. All of averages, stand deviations, and spatial correlations of synthetic events show good agreements with those of the observed events. When only long duration rainfalls are considered, average rainfall amounts in the zones 1-3 are higher and an average rainfall amount in the zone 4 is lower than when all rainfalls are considered. Hence, the location where the long duration rainfalls tend to concentrate over is more upstream than the location where the short duration rainfalls tend to concentrate over. However, the information in the table 5.9 cannot be used to

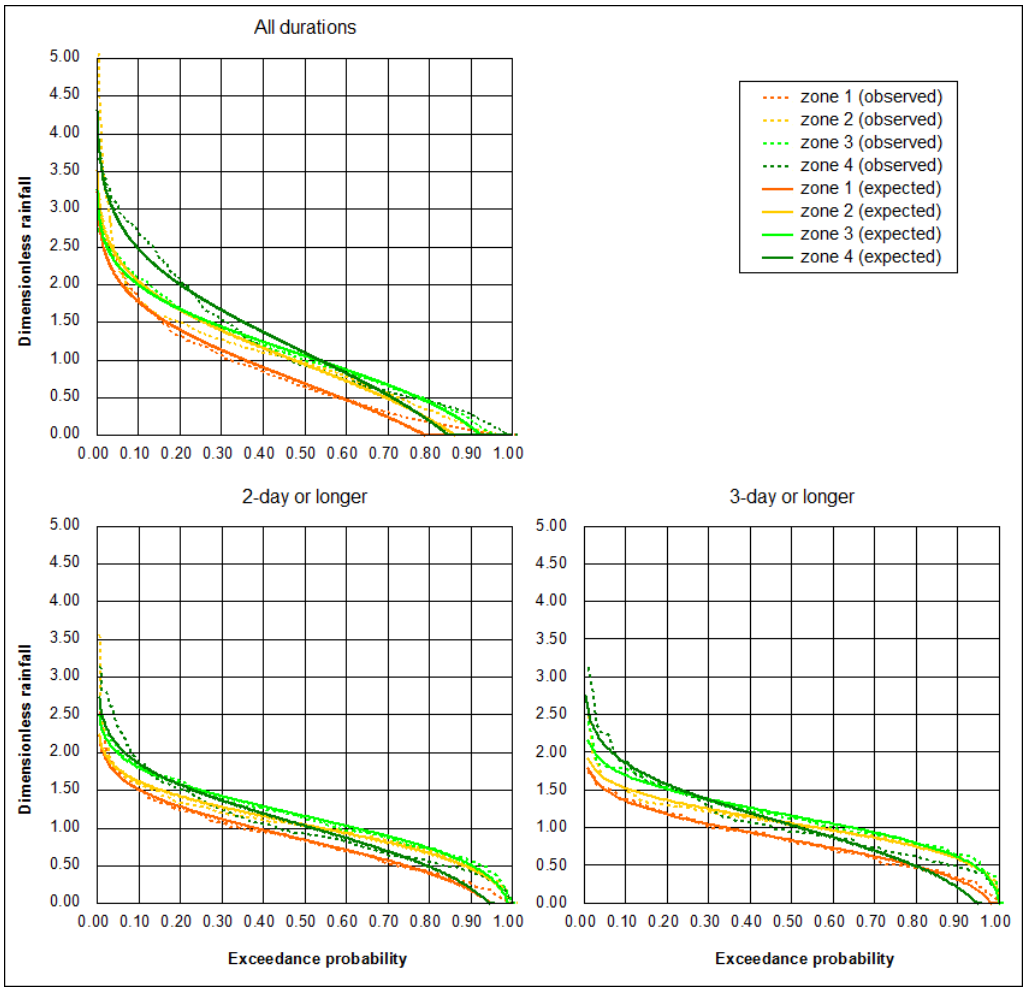

Figure 5.8: Dimensionless zonal rainfall.

Table 5.8: Parameters of the normal probability distribution of dimensionless zonal rainfall, RMSE between observed and expected values, and result of chi-square goodness of fit test.

Rainfall duration	zone	μ	σ	RMSE	χ^2	critical value[a]
All durations	1	0.68299	0.84794	0.0869	36.02	628.75
	2	0.93682	0.86307	0.2235	42.88	683.22
	3	1.05122	0.73598	0.0642	18.93	731.33
	4	1.09418	1.07667	0.1774	216.53	671.71
2 days or longer	1	0.84184	0.52160	0.0630	5.20	269.61
	2	1.04170	0.44978	0.1054	2.29	281.44
	3	1.15603	0.50492	0.0514	1.94	281.44
	4	1.02929	0.64447	0.1473	33.04	269.61
3 days or longer	1	0.82995	0.40852	0.0341	0.33	123.23
	2	1.05375	0.36577	0.0791	0.44	125.46
	3	1.15477	0.42262	0.0550	0.48	125.46
	4	1.06650	0.58129	0.1486	6.70	122.11

[a] The significance level is 0.05.

compare the rainfall amounts among the zones 1-4 because the sizes of these zones are not equal. Nevertheless, since the results of the study 1 suggest that the upstream part of the area has low rainfall amount and the joint between the mountainous region and plain

area has high the probability of consecutive heavy rainfall days (see chapter 4), it can be concluded that the rainfall tends to concentrate over the zones 2-4 rather than the zone 1, and in comparison between short and long duration rainfalls, the long duration rainfall has more likelihood to concentrate over the zones 2-3, the joint area.

Table 5.9: Averages and standard deviations of dimensionless zonal rainfalls.

Rainfall duration	Zone	Average	Standard deviation
All durations	1	0.7948 (0.7976)	0.6672 (0.6837)
(728 observed events)	2	1.0228 (1.0058)	0.7461 (0.7789)
	3	1.1237 (1.0773)	0.7238 (0.6850)
	4	1.1704 (1.2101)	0.8813 (0.9095)
2 days or longer	1	0.8629 (0.8562)	0.4843 (0.4891)
(249 observed events)	2	1.0479 (1.0425)	0.4281 (0.4525)
	3	1.1655 (1.1575)	0.5140 (0.4955)
	4	1.0347 (1.0526)	0.5982 (0.6079)
3 days or longer	1	0.8413 (0.8330)	0.3898 (0.3896)
(104 observed events)	2	1.0548 (1.0538)	0.3479 (0.3623)
	3	1.1591 (1.1548)	0.4273 (0.4122)
	4	1.0637 (1.0785)	0.5522 (0.5576)

The values for the randomized rainfalls are shown outside the parenthesis.
The values for the observed rainfalls are shown inside the parenthesis.

Table 5.10: Spatial correlations among dimensionless zonal rainfalls.

Rainfall duration	Zone	1	2	3	4
All durations	1	1.00 (1.00)	-0.23 (-0.19)	-0.47 (-0.47)	-0.61 (-0.64)
	2	-0.23 (-0.19)	1.00 (1.00)	0.27 (0.27)	-0.45 (-0.47)
	3	-0.47 (-0.47)	0.27 (0.27)	1.00 (1.00)	-0.25 (-0.20)
	4	-0.61 (-0.64)	-0.45 (-0.47)	-0.25 (-0.20)	1.00 (1.00)
2 days or longer	1	1.00 (1.00)	-0.26 (-0.26)	-0.53 (-0.53)	-0.64 (-0.64)
	2	-0.26 (-0.26)	1.00 (1.00)	0.41 (0.41)	-0.42 (-0.42)
	3	-0.53 (-0.53)	0.41 (0.41)	1.00 (1.00)	-0.22 (-0.20)
	4	-0.64 (-0.64)	-0.42 (-0.42)	-0.22 (-0.20)	1.00 (1.00)
3 days or longer	1	1.00 (1.00)	-0.21 (-0.22)	-0.39 (-0.37)	-0.64 (-0.65)
	2	-0.21 (-0.22)	1.00 (1.00)	0.52 (0.54)	-0.48 (-0.48)
	3	-0.39 (-0.37)	0.52 (0.54)	1.00 (1.00)	-0.39 (-0.40)
	4	-0.64 (-0.65)	-0.48 (-0.48)	-0.39 (-0.40)	1.00 (1.00)

The values for the randomized rainfalls are shown outside the parenthesis.
The values for the observed rainfalls are shown inside the parenthesis.

5.3.3 Flood peak from uniform rainfall

A peak discharge at the Sukhothai city when the rainfall is uniform is shown in table 5.11. For 2- and 5-y rainfalls, the highest flood peak occurs when the rainfall duration is 48-h. For 10-y rainfall, the highest flood peak occurs when the rainfall duration is 72-h.

Table 5.12 shows the excess rainfall in each of zones 1-4. Flood water comes from the downstream part (zones 3-4) for 2- and 5-y rainfalls but comes from all parts (zones 1-4) for 10-y rainfall. Even though the rainfall is uniform, the excess rainfall over the upstream part (zones 1-2) is low in comparison to the downstream part because of the high percolation rate over the upstream part (see f_c in table 5.4). However, for a large rainfall, 10-y rainfall, an

Table 5.11: Peak discharge from uniform rainfall.

Rainfall duration	2-y rainfall	5-y rainfall	10-y rainfall
24-h	415.6 cms	792.8 cms	1,186.7 cms
48-h	455.1 cms	910.6 cms	1,457.5 cms
72-h	433.5 cms	895.9 cms	1,461.9 cms

influence of percolation is low, and therefore, the excess rainfall over the upstream part is not much lower than that over the downstream part.

Table 5.12: Peak excess rainfall intensity in each zone from uniform rainfall.

Duration	Return period	Peak rainfall intensity (mm/h)	Peak excess rainfall intensity (mm/h)				
			Zone 1	Zone 2	Zone 3	Zone 4	Average
24-h	2-y	6.6	3.7	3.6	4.4	4.3	4.0
	5-y	9.2	6.3	6.2	8.8	8.6	7.4
	10-y	11.5	8.7	8.5	11.1	10.9	9.7
48-h	2-y	5.7	2.5	2.5	5.1	5.1	3.7
	5-y	7.8	4.5	4.5	7.1	7.1	5.7
	10-y	10.0	6.9	7.0	9.6	9.6	8.2
72-h	2-y	5.0	1.8	1.8	4.4	4.5	3.0
	5-y	6.6	3.5	3.5	6.1	6.1	4.8
	10-y	8.3	5.2	5.3	7.9	8.2	6.5

Fig. 5.9 shows hydrographs from 10 mm 3-h areal excess rainfall when it is uniform and when it concentrates in each zone. A concentration time is 72-h when the excess rainfall is uniform but is 48-h when the excess rainfall concentrates in the downstream part. With this reason, the highest peak discharges from 2- and 5-y rainfalls are associated with 48-h rainfall duration while that from 10-y rainfall is associated with 72-h rainfall duration.

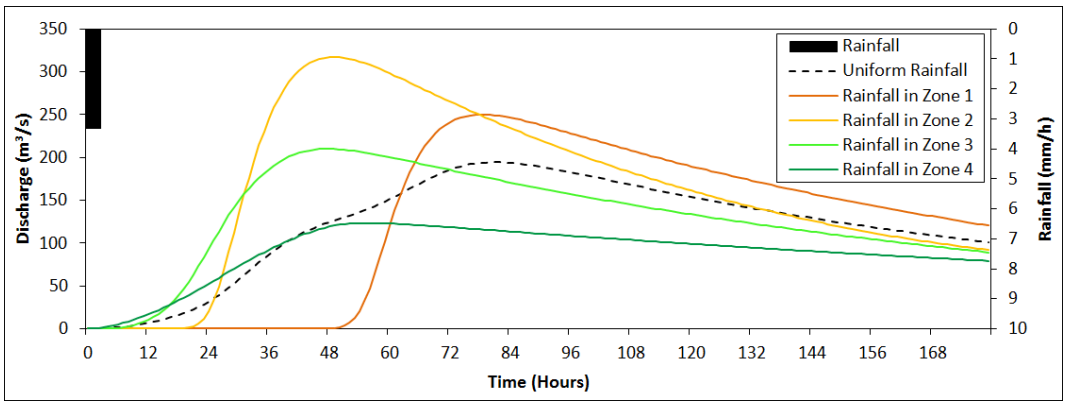

Figure 5.9: Hydrographs from 10 mm 3-h areal excess rainfall when it is uniform and when it concentrates in each zone.

5.3.4 Flood peak from non-uniform rainfall

The simulation of non-uniform rainfall is more complicate than the simulation of uniform rainfall since the rainfall spatial distributions vary upon events. Fig. 5.10 and table 5.13 show information on 1,000 simulated peak discharges at the Sukhothai city from 1,000 non-uniform

rainfalls. The peak discharges from non-uniform rainfalls are variable and the simulation of uniform rainfall can cover only approximately 10-35% of all possible peak discharges. The peak discharges from 24-h rainfall are usually low but highly variable while the peak discharges from 48- and 72-h rainfalls are usually high but not very variable. The high peak discharge usually comes from the long duration rainfall, but in some rare case, the short duration rainfall can produce an extremely high peak discharge.

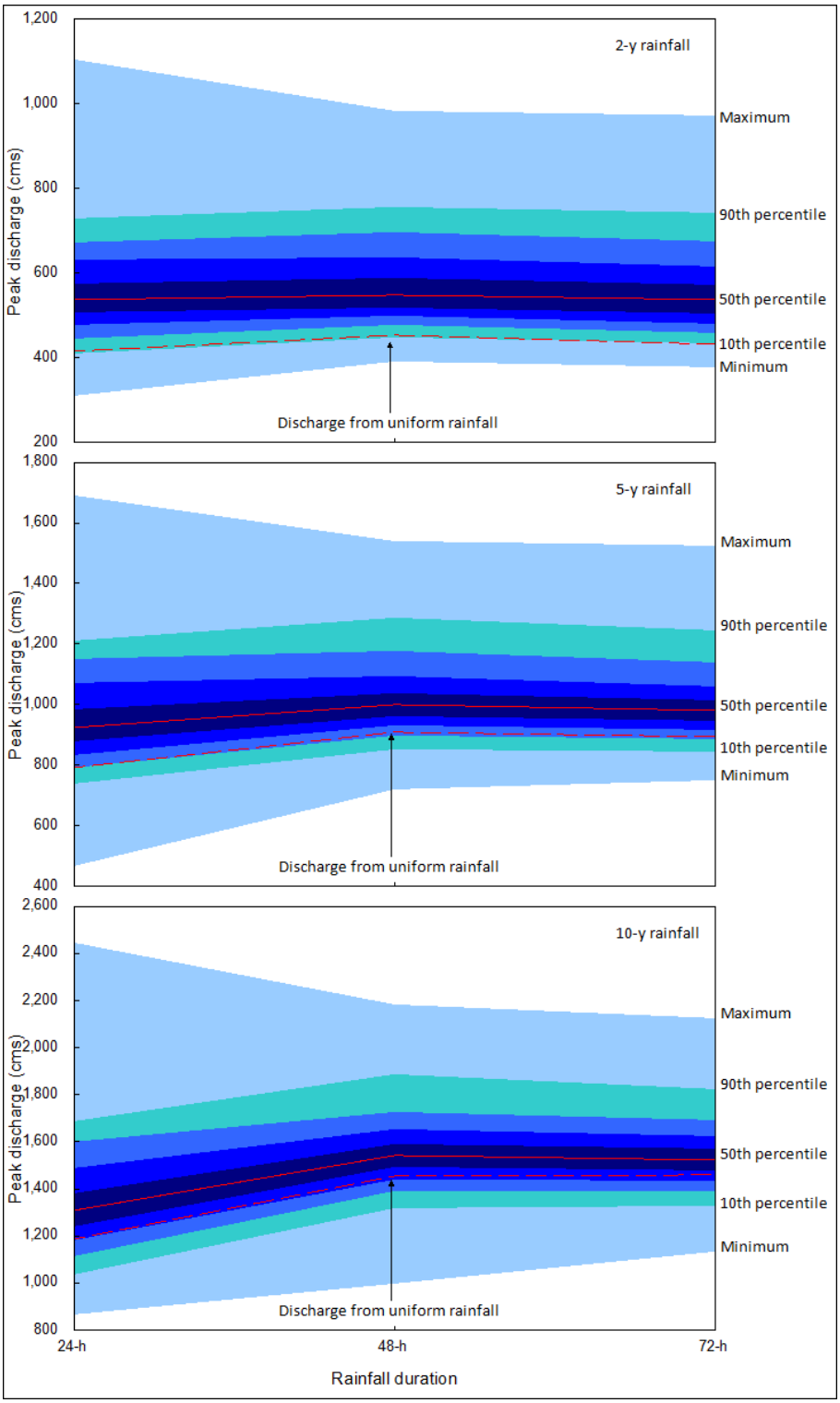

Figure 5.10: Peak discharges from simulated non-uniform rainfalls.

Table 5.13: Average and standard deviation of peak discharge from simulated non-uniform rainfalls.

Duration	Return period	Average (cms)	Standard deviation[a] (cms)
24-h	2-y	564.5	134.0 (23.8%)
	5-y	964.7	195.5 (20.3%)
	10-y	1,348.2	253.7 (18.8%)
48-h	2-y	581.7	119.4 (20.5%)
	5-y	1,034.6	160.0 (15.5%)
	10-y	1,568.6	211.9 (13.5%)
72-h	2-y	565.5	119.6 (21.1%)
	5-y	1,014.4	152.9 (15.1%)
	10-y	1,551.1	194.7 (12.5%)

a Coefficient of variation is shown inside the parenthesis.

The non-uniform rainfall usually gives higher peak discharge than the uniform rainfall does because most rainfalls concentrate over the zones 2-4 which have similar concentration time, approximately 48-h (see Fig. 5.9). It can also be seen in the table 5.13 that in average, the highest peak discharges from all of 2-, 5- and 10-y rainfalls occur when the rainfall duration is 48-h. This result is different from when the rainfall is uniform because in that case, the highest peak discharge from 10-y rainfall occurs when the rainfall duration is 72-h (see table 5.11).

5.3.5 Mechanism of flood peak variation

Since the non-uniform rainfalls give the variable peak discharges, we have identified which characteristic of the spatial distribution has most influence on peak discharge by finding a correlation between the peak discharge and rainfall intensity in each zone. The result is shown in table 5.14. For the short duration rainfall, 24-h rainfall, the peak discharge is correlated with the rainfall over the zones 1-2, the upstream area. For the long duration rainfalls, 48- and 72-h rainfalls, the peak discharges are correlated with the rainfall over the zones 2-3, the joint area.

Table 5.14: Correlation coefficient between peak discharge and rainfall intensity in each zone.

Duration	Return period	Correlation coefficient between peak discharge and rainfall			
		Zone 1	Zone 2	Zone 3	Zone 4
24-h	2-y	0.23	0.49	0.21	-0.61
	5-y	0.33	0.53	0.20	-0.73
	10-y	0.39	0.55	0.19	-0.79
48-h	2-y	-0.10	0.44	0.43	-0.35
	5-y	0.11	0.50	0.38	-0.57
	10-y	0.29	0.52	0.31	-0.73
72-h	2-y	-0.37	0.47	0.60	-0.16
	5-y	-0.07	0.56	0.58	-0.47
	10-y	0.18	0.59	0.53	-0.69

The 24-h rainfall rarely gives the high peak discharge because 24-h is shorter than the concentration time, and moreover, the rainfall amount in the upstream area is usually low. However, due to the short rainfall duration, the variability of peak discharge is high [Ogden and Julien, 1993]. The 24-h rainfall can cause an extremely high peak discharge if it

concentrates over the upstream area. The 48- and 72-h rainfalls usually give the high peak discharges because the concentration times of the area are approximately 48-72 hours depending on rainfall location, and moreover, the long duration rainfall usually concentrates over the joint area.

5.3.5.1 Short duration rainfall

The peak discharge from short duration rainfall is correlated with rainfall over the zones 1-2. The different characteristics between the zones 1-2 and the zones 3-4 are different Manning's coefficient (n) which represents channel roughness, percolation rate (f_c) which represents soil characteristics, surface storage (max $S_{surface}$), and basin coefficient (C_t) which represents steepness (see table 5.4). In order to investigate the main characteristic which causes the peak discharge to strongly responds to the rainfall over the zones 1-2, simulations with the values of C_t, max $S_{surface}$, n, and f_c adjusted to be uniform were carried out and the simulated peak discharge were compared. The results depend on rainfall magnitude and location. The tables 5.15 and 5.16 show peak discharges from sample 2-y 24-h and 10-y 24-h rainfalls, respectively, which concentrate over the mountainous region and plain area when the values of C_t, max $S_{surface}$, n, and f_c are adjusted to be uniform.

Table 5.15: Peak discharges from sample 2-y 24-h rainfalls which concentrate over different locations when the values of C_t, max $S_{surface}$, n, and f_c are adjusted to be uniform.

Adjustment detail	Concentrate over mountain		Concentrate over plain	
	Peak discharge	Difference[a]	Peak discharge	Difference[a]
C_t= 2.9 (as the zones 1-2)	573.6	243.2	818.0	366.1
C_t= 5.8 (as the zones 3-4)	330.4		451.9	
max $S_{surface}$= 0 mm (as the zones 1-2)	692.0	563.0	761.3	381.5
max $S_{surface}$= 30 mm (as the zones 3-4)	129.0		379.8	
n = 0.047 (as the zones 1-2)	510.2	83.2	502.5	35.0
n = 0.019 (as the zones 3-4)	593.4		537.5	
f_c= 2.95 (as the zones 1-2)	453.2	520.9	291.8	422.5
f_c= 0.45 (as the zones 3-4)	974.2		714.3	
No adjustment	541.7	-	539.3	-

a It refers to difference of peak discharges between when parameter values for the zones 1-2 and zones 3-4 are used.
The unit is cms.

It appears that the peak discharges from small rainfall responds to the values of max $S_{surface}$ and f_c rather than the value of C_t, while that from large rainfall responds to the value of C_t rather than the values of max $S_{surface}$ and f_c. However, depending on the rainfall location, the differences among the responses to these 3 values may not be very obvious. Nevertheless, the peak discharge seems not to respond to the value of n. In other words, the peak discharge from the small rainfall responds to the surface storage and soil percolation rate of the rainfall location while the peak discharge from the large rainfall responds to the steepness of the rainfall location, but both the peak discharges from small and large rainfalls do not respond to the channel roughness. The reasons why peak discharge responds to the rainfall in zones 1-2 rather than that the zones 3-4 are different for small and large rainfalls. For small rainfalls, it is because the zones 1-2 have low surface storage. For the large rainfall, it is because the zones 1-2 have high steepness.

Table 5.16: Peak discharges from sample 10-y 24-h rainfalls which concentrate over different locations when the values of C_t, max $S_{surface}$, n, and f_c are adjusted to be uniform.

Adjustment detail	Concentrate over mountain		Concentrate over plain	
	Peak discharge	Difference[a]	Peak discharge	Difference[a]
C_t= 2.9 (as the zones 1-2)	1,534.2	672.9	1,971.0	896.5
C_t= 5.8 (as the zones 3-4)	861.3		1,074.5	
max $S_{surface}$= 0 mm (as the zones 1-2)	1,617.9	640.6	1,499.5	377.6
max $S_{surface}$= 30 mm (as the zones 3-4)	977.3		1,121.9	
n = 0.047 (as the zones 1-2)	1,317.2	207.2	1,197.5	70.7
n = 0.019 (as the zones 3-4)	1,524.4		1,268.2	
f_c= 2.95 (as the zones 1-2)	1,281.5	652.0	993.5	518.0
f_c= 0.45 (as the zones 3-4)	1,933.5		1,511.5	
No adjustment	1,415.9	-	1,278.8	-

a It refers to difference of peak discharges between when parameter values for the zones 1-2 and zones 3-4 are used.
The unit is cms.

5.3.5.2 Long duration rainfall

In comparison to the short duration rainfall, the peak discharge from the long duration rainfall does not respond to the rainfall in the zone 1. Simulations of long duration rainfalls with the values of C_t, max $S_{surface}$, n, and f_c adjusted to be uniform were carried out to investigate the mechanism. The results are shown in tables 5.17 and 5.18, for 2-y 48-h and 10-y 48-h rainfalls, respectively.

Table 5.17: Peak discharges from sample 2-y 48-h rainfalls which concentrate over different locations when the values of C_t, max $S_{surface}$, n, and f_c are adjusted to be uniform.

Adjustment detail	Concentrate over mountain		Concentrate over plain	
	Peak discharge	Difference[a]	Peak discharge	Difference[a]
C_t= 2.9 (as the zones 1-2)	575.0	236.9	885.6	398.2
C_t= 5.8 (as the zones 3-4)	338.1		478.4	
max $S_{surface}$= 0 mm (as the zones 1-2)	721.3	551.7	779.4	371.3
max $S_{surface}$= 30 mm (as the zones 3-4)	169.6		408.1	
n = 0.047 (as the zones 1-2)	490.1	80.4	524.8	35.4
n = 0.019 (as the zones 3-4)	570.5		560.2	
f_c= 2.95 (as the zones 1-2)	365.4	792.5	210.1	762.7
f_c= 0.45 (as the zones 3-4)	1,157.9		972.9	
No adjustment	517.9	-	560.2	-

a It refers to difference of peak discharges between when parameter values for the zones 1-2 and zones 3-4 are used.
The unit is cms.

It appears that the peak discharges mainly respond to the value of f_c for both small and large rainfalls. The responses to the value of C_t and max $S_{surface}$ are less obvious than those to the value of f_c. However, similarly the peak discharges from the short duration rainfall, the peak discharge from the small rainfall responds to the value of max $S_{surface}$ more obviously than the value of C_t while the peak discharge from large rainfall responds to the value of C_t more obviously than the value of max $S_{surface}$. The peak discharge mainly responds to the soil percolation rate of the rainfall location because of the fact that the longer rainfall has lower intensity which causes the stronger influence of the percolation. Apart from the soil percolation rate, the peak discharge responds to the surface storage when the rainfall is

Table 5.18: Peak discharges from sample 10-y 48-h rainfalls which concentrate over different locations when the values of C_t, max $S_{surface}$, n, and f_c are adjusted to be uniform.

Adjustment detail	Concentrate over mountain		Concentrate over plain	
	Peak discharge	Difference[a]	Peak discharge	Difference[a]
C_t= 2.9 (as the zones 1-2)	1,870.9	814.3	2,201.2	992.9
C_t= 5.8 (as the zones 3-4)	1,056.6		1,208.4	
max $S_{surface}$= 0 mm (as the zones 1-2)	1,818.6	652.0	1,664.6	425.7
max $S_{surface}$= 30 mm (as the zones 3-4)	1,166.6		1,238.8	
n = 0.047 (as the zones 1-2)	1,502.6	204.3	1,388.5	135.0
n = 0.019 (as the zones 3-4)	1,706.9		1,523.5	
f_c= 2.95 (as the zones 1-2)	1,274.7	1,182.5	982.6	1,137.0
f_c= 0.45 (as the zones 3-4)	2,457.2		2,119.6	
No adjustment	1,608.8	-	1,451.3	-

a It refers to difference of peak discharges between when parameter values for the zones 1-2 and zones 3-4 are used.
The unit is cms.

small and responds to the steepness when the rainfall is large similarly to the peak discharge from the short duration rainfall.

In the zone 1, due to the high soil percolation rate in conjunction with low probability of heavy rainfall, most rainwater is likely to become percolation loss. With this reason, the correlation between the peak discharge and rainfall in the zone 1 is weak. In the zone 2, even though the soil percolation rate is high, there is some probability of heavy rainfalls which are not much influenced by the percolation. With this reason, the correlation between the peak discharge and rainfall in the zone 2 is still strong. The table 5.19 shows the average excess rainfall intensity in each of the zones 1-4. It can be seen that the excess rainfall intensity in the zone 1 is low and the correlation coefficient between the peak discharge and rainfall in this zone (see table 5.14) varies upon the excess rainfall intensity while the excess rainfall intensity in the zone 2 is higher than that in the zone 1 and the correlation coefficient between the peak discharge and rainfall in this zone is always high regardless of the excess rainfall intensity.

Table 5.19: Average peak excess rainfall intensity in each zone from simulated non-uniform rainfalls.

Duration	Return period	Average peak excess rainfall intensity (mm/h)				
		Zone 1	Zone 2	Zone 3	Zone 4	Average
24-h	2-y	3.2	4.3	6.0	6.5	4.8
	5-y	5.2	6.9	9.3	9.7	7.5
	10-y	7.0	9.2	12.2	12.5	9.9
48-h	2-y	2.2	3.0	5.5	4.6	3.6
	5-y	3.8	5.0	8.1	7.0	5.7
	10-y	5.7	7.4	10.8	9.5	8.0
72-h	2-y	1.4	2.2	4.8	4.3	3.0
	5-y	2.6	3.9	6.9	6.4	4.7
	10-y	4.0	5.7	9.0	8.4	6.5

Between the zones 3 and 4, the main different characteristic is the distance to the river. Sub-areas in the zone 3 have short centroid distances while the zone 4 has a very long centroid distance (see centroid distance of sub-areas Y6, Y3A, Y33, and Y4 in table 5.3). In the zone 3, the short centroid distances cause the rainwater to be drained to the stream

more quickly, and therefore, the excess rainfall in the zone 3 causes the higher peak discharge than the excess rainfall in the zone 4 does (see Fig. 5.9). In the zone 4, due to the long centroid distance, the rainwater was drained very slowly, and therefore the peak discharge from the excess rainfall in the zone 4 is low. With this reason, the correlation between the peak discharge and rainfall in the zone 4 is always weak.

5.4 Conclusions

Floods in the Sukhothai city from uniform and non-uniform rainfalls over the middle and lower Yom basin were simulated. The rainfalls were spatially distributed into 4 zones. The most upstream area was referred as "zone 1" and the most downstream area was referred as "zone 4". The zone 1 was a mountainous region with high steepness and high soil percolation rate. The zone 2 was similar to the zone 1 but the stream length to the Sukhothai city was shorter. The zone 3 was a plain area with low steepness and low soil percolation rate. It also has a large surface storage. The zone 4 was similar to the zone 3 but the centroid distance was longer. The rainfall tends to concentrate over the zones 2-4 rather than the zone 1, and in comparison among 24-, 48-, and 72-h rainfalls, the 48- and 72-h rainfalls have more likelihood to concentrate over the zones 2-3.

When the rainfall is uniform, the highest flood peak is coincided with 48-h rainfall duration for 2- and 5-y rainfalls but is coincided with 72-h rainfall duration for 10-y rainfall. The reason is that the concentration time is 72-h in average over the area but is 48-h for the downstream part. For 2- and 5-y rainfalls, even though the rainfall is uniform, the influence of percolation over the upstream area causes the loss of rainwater, and therefore, the flood water comes from the downstream part. However, for 10-y rainfall, because of the high intensity, the influence of percolation is less, and therefore the flood water comes from upstream and downstream parts more uniformly.

However, in comparison to flood peaks from the non-uniform rainfall, the flood peak from the uniform rainfall can cover only approximately 10-35% of possible floods. Flood peaks from the non-uniform rainfalls are usually high and the highest flood peak usually comes from 48-h rainfall duration for all of 2-, 5-, and 10-y rainfalls because the rainfalls tend to concentrate over the zones 2-4 rather than the zone 1. The zones 2-4 have the similar concentration time, 48-h.

The flood peak from 24-h rainfall tends to be high when the rainfall concentrates over the zone 1-2 (upstream area) while those from 48- and 72-h rainfalls tend to be high when the rainfalls concentrate over the zones 2-3 (joint area). The flood peak from 24-h rainfall is usually low because the duration is shorter than the concentration time and the rainfall tends not to concentrate over the upstream area. However, if the rainfall concentrates over the upstream area the 24-h rainfall can give a very high flood peak. The flood peaks from 48- and 72-h rainfalls are usually high because the durations are close to the concentration time and 48- and 72-h rainfalls tend to concentrate over the joint area. The flood peaks from these rainfalls are not very variable because the spatial distributions of 48- and 72-h rainfalls are not very variable.

For the short duration rainfall, the flood peak responds to the rainfall in the zones 1-2 because these zones have low surface storage and high soil percolation rate. The surface storage is dominant for a small rainfall while the soil percolation rate is dominant for a large rainfall. For the long duration rainfall, the flood peak responds to the rainfall in the zones 2-3 because of the lower intensity than the short duration rainfall. The low rainfall intensity causes an influence of the soil percolation rate to be strong. Even though both the zones

1-2 have low surface storage and high steepness, the low intensity of the rainfall over the zone 1 causes the influence of the soil percolation to be dominant, and therefore, most of the rainwater in the zone 1 becomes percolation loss. With this reason, the response of the flood peak to the rainfall in this zone is weak. For the zone 2, since the rainfall intensity over this zone is usually higher than that over the zone 1, the influence of the percolation is less, and therefore, the response of the flood peak to the rainfall in this zone is still strong. For the zones 3-4, because the zone 3 has a short distance to the main stream while the zone 4 has a long distance to the main stream, the response of the flood peak to the rainfall in the zone 3 is much stronger than the response of the flood peak to the rainfall in the zone 4.

Chapter 6

Conclusions

Even though it has been suggested that the flood peak is affected by rainfall temporal distribution and spatial hydraulic conductivity rather than the rainfall spatial distribution, some studies have found that the rainfall spatial distribution can affect the flood peak when the duration is less than the time to equilibrium and the basin is non-uniform. Recently, many studies applied the Monte Carlo analysis to simulate floods from various spatial rainfalls and have found that the simulated flood peaks can be varied by rainfall spatial distribution. Some physical mechanism regarding the basin characteristics were also discussed. Nevertheless, there is still lack of information on prioritization of each characteristic. This study simulated the peak discharge from various spatial rainfalls, determined the flood peaks, and identified the mechanism behind the response of flood peaks to rainfall spatial distribution.

The middle and lower Yom basin, Thailand, was selected for this study because it was a basin with long distance from the upstream area to the downstream area, has different characteristics between the upstream and downstream areas, and the influence of control structures on a flow is very small. The downstream area is a plain area, consisted of fine-textured soil, and covered by agricultural area while the upstream part is a mountainous region, consisted of coarser-textured soil, and covered by forest area. According to the exist reports, most floods are coincide with consecutive rainfall days and usually occur during the end of the southwest monsoon period where there was a high rainfall amount in conjunction with a nearly saturated soil due to previous rainfalls. Nevertheless, there was still no relevant study on spatial characteristics of consecutive rainfall days.

In the first part of the study, we identified the spatial characteristics of consecutive rainfall days over the northern Thailand in where the Yom basin is located, according to the Markov chain model and chi-square test of independence, 0.0-10.0 mm rainfall days are not consecutive while >10.0 mm rainfall days are consecutive all over the northern Thailand and >35.0 mm rainfall days are obviously consecutive over the joint between the mountainous region and plain area. According to the student-t test, the mountainous region has lower rainfall amount on >10.0 mm rainfall days than the plain area. Therefore, we successfully established the spatial characteristics of rainfalls over the mountainous region, plain area, and joint area.

In the second part of the study, we developed the conceptual model from the HEC-HMS and HEC-RAS models to simulate floods in the Sukhothai city from spatial rainfall over the middle and lower Yom basin. In the model, there were 4 zones to distribute the rainfall. The upper upstream zone, zone 1, was the steep mountainous region with high soil percolation rate. The lower upstream zone, zone 2, was similar to the zone 1. The upper downstream area, zone 3, was the plain area with low soil percolation rate and short

distance to the stream. The lower downstream area, zone 4, was similar to the zone 3 but had a long distance to the stream. The simulated rainfall amounts were 2-, 5-, and 10-y rainfalls under durations of 24-, 48-, and 72-h. The rainfall amounts were determined by a frequency analysis using the GEV distribution. The rainfall hyetograph was designed by an alternating block method. The rainfall spatial distribution was determined by Monte Carlo analysis using the Normal distribution and Cholesky randomization. With the Monte Carlo analysis and Cholesky randomization 1,000 rainfalls were randomly generated under the observed scale parameter, location parameter, and spatial correlation. The rainfall tends to concentrate over the zones 2-4 rather than the zone 1, and in comparison among 24-, 48-, and 72-h rainfalls, the 48- and 72-h rainfalls have more likelihood to concentrate over the zones 2-3.

When the rainfall is uniform, the 2- and 5-y rainfalls give the highest flood peak when the duration is 48-h while the 10-y rainfall gives the highest flood peak when the duration is 72-h. The variation of rainfall duration which gives the highest flood peak appears to be caused by a non-uniform percolation rate which causes the flood water to come from the downstream area for the low intensity rainfall, 2- and 5-y rainfalls, but come from both downstream and upstream areas for the high intensity rainfall, 10-y rainfall.

However, in comparison with non-uniform rainfalls, the flood peak from uniform rainfall can cover only approximately 10-35% of possible flood peaks because the rainfall tends to concentrate over the zones 2-4 which have similar concentration time, 48-h, and not to concentrate over the zone 1 which has a concentration time of 72-h. With the same reason, all of 2-, 5-, and 10-y rainfalls tend to give the highest flood peak when the duration is 48-h. The flood from short duration rainfall, 24-h rainfall, is usually low but has high variability and is high when the rainfall concentrates over the zones 1-2, mountainous region. The floods from long duration rainfalls, 48- and 72-h rainfalls, are usually high but have low variability and are high when the rainfall concentrates over the zones 2-3, joint area. Usually, the high flood peak in the area comes from the long duration rainfalls because the joint area has high probability of consecutive heavy rainfall days, but the short duration rainfall can still give an extremely high flood peak if it concentrates over the mountainous region. Nevertheless, because the rainfall rarely concentrates over the mountainous region, the probability of the extremely high flood peak from the short duration rainfall is low.

The reason why the flood peaks from short and long duration rainfalls respond to the rainfall at the different locations is that the flood peak mainly responds to surface storage and steepness of a rainfall location for the short duration rainfall but mainly responds to soil percolation rate for the long duration rainfall. For the short duration rainfall, the surface storage is dominant when the rainfall is small while the steepness is dominant when the rainfall is large. Both low surface storage and high steepness are associated with the zones 1-2. With these reasons, the flood peak responds to the rainfall in the zones 1-2. For the long duration rainfall, apart from the influence of the soil percolation rate, the influences of the surface storage and steepness are similar to those for the short duration rainfall. The high soil percolation rate is associated with the zones 1-2. With this reason, the response of the flood peak to the rainfall in the zone 1 is weak. For the zone 2 since it usually has high rainfall amount, the influence of the percolation over that zone is less, and therefore, while the response of the flood peak to the rainfall in the zone 2 is still strong. Apart from the influences of the surface storage, steepness, and soil percolation rate, there is also an influence of the distance from the rainfall location to the channel which causes the response of the flood peak to the rainfall in the zone 4 weak in comparison to the response of the flood peak to the rainfall in the zone 3.

Acknowledgements

My heartfelt appreciation goes to Prof. Dr. Minjiao Lu whose comments and suggestions were of inestimable value for my study. I am also indebt Assoc. Prof. Dr. Srilert Chotpantarat from Chulalongkorn University, Thailand, whose comments made enormous contribution to my work. The Royal Irrigation Department and Thai Meteorological Department should also be recognized as data providers. Moreover, I would like to express my gratitude to my family and friends for their moral support and warm encouragement. Finally, I would like to thank MEXT for a grant that made it possible to complete this study.

Bibliography

C. D. Ahrens. *Meteorology Today: An Introduction to Weather, Climate, and the Environment* (9th Edition). Brooks/Cole, U.S., 2009.

D. J. Allcroft and C. A. Glasbey. A latent Gaussian Markov random-field model for spatiotemporal rainfall disaggregation. *Journal of the Royal Statistical Society: Series C (Applied Statistics)*, 52(4):487–498, 2003.

A. Bárdossy and G. G. S. Pegram. Copula based multisite model for daily precipitation simulation. *Hydrology and Earth System Sciences*, 13(12):2299–2314, 2009.

P. B. Bedient and W. C. Huber. *Hydrology and Floodplain Analysis* (2nd Edition). Addison-Wesley, U.S., 1992.

V. A. Bell and R. J. Moore. The sensitivity of catchment runoff models to rainfall data at different spatial scales. *Hydrology and Earth System Sciences*, 4(4):653–667, 2000.

G. W. Brunner. *HEC-RAS, River Analysis System Hydraulic References Manual* (Version 4.1). U.S. Army Corps of Engineers, Hydrologic Engineering Center, U.S., 2010.

V. T. Chow, D. R. Maidment, and L. W. Mays. *Applied Hydrology.* McGraw-Hill, U.S., 1988.

A. Crisci, B. Gozzini, F. Meneguzzo, S. Pagliara, and G. Maracchi. Extreme rainfall in a changing climate: regional analysis and hydrological implications in Tuscany. *Hydrological Processes*, 16(6):1261–1274, 2002.

R. Cronshey. *Urban Hydrology for Small Watersheds* (2nd Edition). U.S. Department of Agriculture, Soil Conservation Service, U.S., 1986.

S. D. Dahale, N. Panchawagh, S. V. Singh, E. R. Ranatunge, and M. Brikshavana. Persistence in rainfall occurrence over Tropical south-east Asia and equatorial Pacific. *Theoretical and Applied Climatology*, 49(1):27–39, 1994.

A. G. Dastidar, D. Ghosh, S. Dasgupta, and U. K. De. Higher order Markov chain models for monsoon rainfall over West Bengal, India. *Indian Journal of Radio & Space Physics*, 39(1):39–44, 2010.

A. C. Davison, S. A. Padoan, and M. Ribatet. Statistical modeling of spatial extremes. *Statistical Science*, 27(2):161–186, 2012.

L. de Haan. A spectral representation for max-stable processes. *The Annals of Probability*, 12(4):1194–1204, 1984.

L. de Haan and A. Ferreira. *Extreme value theory: an introduction*. Springer Science & Business Media, 2006.

A. D. Feldman. *Hydrologic Modeling System HEC-HMS: Technical Reference Manual*. U.S. Army Corps of Engineers, Hydrologic Engineering Center, U.S., 2000.

S. Feng, S. Nadarajah, and Q. Hu. Modeling annual extreme precipitation in China using the generalized extreme value distribution. *Journal of the Meteorological Society of Japan*, 85(5):599–613, 2007.

A. K. Fleig and D. Wilson. *NIFS – Flood Estimation in Small Catchments*. Norwegian Water Resources and Energy Directorate, Norway, 2013.

S. Golian, B. Saghafian, and R. Maknoon. Derivation of probabilistic thresholds of spatially distributed rainfall for flood forecasting. *Water Resources Management*, 24(13):3547–3559, 2010.

S. Golian, B. Saghafian, M. Elmi, and R. Maknoon. Probabilistic rainfall thresholds for flood forecasting: evaluating different methodologies for modelling rainfall spatial correlation (or dependence). *Hydrological Processes*, 25(13):2046–2055, 2011.

Y. Gong, X. Liang, X. Li, J. Li, X. Fang, and R. Song. Influence of rainfall characteristics on Total suspended solids in urban runoff: A case study in Beijing, China. *Water*, 8(7): 278, 2016.

C. T. Haan, H. P. Johnson, D. L. Brakensiek, et al. *Hydrologic Modeling of Small Watersheds*. American Society of Agricultural Engineers, U.S., 1982.

A. Haghnegahdar, B. A. Tolson, J. R. Craig, and K. T. Paya. Assessing the performance of a semi-distributed hydrological model under various watershed discretization schemes. *Hydrological Processes*, 29(18):4018–4031, 2015.

N. J. Higham. *Computing the Nearest Correlation Matrix—a Problem from Finance*. Manchester Institute for Mathematical Sciences, School of Mathematics, University of Manchester, U.K., 2002.

M. M. Hossain and S. Anam. Identifying the dependency pattern of daily rainfall of Dhaka station in Bangladesh using Markov chain and logistic regression model. *Agricultural Sciences*, 3(3):385–391, 2012.

F. A. Huff. Time distribution of rainfall in heavy storms. *Water Resources Research*, 3(4): 1007–1019, 1967.

P. B. Hunukumbura and Y. Tachikawa. River discharge projection under climate change in the Chao Phraya River basin, Thailand, using the MRI-GCM3.1S dataset. *Journal of the Meteorological Society of Japan*, 90A:137–150, 2012.

R. Huser and A. C. Davison. Space–time modelling of extreme events. *Journal of the Royal Statistical Society: Series B (Statistical Methodology)*, 76(2):439–461, 2014.

Hydro and Agro Informatics Institute. *Summary of Thailand Water Situation in 2548 and 2549 B.E.* Hydro and Agro Informatics Institute, Thailand, 2008a. (in Thai).

Hydro and Agro Informatics Institute. *Summary of Thailand Water Situation in 2550 B.E.* Hydro and Agro Informatics Institute, Thailand, 2008b. (in Thai).

Hydro and Agro Informatics Institute. *Summary of Thailand Water Situation in 2551 B.E.* Hydro and Agro Informatics Institute, Thailand, 2009. (in Thai).

Z. Kabluchko and M. Schlather. Ergodic properties of max-infinitely divisible processes. *Stochastic Processes and their Applications*, 120(3):281–295, 2010.

P. Klongvessa and S. Chotpantarat. Flood mitigation due to extreme rainfall events in the inner Bangkok, Thailand. *Natural Hazards*, 73(3):1957–1975, 2014.

M.R. Knebl, Z.L. Yang, K. Hutchison, and D.R. Maidment. Regional scale flood modeling using NEXRAD rainfall, GIS, and HEC-HMS/RAS: a case study for the San Antonio River Basin Summer 2002 storm event. *Journal of Environmental Management*, 75(4): 325–336, 2005.

S. Kotsuki and K. Tanaka. Impacts of mid-rainy season rainfall on runoff into the Chao Phraya River, Thailand. *Journal of Disaster Research*, 8(3):397–405, 2013.

E. Kreyszig. *Advanced Engineering Mathematics* (8th Edition). John Wiley & Sons, U.S., 1999.

K. Kuraji, M. Gomyo, and K. Punyatrong. Inter-annual and spatial variation of altitudinal increase in rainfall over Mount Inthanon and Mae Chaem Watershed, Northern Thailand. *Hydrological Research Letters*, 3:18–21, 2009.

S. Kure and T. Tebakari. Hydrological impact of regional climate change in the Chao Phraya River Basin, Thailand. *Hydrological Research Letters*, 6:53–58, 2012.

G. Lee, Y. Tachikawa, T. Sayama, and K. Takara. Effect of spatial variability of rainfall on catchment responses in mesoscale mountainous area. *Annual Journal of Hydraulic Engineering*, 53:7–12, 2009.

S. K. Lee, B. E. Mapes, C. Wang, D. B. Enfield, and S. J. Weaver. Springtime ENSO phase evolution and its relation to rainfall in the continental US. *Geophysical Research Letters*, 41(5):1673–1680, 2014.

K. Leewatjanakul. *Hydrology* (3rd Edition). SPEC, Thailand, 2009. (in Thai).

N. Mahavik, T. Satomura, S. Shige, B. Sysouphanthavong, S. Phonevilay, M. Wakabayashi, and S. Baimoung. Rainfall pattern over the middle of Indochina Peninsula during 2009–2010 summer monsoon. *Hydrological Research Letters*, 8(1):57–63, 2014.

S. P. Mandal and A. Chakrabarty. Flash flood risk assessment for upper Teesta river basin: using the hydrological modeling system (HEC-HMS) software. *Modeling Earth Systems and Environment*, 2(2):59, 2016.

E. S. Martins and J. R. Stedinger. Generalized maximum-likelihood generalized extreme-value quantile estimators for hydrologic data. *Water Resources Research*, 36(3):737–744, 2000.

S. E. Moon, S. B. Ryoo, and J. G. Kwon. A Markov chain model for daily precipitation occurrence in South Korea. *International Journal of Climatology*, 14(9):1009–1016, 1994.

J. R. Nimmo. Vadose water. *Encyclopedia of Inland Waters*, 1:766–777, 2009.

F. L. Ogden and P. Y. Julien. Runoff sensitivity to temporal and spatial rainfall variability at runoff plane and small basin scales. *Water Resources Research*, 29(8):2589–2597, 1993.

K. Okumura, T. Satomura, T. Oki, and W. Khantiyanan. Diurnal variation of precipitation by moving mesoscale systems: Radar observations in northern Thailand. *Geophysical Research Letters*, 30(20):2073, 2003.

A. Overeem, A. Buishand, and I. Holleman. Rainfall depth-duration-frequency curves and their uncertainties. *Journal of Hydrology*, 348(1–2):124–134, 2008.

V. M. Ponce. Kinematic wave controversy. *Journal of Hydraulic Engineering*, 117(4):511–525, 1991.

S. Prajamwong and P. Suppataratarn. *Integrated Flood Mitigation Management in the Lower Chao Phraya River Basin*. Thailand Development Research Institute, Thailand, 2007.

P. V. S. Raju, U. C. Mohanty, P. L. S. Rao, and R. Bhatla. The contrasting features of Asian summer monsoon during surplus and deficient rainfall over India. *International Journal of Climatology*, 22(15):1897–1914, 2002.

Royal Irrigation Department. *Plan for Protection and Mitigation of Water-related Disasters (Rainy Season) in 2558 B.E.* Royal Irrigation Department, Office of Water Management and Hydrology, Thailand, 2015. (in Thai).

B. Saghafian, S. Golian, and A. Ghasemi. Flood frequency analysis based on simulated peak discharges. *Natural Hazards*, 71(1):403–417, 2014.

T. Sayama, Y. Tatebe, Y. Iwami, and S. Tanaka. Hydrologic sensitivity of flood runoff and inundation: 2011 Thailand floods in the Chao Phraya River basin. *Natural Hazards and Earth System Science*, 15(7):1617–1630, 2015.

T. Sayama, Y. Tatebe, and S. Tanaka. An emergency response-type rainfall-runoff-inundation simulation for 2011 Thailand floods. *Journal of Flood Risk Management*, 10 (1):65–78, 2017.

M. Schlather. Models for stationary max-stable random fields. *Extremes*, 5(1):33–44, 2002.

D. J. Sheskin. *Handbook of Parametric and Nonparametric Statistical Procedures*. CRC Press, U.S., 1996.

V. P. Singh. *Elementary Hydrology*. Pearson College Division, U.S., 1992.

V. P. Singh. Effect of spatial and temporal variability in rainfall and watershed characteristics on stream flow hydrograph. *Hydrological Processes*, 11(12):1649–1669, 1997.

F. F. Snyder. Synthetic unit-graphs. *Eos, Transactions American Geophysical Union*, 19(1): 447–454, 1938.

D. U. J. Sonnadara and D. R. Jayewardene. A Markov chain probability model to describe wet and dry patterns of weather at Colombo. *Theoretical and Applied Climatology*, 119 (1–2):333–340, 2015.

A. Sriariyawat, K. Pakoksung, T. Sayama, S. Tanaka, and S. Koontanakulvong. Approach to estimate the flood damage in Sukhothai Province using flood simulation. *Journal of Disaster Research*, 8(3):406–414, 2013.

K. Subramanya. *Engineering Hydrology* (3rd Edition). Tata McGraw-Hill, India, 2008.

S. Suriya and B.V. Mudgal. Impact of urbanization on flooding: The Thirusoolam sub watershed–A case study. *Journal of Hydrology*, 412–413:210–219, 2012.

A. M. Szyniszewska and P. R. Waylen. Determining the daily rainfall characteristics from the monthly rainfall totals in central and northeastern Thailand. *Applied Geography*, 35 (1–2):377–393, 2012.

H. G. Takahashi. Seasonal changes in diurnal rainfall cycle over and around the Indochina Peninsula observed by TRMM-PR. *Advances in Geosciences*, 25:23–28, 2010.

H. G. Takahashi, H. Fujinami, T. Yasunari, and J. Matsumoto. Diurnal rainfall pattern observed by Tropical Rainfall Measuring Mission Precipitation Radar (TRMM-PR) around the Indochina peninsula. *Journal of Geophysical Research*, 115(D7):D07109, 2010.

Thai Meteorological Department. *The Climate of Thailand*. Thai Meteorological Department, Thailand, 2015.

The World Bank. *Thai Flood 2011: Rapid Assessment for Resilient Recovery and Reconstruction Planning*. The World Bank, Thailand, 2012.

T. Tingsanchali and F. Karim. Flood-hazard assessment and risk-based zoning of a tropical flood plain: case study of the Yom River, Thailand. *Hydrological Sciences Journal–Journal des Sciences Hydrologiques*, 55(2):145–161, 2010.

Y. Tramblay, C. Bouvier, P. A. Ayral, and A. Marchandise. Impact of rainfall spatial distribution on rainfall-runoff modelling efficiency and initial soil moisture conditions estimation. *Natural Hazards and Earth System Sciences*, 11:157–170, 2011.

L. L. Weiss. Sequences of wet and dry days described by a Markov chain probability model. *Monthly Weather Review*, 92(4):169–176, 1964.

S. Yokoi and T. Satomura. Geographical distribution of variance of intraseasonal variations in western Indochina as revealed from radar reflectivity data. *Journal of Climate*, 21(19): 5154–5161, 2008.

D. Zoccatelli, M. Borga, A. Viglione, G. B. Chirico, and G. Blöschl. Spatial moments of catchment rainfall: rainfall spatial organisation, basin morphology, and flood response. *Hydrology and Earth System Sciences*, 15:3767–3783, 2011.

Appendix A

Proof of method

A.1 Markov chain probability model

The proofs regarding the Markov chain probability model are from Weiss [1964] and Sonnadara and Jayewardene [2015].

A.1.1 Rainfall day probability

Let p_1 be a rainfall day probability. A dry day probability can be calculated as $1 - p_1$. Let p_{01} be a transition probability from dry day to rainfall day, and let p_{11} be a transition probability from rainfall day to rainfall day. A probability that a rainfall day after a dry day occurs is $(1 - p_1)p_{01}$ and the probability that a rainfall day after a rainfall day occurs is $p_1 p_{11}$. Since every rainfall day should be either the rainfall day after the dry day or the rainfall day after the rainfall day, p_1 can be calculated by the equation A.1.

$$p_1 = (1 - p_1)p_{01} + p_1 p_{11} \tag{A.1}$$

From the equation A.1, p_1 can be written in terms of p_{01} and p_{11} as the equation A.2.

$$p_1 = \frac{p_{01}}{1 + p_{01} - p_{11}} \tag{A.2}$$

A.1.2 Consecutive rainfall days probability

Define L consecutive rainfall days as a period of $L + 1$ days the last day of which was a dry day and the others L day of which were rainfall days. Denote its probability by p_L^*. With this definition the L consecutive rainfall days occur when the following 3 conditions are satisfied,

1. There is a rainfall day. The probability that this condition is satisfied is p_1.

2. The $L - 1$ days which follow that rainfall day must be rainfall days. The probability that this condition is satisfied is p_{11}^{L-1}.

3. The day after the last day of those rainfall days must become a dry day. The probability that this condition is satisfied is $1 - p_{11}$ since the transition probability from rainfall day to dry day is the complement of the transition probability from rainfall day to rainfall day.

Hence, the value of p_L^* can be calculated as $p_1 p_{11}^{L-1}(1 - p_{11})$. From the equation A.2, p_L^* can be written in terms of p_{01} and p_{11} as the equation A.3.

$$p_L^* = \frac{p_{01}(1-p_{11})p_{11}^{L-1}}{1+p_{01}-p_{11}} \tag{A.3}$$

It should be noted that the day before those $L+1$ can be any of dry day or rainfall day. Hence, the L consecutive rainfall days refers to the consecutive rainfall days with the length of equal to or more than L days. Denote the probability of consecutive rainfall days with the length of more than L days by p_L. Since the length of consecutive rainfall days is discrete, the probability of consecutive rainfall days with the length of more than L days is the same as the probability of consecutive rainfall days with the length of equal to or more than $L+1$ days. Therefore, p_L can be calculated as the equation A.4.

$$p_L = p_{L+1}^* = \frac{p_{01}(1-p_{11})p_{11}^{L}}{1+p_{01}-p_{11}} \tag{A.4}$$

A.1.3 Average length of consecutive rainfall days

Given a condition that the previous day is a rainfall day, the L consecutive rainfall days occur when the following 2 conditions are satisfied,

1. The $L-1$ days which follow that previous day must still be rainfall days. The probability that this condition is satisfied is p_{11}^{L-1}.

2. The day after the last day of those rainfall days must become a dry day. The probability that this condition is satisfied is $1-p_{11}$.

Hence, the probability that the rainfall days are consecutive for L days can be calculated as $p_{11}^{L-1}(1-p_{11})$. Denote the average length of consecutive rainfall days by $\bar{L}$. The value of $\bar{L}$ can be calculated as the equation A.5.

$$\bar{L} = \sum_{L=1}^{\infty} L p_{11}^{L-1}(1-p_{11}) = \frac{1}{1-p_{11}} \tag{A.5}$$

A.2 Cholesky randomization

Let C be a correlation matrix of desired random vectors and let $v_1 = [\ v_{11}\ \ v_{21}\ \ \cdots\ \ v_{r1}\ ]$, $v_2 = [\ v_{12}\ \ v_{22}\ \ \cdots\ \ v_{r2}\ ]$, ..., $v_c = [\ v_{1c}\ \ v_{2c}\ \ \cdots\ \ v_{rc}\ ]$ be uncorrelated random vectors where all elements of these vectors are randomly generated under a population mean of 0 and a population standard deviation of 1. The matrix of the uncorrelated random number ($V_{uncorrelated}$) can be written as the equation A.6.

$$V_{uncorrelated} = \begin{bmatrix} v_{11} & v_{12} & \cdots & v_{1c} \\ v_{21} & v_{22} & \cdots & v_{2c} \\ \vdots & \vdots & \ddots & \vdots \\ v_{r1} & v_{r2} & \cdots & v_{rc} \end{bmatrix} \tag{A.6}$$

With the mean of 0 and standard deviation of 1, the correlation coefficient between the vector v_{i_1} and v_{i_2} where $i_1 \in \{1,2,...,c\}$ and $i_2 \in \{1,2,...,c\}$ is $E(v_{i_1}v_{i_2})$ where E is an expectation operator. The correlation matrix among the vectors $v_1 = [\ v_{11}\ \ v_{21}\ \ \cdots\ \ v_{r1}\ ]$, $v_2 = [\ v_{12}\ \ v_{22}\ \ \cdots\ \ v_{r2}\ ]$, ..., $v_c = [\ v_{1c}\ \ v_{2c}\ \ \cdots\ \ v_{rc}\ ]$ is $E(V_{uncorrelated}^T V_{uncorrelated})$. Because the vectors $v_1 = [\ v_{11}\ \ v_{21}\ \ \cdots\ \ v_{r1}\ ]$, $v_2 = [\ v_{12}\ \ v_{22}\ \ \cdots\ \ v_{r2}\ ]$, ..., $v_c = [\ v_{1c}\ \ v_{2c}\ \ \cdots\ \ v_{rc}\ ]$ are uncorrelated, $E(v_{i_1}v_{i_2})$ is 0 when $i_1 \neq i_2$ and is 1 when $i_1 = i_2$. Therefore, we have the equation A.7.

$$E(V_{uncorrelated}^T V_{uncorrelated}) = I \tag{A.7}$$

Let Z be a triangular matrix which satisfies the equation A.8 and let $V_{correlated}$ be the matrix which satisfies the equation A.9.

$$Z^T Z = C \tag{A.8}$$

$$V_{correlated} = V_{uncorrelated} Z \tag{A.9}$$

The co-variance matrix among the vectors in the matrix $V_{correlated}$ can be written as $E(V_{correlated}^T V_{correlated})$. From the equations A.7, A.8, and A.9, we have the equation A.10.

$$\begin{aligned} E(V_{correlated}^T V_{correlated}) &= E((V_{uncorrelated} Z)^T (V_{uncorrelated} Z)) \\ &= E(Z^T V_{uncorrelated}^T V_{uncorrelated} Z) \\ &= Z^T E(V_{uncorrelated}^T V_{uncorrelated}) Z \\ &= Z^T I Z \\ &= Z^T Z \\ &= C \end{aligned} \tag{A.10}$$

Therefore, the co-variance matrix among the vectors in the matrix $V_{correlated}$ is a correlation matrix C.

Appendix B

Algorithm

B.1 Linearization of differential equations in HEC-RAS model

The linearization of equations of the principles of conservation of mass (equation 5.6) and conservation of momentum (equation 5.7), in the HEC-RAS model are from Brunner [2010]. Denotations in this section are as same as those in the section 5.2.1.2.

B.1.1 Equation of principle of conservation of mass

At the time t and spatial location x, determine the finite differences in the equation 5.15.

For the finite difference $\frac{\Delta A_C}{\Delta t}\Delta x_C$, apply the equation 5.11 to $\frac{\Delta A_C}{\Delta t}$ and apply the equation 5.20 with $A = A_C$. The result is as the equation B.1.

$$\begin{aligned}
\frac{\Delta A_C}{\Delta t}\Delta x_C &= 0.5\Delta x_C \frac{\left(A_{C,x+\Delta x}^{t+\Delta t} - A_{C,x+\Delta x}^{t}\right) + \left(A_{C,x}^{t+\Delta t} - A_{C,x}^{t}\right)}{\Delta t} \\
&= 0.5\Delta x_C \frac{\left(\frac{dA_C}{dz}\right)_{z_x^t}\left(z_x^{t+\Delta t} - z_x^t\right) + \left(\frac{dA_C}{dz}\right)_{z_{x+\Delta x}^t}\left(z_{x+\Delta x}^{t+\Delta t} - z_{x+\Delta x}^t\right)}{\Delta t} \\
&= \frac{0.5\Delta x_C}{\Delta t}\left(\frac{dA_C}{dz}\right)_{z_x^t}\left(z_x^{t+\Delta t} - z_x^t\right) + \frac{0.5\Delta x_C}{\Delta t}\left(\frac{dA_C}{dz}\right)_{z_{x+\Delta x}^t}\left(z_{x+\Delta x}^{t+\Delta t} - z_{x+\Delta x}^t\right)
\end{aligned} \tag{B.1}$$

For the finite difference $\frac{\Delta A_F}{\Delta t}\Delta x_F$, apply the equation 5.11 to $\frac{\Delta A_F}{\Delta t}$ and apply the equation 5.20 with $A = A_F$. The result is as the equation B.2.

$$\begin{aligned}
\frac{\Delta A_F}{\Delta t}\Delta x_F &= 0.5\Delta x_F \frac{\left(A_{F,x+\Delta x}^{t+\Delta t} - A_{F,x+\Delta x}^{t}\right) + \left(A_{F,x}^{t+\Delta t} - A_{F,x}^{t}\right)}{\Delta t} \\
&= 0.5\Delta x_F \frac{\left(\frac{dA_F}{dz}\right)_{z_x^t}\left(z_x^{t+\Delta t} - z_x^t\right) + \left(\frac{dA_F}{dz}\right)_{z_{x+\Delta x}^t}\left(z_{x+\Delta x}^{t+\Delta t} - z_{x+\Delta x}^t\right)}{\Delta t} \\
&= \frac{0.5\Delta x_F}{\Delta t}\left(\frac{dA_F}{dz}\right)_{z_x^t}\left(z_x^{t+\Delta t} - z_x^t\right) + \frac{0.5\Delta x_F}{\Delta t}\left(\frac{dA_F}{dz}\right)_{z_{x+\Delta x}^t}\left(z_{x+\Delta x}^{t+\Delta t} - z_{x+\Delta x}^t\right)
\end{aligned} \tag{B.2}$$

For the finite difference $\frac{\Delta S}{\Delta t}\Delta x_F$, apply the equation 5.11 to $\frac{\Delta S}{\Delta t}$ and apply the equation 5.21. The result is as the equation B.3.

$$\begin{aligned}\frac{\Delta S}{\Delta t}\Delta x_F &= 0.5\Delta x_F \frac{\left(S_{x+\Delta x}^{t+\Delta t} - S_{x+\Delta x}^{t}\right) + \left(S_{x}^{t+\Delta t} - S_{x}^{t}\right)}{\Delta t} \\ &= 0.5\Delta x_F \frac{\left(\frac{dS}{dz}\right)_{z_x^t}\left(z_x^{t+\Delta t} - z_x^t\right) + \left(\frac{dS}{dz}\right)_{z_{x+\Delta x}^t}\left(z_{x+\Delta x}^{t+\Delta t} - z_{x+\Delta x}^t\right)}{\Delta t} \\ &= \frac{0.5\Delta x_F}{\Delta t}\left(\frac{dS}{dz}\right)_{z_x^t}\left(z_x^{t+\Delta t} - z_x^t\right) + \frac{0.5\Delta x_F}{\Delta t}\left(\frac{dS}{dz}\right)_{z_{x+\Delta x}^t}\left(z_{x+\Delta x}^{t+\Delta t} - z_{x+\Delta x}^t\right)\end{aligned} \tag{B.3}$$

For the finite difference ΔQ, according the equation 5.12 with $f = Q$, we have the equation B.4.

$$\begin{aligned}\frac{\Delta Q}{\Delta x} &= \frac{\left(Q_{x+\Delta x}^t - Q_x^t\right) + \theta\left(\left(Q_{x+\Delta x}^{t+\Delta t} - Q_{x+\Delta x}^t\right) - \left(Q_x^{t+\Delta t} - Q_x^t\right)\right)}{\Delta x} \\ \Delta Q &= \left(Q_{x+\Delta x}^t - Q_x^t\right) + \theta\left(Q_{x+\Delta x}^{t+\Delta t} - Q_{x+\Delta x}^t\right) - \theta\left(Q_x^{t+\Delta t} - Q_x^t\right)\end{aligned} \tag{B.4}$$

Replace the finite difference in the equation 5.15 using the equations B.1-B.4 and divide the whole equation by Δx_e. The result is as the equation B.5,

$$C_{Q1}\left(Q_x^{t+\Delta t} - Q_x^t\right) + C_{z1}\left(z_x^{t+\Delta t} - z_x^t\right) + C_{Q2}\left(Q_{x+\Delta x}^{t+\Delta t} - Q_{x+\Delta x}^t\right) + C_{z2}\left(z_{x+\Delta x}^{t+\Delta t} - z_{x+\Delta x}^t\right) = C_B \tag{B.5}$$

where the coefficients C_{Q1}, C_{z1}, C_{Q2}, C_{z2}, and C_B are as the equations B.6, B.7, B.8, B.9, and B.10, respectively.

$$C_{Q1} = \frac{-\theta}{\Delta x_e} \tag{B.6}$$

$$C_{z1} = \frac{0.5}{\Delta t \Delta x_e}\left(\Delta x_C\left(\frac{dA_C}{dz}\right)_{z_x^t} + \Delta x_F\left(\frac{dA_F}{dz} + \frac{dS}{dz}\right)_{z_x^t}\right) \tag{B.7}$$

$$C_{Q2} = \frac{\theta}{\Delta x_e} \tag{B.8}$$

$$C_{z2} = \frac{0.5}{\Delta t \Delta x_e}\left(\Delta x_C\left(\frac{dA_C}{dz}\right)_{z_{x+\Delta x}^t} + \Delta x_F\left(\frac{dA_F}{dz} + \frac{dS}{dz}\right)_{z_{x+\Delta x}^t}\right) \tag{B.9}$$

$$C_B = \frac{\bar{Q}_l - \left(Q_{x+\Delta x}^t - Q_x^t\right)}{\Delta x_e} \tag{B.10}$$

B.1.2 Equation of principle of conservation of momentum

At the time t and spatial location x, determine the finite differences in the equation 5.16.

For the finite difference $\frac{\Delta(Q_C\Delta x_C+Q_F\Delta x_F)}{\Delta t\Delta x_e}$, write Q_C and Q_F as $Q\phi$ and $Q(1-\phi)$, respectively, apply the equation 5.11 to $\frac{\Delta(Q\phi)}{\Delta t}$ and $\frac{\Delta(Q(1-\phi))}{\Delta t}$, and apply the equation 5.25. The result is as the equation B.11.

$$
\begin{aligned}
\frac{\Delta\left(Q_C\Delta x_C+Q_F\Delta x_F\right)}{\Delta t\Delta x_e} &= \frac{\Delta x_C\Delta Q_C+\Delta x_F\Delta Q_F}{\Delta t\Delta x_e}\\
&= \frac{\Delta x_C\Delta\left(Q\phi\right)}{\Delta t\Delta x_e}+\frac{\Delta x_F\Delta\left(Q(1-\phi)\right)}{\Delta t\Delta x_e}\\
&= \frac{0.5\Delta x_C}{\Delta t\Delta x_e}\left(\left((Q\phi)^{t+\Delta t}_{x+\Delta x}-(Q\phi)^{t}_{x+\Delta x}\right)+\left((Q\phi)^{t+\Delta t}_{x}-(Q\phi)^{t}_{x}\right)\right)\\
&\quad+\frac{0.5\Delta x_F}{\Delta t\Delta x_e}\left[\left((Q(1-\phi))^{t+\Delta t}_{x+\Delta x}-(Q(1-\phi))^{t}_{x+\Delta x}\right)\right.\\
&\quad\left.+\left((Q(1-\phi))^{t+\Delta t}_{x}-(Q(1-\phi))^{t}_{x}\right)\right]\\
&= \frac{0.5\Delta x_C}{\Delta t\Delta x_e}\left(\left(Q^{t+\Delta t}_{x+\Delta x}\phi^{t}_{x+\Delta x}-Q^{t}_{x+\Delta x}\phi^{t}_{x+\Delta x}\right)+\left(Q^{t+\Delta t}_{x}\phi^{t}_{x}-Q^{t}_{x}\phi^{t}_{x}\right)\right)\\
&\quad+\frac{0.5\Delta x_F}{\Delta t\Delta x_e}\left[\left(Q^{t+\Delta t}_{x+\Delta x}\left(1-\phi^{t}_{x+\Delta x}\right)-Q^{t}_{x+\Delta x}\left(1-\phi^{t}_{x+\Delta x}\right)\right)\right.\\
&\quad\left.+\left(Q^{t+\Delta t}_{x}\left(1-\phi^{t}_{x}\right)-Q^{t}_{x}\left(1-\phi^{t}_{x}\right)\right)\right]\\
&= \frac{0.5\Delta x_C\phi^{t}_{x+\Delta x}}{\Delta t\Delta x_e}\left(Q^{t+\Delta t}_{x+\Delta x}-Q^{t}_{x+\Delta x}\right)+\frac{0.5\Delta x_C\phi^{t}_{x}}{\Delta t\Delta x_e}\left(Q^{t+\Delta t}_{x}-Q^{t}_{x}\right)\\
&\quad+\frac{0.5\Delta x_F\left(1-\phi^{t}_{x+\Delta x}\right)}{\Delta t\Delta x_e}\left(Q^{t+\Delta t}_{x+\Delta x}-Q^{t}_{x+\Delta x}\right)\\
&\quad+\frac{0.5\Delta x_F\left(1-\phi^{t}_{x}\right)}{\Delta t\Delta x_e}\left(Q^{t+\Delta t}_{x}-Q^{t}_{x}\right) \qquad \text{(B.11)}
\end{aligned}
$$

For the finite difference $\frac{\Delta(\beta VQ)}{\Delta x_e}$, apply the equations 5.12, 5.26, and 5.27. The result is as the equation B.12.

$$
\begin{aligned}
\frac{\Delta\left(\beta VQ\right)}{\Delta x_e} &= \frac{(\beta VQ)^{t}_{x+\Delta x}-(\beta VQ)^{t}_{x}}{\Delta x_e}\\
&\quad+\frac{\theta\left(\left((\beta VQ)^{t+\Delta t}_{x+\Delta x}-(\beta VQ)^{t}_{x+\Delta x}\right)-\left((\beta VQ)^{t+\Delta t}_{x}-(\beta VQ)^{t}_{x}\right)\right)}{\Delta x_e}\\
&= \frac{\beta^{t}_{x+\Delta x}V^{t}_{x+\Delta x}Q^{t}_{x+\Delta x}-\beta^{t}_{x}V^{t}_{x}Q^{t}_{x}}{\Delta x_e}\\
&\quad+\frac{\theta\left(\left(\beta^{t}_{x+\Delta x}V^{t}_{x+\Delta x}Q^{t+\Delta t}_{x+\Delta x}-\beta^{t}_{x+\Delta x}V^{t}_{x+\Delta x}Q^{t}_{x+\Delta x}\right)-\left(\beta^{t}_{x}V^{t}_{x}Q^{t+\Delta t}_{x}-\beta^{t}_{x}V^{t}_{x}Q^{t}_{x}\right)\right)}{\Delta x_e}\\
&= \frac{\beta^{t}_{x+\Delta x}V^{t}_{x+\Delta x}Q^{t}_{x+\Delta x}-\beta^{t}_{x}V^{t}_{x}Q^{t}_{x}}{\Delta x_e}+\frac{\theta\beta^{t}_{x+\Delta x}V^{t}_{x+\Delta x}}{\Delta x_e}\left(Q^{t+\Delta t}_{x+\Delta x}-Q^{t}_{x+\Delta x}\right)
\end{aligned}
$$

$$-\frac{\theta\beta_x^t V_x^t}{\Delta x_e}\left(Q_x^{t+\Delta t}-Q_x^t\right) \tag{B.12}$$

For the finite difference $g\bar{A}\frac{\Delta z}{\Delta x_e}$, apply the equation 5.10 to $\bar{A}$, apply the equation 5.12 to $\frac{\Delta z}{\Delta x_e}$, and apply the equations 5.20 and 5.28. The result is as the equation B.13.

$$\begin{aligned}
g\bar{A}\frac{\Delta z}{\Delta x_e} &= g\left(0.5\left(A_{x+\Delta x}^t+A_x^t\right)+0.5\theta\left(\left(A_{x+\Delta x}^{t+\Delta t}-A_{x+\Delta x}^t\right)+\left(A_x^{t+\Delta t}-A_x^t\right)\right)\right)\\
&\quad\times\frac{\left(z_{x+\Delta x}^t-z_x^t\right)+\theta\left(\left(z_{x+\Delta x}^{t+\Delta t}-z_{x+\Delta x}^t\right)-\left(z_x^{t+\Delta t}-z_x^t\right)\right)}{\Delta x_e}\\
&= \frac{0.5g\left(A_{x+\Delta x}^t+A_x^t\right)\left(z_{x+\Delta x}^t-z_x^t\right)}{\Delta x_e}\\
&\quad+\frac{0.5\theta g\left(A_{x+\Delta x}^t+A_x^t\right)\left(\left(z_{x+\Delta x}^{t+\Delta t}-z_{x+\Delta x}^t\right)-\left(z_x^{t+\Delta t}-z_x^t\right)\right)}{\Delta x_e}\\
&\quad+\frac{0.5\theta g\left(\left(A_{x+\Delta x}^{t+\Delta t}-A_{x+\Delta x}^t\right)+\left(A_x^{t+\Delta t}-A_x^t\right)\right)\left(z_{x+\Delta x}^t-z_x^t\right)}{\Delta x_e}\\
&= \frac{0.5g\left(A_{x+\Delta x}^t+A_x^t\right)\left(z_{x+\Delta x}^t-z_x^t\right)}{\Delta x_e}\\
&\quad+\frac{0.5\theta g\left(A_{x+\Delta x}^t+A_x^t\right)\left(\left(z_{x+\Delta x}^{t+\Delta t}-z_{x+\Delta x}^t\right)-\left(z_x^{t+\Delta t}-z_x^t\right)\right)}{\Delta x_e}\\
&\quad+\frac{0.5\theta g\left(\left(\frac{dA}{dz}\right)_{z_{x+\Delta x}^t}\left(z_{x+\Delta x}^{t+\Delta t}-z_{x+\Delta x}^t\right)+\left(\frac{dA}{dz}\right)_{z_x^t}\left(z_x^{t+\Delta t}-z_x^t\right)\right)\left(z_{x+\Delta x}^t-z_x^t\right)}{\Delta x_e}\\
&= \frac{0.5g\left(A_{x+\Delta x}^t+A_x^t\right)\left(z_{x+\Delta x}^t-z_x^t\right)}{\Delta x_e}+\frac{0.5\theta g\left(A_{x+\Delta x}^t+A_x^t\right)}{\Delta x_e}\left(z_{x+\Delta x}^{t+\Delta t}-z_{x+\Delta x}^t\right)\\
&\quad-\frac{0.5\theta g\left(A_{x+\Delta x}^t+A_x^t\right)}{\Delta x_e}\left(z_x^{t+\Delta t}-z_x^t\right)\\
&\quad+\frac{0.5\theta g\left(z_{x+\Delta x}^t-z_x^t\right)}{\Delta x_e}\left(\frac{dA}{dz}\right)_{z_{x+\Delta x}^t}\left(z_{x+\Delta x}^{t+\Delta t}-z_{x+\Delta x}^t\right)\\
&\quad+\frac{0.5\theta g\left(z_{x+\Delta x}^t-z_x^t\right)}{\Delta x_e}\left(\frac{dA}{dz}\right)_{z_x^t}\left(z_x^{t+\Delta t}-z_x^t\right)
\end{aligned} \tag{B.13}$$

For the finite difference $g\bar{A}\left(\bar{S}_f+\bar{S}_h\right)$, apply the equation 5.10 to $\bar{A}$, $\bar{S}_f$, and $\bar{S}_h$ and apply the equations 5.20, 5.22, 5.23, and 5.28. The result is as the equation B.14.

$$\begin{aligned}
g\bar{A}\left(\bar{S}_f+\bar{S}_h\right) &= g\left(0.5\left(A_{x+\Delta x}^t+A_x^t\right)+0.5\theta\left(\left(A_{x+\Delta x}^{t+\Delta t}-A_{x+\Delta x}^t\right)+\left(A_x^{t+\Delta t}-A_x^t\right)\right)\right)\\
&\quad\times\left[0.5\left(S_{f,x+\Delta x}^t+S_{fx}^t\right)+0.5\theta\left(\left(S_{f,x+\Delta x}^{t+\Delta t}-S_{f,x+\Delta x}^t\right)+\left(S_{fx}^{t+\Delta t}-S_{fx}^t\right)\right)\right.\\
&\quad\left.+0.5\left(S_{h,x+\Delta x}^t+S_{hx}^t\right)+0.5\theta\left(\left(S_{h,x+\Delta x}^{t+\Delta t}-S_{h,x+\Delta x}^t\right)+\left(S_{hx}^{t+\Delta t}-S_{hx}^t\right)\right)\right]
\end{aligned}$$

$$
\begin{aligned}
= \; & 0.25g\left(A^t_{x+\Delta x}+A^t_x\right)\left(S^t_{f,x+\Delta x}+S^t_{fx}\right)\\
& +0.25\theta g\left(A^t_{x+\Delta x}+A^t_x\right)\left(\left(S^{t+\Delta t}_{f,x+\Delta x}-S^t_{f,x+\Delta x}\right)+\left(S^{t+\Delta t}_{fx}-S^t_{fx}\right)\right)\\
& +0.25\theta g\left(\left(A^{t+\Delta t}_{x+\Delta x}-A^t_{x+\Delta x}\right)+\left(A^{t+\Delta t}_{x}-A^t_{x}\right)\right)\left(S^t_{f,x+\Delta x}+S^t_{fx}\right)\\
& +0.25g\left(A^t_{x+\Delta x}+A^t_x\right)\left(S^t_{h,x+\Delta x}+S^t_{hx}\right)\\
& +0.25\theta g\left(A^t_{x+\Delta x}+A^t_x\right)\left(\left(S^{t+\Delta t}_{h,x+\Delta x}-S^t_{h,x+\Delta x}\right)+\left(S^{t+\Delta t}_{hx}-S^t_{hx}\right)\right)\\
& +0.25\theta g\left(\left(A^{t+\Delta t}_{x+\Delta x}-A^t_{x+\Delta x}\right)+\left(A^{t+\Delta t}_{x}-A^t_{x}\right)\right)\left(S^t_{h,x+\Delta x}+S^t_{hx}\right)
\end{aligned}
$$

$$
\begin{aligned}
= \; & 0.25g\left(A^t_{x+\Delta x}+A^t_x\right)\left(S^t_{f,x+\Delta x}+S^t_{fx}\right)\\
& +0.25\theta g\left(A^t_{x+\Delta x}+A^t_x\right)\left[\left(\frac{\partial S_f}{\partial z}\right)_{z^t_{x+\Delta x},Q^t_{x+\Delta x}}\left(z^{t+\Delta t}_{x+\Delta x}-z^t_{x+\Delta x}\right)\right.\\
& \left.+\left(\frac{\partial S_f}{\partial Q}\right)_{z^t_{x+\Delta x},Q^t_{x+\Delta x}}\left(Q^{t+\Delta t}_{x+\Delta x}-Q^t_{x+\Delta x}\right)+\left(\frac{\partial S_f}{\partial z}\right)_{z^t_x,Q^t_x}\left(z^{t+\Delta t}_{x}-z^t_x\right)\right.\\
& \left.+\left(\frac{\partial S_f}{\partial Q}\right)_{z^t_x,Q^t_x}\left(Q^{t+\Delta t}_{x}-Q^t_x\right)\right]\\
& +0.25\theta g\left(S^t_{f,x+\Delta x}+S^t_{fx}\right)\left[\left(\frac{dA}{dz}\right)_{z^t_{x+\Delta x}}\left(z^{t+\Delta t}_{x+\Delta x}-z^t_{x+\Delta x}\right)\right.\\
& \left.+\left(\frac{dA}{dz}\right)_{z^t_x}\left(z^{t+\Delta t}_{x}-z^t_x\right)\right]\\
& +0.25g\left(A^t_{x+\Delta x}+A^t_x\right)\left(S^t_{h,x+\Delta x}+S^t_{hx}\right)\\
& +0.25\theta g\left(A^t_{x+\Delta x}+A^t_x\right)\left[\left(\frac{\partial S_h}{\partial z}\right)_{z^t_{x+\Delta x},Q^t_{x+\Delta x}}\left(z^{t+\Delta t}_{x+\Delta x}-z^t_{x+\Delta x}\right)\right.\\
& \left.+\left(\frac{\partial S_h}{\partial Q}\right)_{z^t_{x+\Delta x},Q^t_{x+\Delta x}}\left(Q^{t+\Delta t}_{x+\Delta x}-Q^t_{x+\Delta x}\right)+\left(\frac{\partial S_h}{\partial z}\right)_{z^t_x,Q^t_x}\left(z^{t+\Delta t}_{x}-z^t_x\right)\right.\\
& \left.+\left(\frac{\partial S_h}{\partial Q}\right)_{z^t_x,Q^t_x}\left(Q^{t+\Delta t}_{x}-Q^t_x\right)\right]\\
& +0.25\theta g\left(S^t_{h,x+\Delta x}+S^t_{hx}\right)\left[\left(\frac{dA}{dz}\right)_{z^t_{x+\Delta x}}\left(z^{t+\Delta t}_{x+\Delta x}-z^t_{x+\Delta x}\right)\right.\\
& \left.+\left(\frac{dA}{dz}\right)_{z^t_x}\left(z^{t+\Delta t}_{x}-z^t_x\right)\right]
\end{aligned}
$$

$$
\begin{aligned}
= \; & 0.25g\left(A^t_{x+\Delta x}+A^t_x\right)\left(S^t_{f,x+\Delta x}+S^t_{fx}\right)\\
& +0.25\theta g\left(A^t_{x+\Delta x}+A^t_x\right)\left(\frac{\partial S_f}{\partial z}\right)_{z^t_{x+\Delta x},Q^t_{x+\Delta x}}\left(z^{t+\Delta t}_{x+\Delta x}-z^t_{x+\Delta x}\right)\\
& +0.25\theta g\left(A^t_{x+\Delta x}+A^t_x\right)\left(\frac{\partial S_f}{\partial Q}\right)_{z^t_{x+\Delta x},Q^t_{x+\Delta x}}\left(Q^{t+\Delta t}_{x+\Delta x}-Q^t_{x+\Delta x}\right)
\end{aligned}
$$

$$
\begin{aligned}
&+0.25\theta g\left(A_{x+\Delta x}^{t}+A_{x}^{t}\right)\left(\frac{\partial S_f}{\partial z}\right)_{z_x^t,Q_x^t}\left(z_x^{t+\Delta t}-z_x^t\right)\\
&+0.25\theta g\left(A_{x+\Delta x}^{t}+A_{x}^{t}\right)\left(\frac{\partial S_f}{\partial Q}\right)_{z_x^t,Q_x^t}\left(Q_x^{t+\Delta t}-Q_x^t\right)\\
&+0.25\theta g\left(S_{f,x+\Delta x}^{t}+S_{fx}^{t}\right)\left(\frac{dA}{dz}\right)_{z_{x+\Delta x}^t}\left(z_{x+\Delta x}^{t+\Delta t}-z_{x+\Delta x}^t\right)\\
&+0.25\theta g\left(S_{f,x+\Delta x}^{t}+S_{fx}^{t}\right)\left(\frac{dA}{dz}\right)_{z_x^t}\left(z_x^{t+\Delta t}-z_x^t\right)\\
&+0.25g\left(A_{x+\Delta x}^{t}+A_{x}^{t}\right)\left(S_{h,x+\Delta x}^{t}+S_{hx}^{t}\right)\\
&+0.25\theta g\left(A_{x+\Delta x}^{t}+A_{x}^{t}\right)\left(\frac{\partial S_h}{\partial z}\right)_{z_{x+\Delta x}^t,Q_{x+\Delta x}^t}\left(z_{x+\Delta x}^{t+\Delta t}-z_{x+\Delta x}^t\right)\\
&+0.25\theta g\left(A_{x+\Delta x}^{t}+A_{x}^{t}\right)\left(\frac{\partial S_h}{\partial Q}\right)_{z_{x+\Delta x}^t,Q_{x+\Delta x}^t}\left(Q_{x+\Delta x}^{t+\Delta t}-Q_{x+\Delta x}^t\right)\\
&+0.25\theta g\left(A_{x+\Delta x}^{t}+A_{x}^{t}\right)\left(\frac{\partial S_h}{\partial z}\right)_{z_x^t,Q_x^t}\left(z_x^{t+\Delta t}-z_x^t\right)\\
&+0.25\theta g\left(A_{x+\Delta x}^{t}+A_{x}^{t}\right)\left(\frac{\partial S_h}{\partial Q}\right)_{z_x^t,Q_x^t}\left(Q_x^{t+\Delta t}-Q_x^t\right)\\
&+0.25\theta g\left(S_{h,x+\Delta x}^{t}+S_{hx}^{t}\right)\left(\frac{dA}{dz}\right)_{z_{x+\Delta x}^t}\left(z_{x+\Delta x}^{t+\Delta t}-z_{x+\Delta x}^t\right)\\
&+0.25\theta g\left(S_{h,x+\Delta x}^{t}+S_{hx}^{t}\right)\left(\frac{dA}{dz}\right)_{z_x^t}\left(z_x^{t+\Delta t}-z_x^t\right) \qquad \text{(B.14)}
\end{aligned}
$$

Replace the terms in the equation 5.16 using the equations B.11-B.14. The result is as the equation B.15,

$$
M_{Q1}\left(Q_x^{t+\Delta t}-Q_x^t\right)+M_{z1}\left(z_x^{t+\Delta t}-z_x^t\right)+M_{Q2}\left(Q_{x+\Delta x}^{t+\Delta t}-Q_{x+\Delta x}^t\right)+M_{z2}\left(z_{x+\Delta x}^{t+\Delta t}-z_{x+\Delta x}^t\right)=M_B \qquad \text{(B.15)}
$$

where the coefficients M_{Q1}, M_{z1}, M_{Q2}, M_{z2}, and M_B are as the equations B.16, B.17, B.18, B.19, and B.20, respectively.

$$
\begin{aligned}
M_{Q1} &= \frac{0.5\left(\Delta x_C\phi_x^t+\Delta x_F\left(1-\phi_x^t\right)\right)}{\Delta t\Delta x_e}-\frac{\theta\beta_x^tV_x^t}{\Delta x_e}\\
&\quad +0.25\theta g\left(A_{x+\Delta x}^{t}+A_{x}^{t}\right)\left(\left(\frac{\partial S_f}{\partial Q}\right)_{z_x^t,Q_x^t}+\left(\frac{\partial S_h}{\partial Q}\right)_{z_x^t,Q_x^t}\right) \qquad \text{(B.16)}
\end{aligned}
$$

$$
\begin{aligned}
M_{z1} &= -\frac{0.5\theta g\left(A_{x+\Delta x}^{t}+A_{x}^{t}\right)}{\Delta x_e}+\frac{0.5\theta g\left(z_{x+\Delta x}^{t}-z_x^t\right)}{\Delta x_e}\left(\frac{dA}{dz}\right)_{z_x^t}\\
&\quad +0.25\theta g\left(A_{x+\Delta x}^{t}+A_{x}^{t}\right)\left(\left(\frac{\partial S_f}{\partial z}\right)_{z_x^t,Q_x^t}+\left(\frac{\partial S_h}{\partial z}\right)_{z_x^t,Q_x^t}\right)
\end{aligned}
$$

$$+0.25\theta g\left(\left(S^t_{f,x+\Delta x}+S^t_{fx}\right)+\left(S^t_{h,x+\Delta x}+S^t_{hx}\right)\right)\left(\frac{dA}{dz}\right)_{z^t_x} \tag{B.17}$$

$$\begin{aligned} M_{Q2} &= \frac{0.5\left(\Delta x_C\phi^t_{x+\Delta x}+\Delta x_F\left(1-\phi^t_{x+\Delta x}\right)\right)}{\Delta t\Delta x_e}+\frac{\theta\beta^t_{x+\Delta x}V^t_{x+\Delta x}}{\Delta x_e} \\ &\quad +0.25\theta g\left(A^t_{x+\Delta x}+A^t_x\right)\left(\left(\frac{\partial S_f}{\partial Q}\right)_{z^t_{x+\Delta x},Q^t_{x+\Delta x}}+\left(\frac{\partial S_h}{\partial Q}\right)_{z^t_{x+\Delta x},Q^t_{x+\Delta x}}\right) \end{aligned} \tag{B.18}$$

$$\begin{aligned} M_{z2} &= \frac{0.5\theta g\left(A^t_{x+\Delta x}+A^t_x\right)}{\Delta x_e}+\frac{0.5\theta g\left(z^t_{x+\Delta x}-z^t_x\right)}{\Delta x_e}\left(\frac{dA}{dz}\right)_{z^t_{x+\Delta x}} \\ &\quad +0.25\theta g\left(A^t_{x+\Delta x}+A^t_x\right)\left(\left(\frac{\partial S_f}{\partial z}\right)_{z^t_{x+\Delta x},Q^t_{x+\Delta x}}+\left(\frac{\partial S_h}{\partial z}\right)_{z^t_{x+\Delta x},Q^t_{x+\Delta x}}\right) \\ &\quad +0.25\theta g\left(\left(S^t_{f,x+\Delta x}+S^t_{fx}\right)+\left(S^t_{h,x+\Delta x}+S^t_{hx}\right)\right)\left(\frac{dA}{dz}\right)_{z^t_{x+\Delta x}} \end{aligned} \tag{B.19}$$

$$\begin{aligned} M_B &= -\frac{\beta^t_{x+\Delta x}V^t_{x+\Delta x}Q^t_{x+\Delta x}-\beta^t_xV^t_xQ^t_x}{\Delta x_e}-\frac{0.5g\left(A^t_{x+\Delta x}+A^t_x\right)\left(z^t_{x+\Delta x}-z^t_x\right)}{\Delta x_e} \\ &\quad -0.25g\left(A^t_{x+\Delta x}+A^t_x\right)\left(\left(S^t_{f,x+\Delta x}+S^t_{fx}\right)+\left(S^t_{h,x+\Delta x}+S^t_{hx}\right)\right) \end{aligned} \tag{B.20}$$

B.2 Cholesky decomposition

Cholesky decomposition is the method to determine a triangular matrix Z such that $Z^TZ = C$ for a specified symmetric matrix C.

B.2.1 Decomposition for 2×2 matrix

Write the symmetric matrix C as the equation B.21 and write the triangular matrix Z as the equation B.22.

$$C=\begin{bmatrix} c_{11} & c_{12} \\ c_{12} & c_{22} \end{bmatrix} \tag{B.21}$$

$$Z=\begin{bmatrix} z_{11} & z_{12} \\ 0 & z_{22} \end{bmatrix} \tag{B.22}$$

Since $Z^TZ = C$, we have the equation B.23.

$$\begin{bmatrix} z_{11} & 0 \\ z_{12} & z_{22} \end{bmatrix}\begin{bmatrix} z_{11} & z_{12} \\ 0 & z_{22} \end{bmatrix}=\begin{bmatrix} c_{11} & c_{12} \\ c_{12} & c_{22} \end{bmatrix} \tag{B.23}$$

Therefore, $z_{11}^2 = c_{11}$, $z_{11}z_{12} = c_{12}$, and $z_{12}^2 + z_{22}^2 = c_{22}$.
Hence, $z_{11} = \sqrt{c_{11}}$, $z_{12} = c_{12}/z_{11}$, and $z_{22} = \sqrt{c_{22} - z_{12}^2}$.
Then, $z_{12} = c_{12}/\sqrt{c_{11}}$ and $z_{22} = \sqrt{c_{22} - (c_{12}^2/c_{11})}$.

The matrix Z can be written in terms of elements in the matrix C as the equation B.22.

$$Z = \begin{bmatrix} \sqrt{c_{11}} & c_{12}/\sqrt{c_{11}} \\ 0 & \sqrt{c_{22} - (c_{12}^2/c_{11})} \end{bmatrix} \tag{B.24}$$

B.2.2 Decomposition for $n \times n$ matrix where $n > 2$

Write the symmetric matrix C as the equation B.25 and write the triangular matrix Z as the equation B.26,

$$C = \begin{bmatrix} c_{11} & C_{1,2:n} \\ C_{1,2:n}^T & C_{2:n,2:n} \end{bmatrix} \tag{B.25}$$

$$Z = \begin{bmatrix} z_{11} & Z_{1,2:n} \\ 0 & Z_{2:n,2:n} \end{bmatrix} \tag{B.26}$$

where $C_{1,2:n}$ and $Z_{1,2:n}$ are $1 \times (n-1)$ matrices, $C_{2:n,2:n}$ is a $(n-1) \times (n-1)$ symmetric matrix, and $Z_{2:n,2:n}$ is a $(n-1) \times (n-1)$ upper triangular matrix.

Since $Z^T Z = C$, we have the equation B.27.

$$\begin{bmatrix} z_{11} & 0 \\ Z_{1,2:n}^T & Z_{2:n,2:n}^T \end{bmatrix} \begin{bmatrix} z_{11} & Z_{1,2:n} \\ 0 & Z_{2:n,2:n} \end{bmatrix} = \begin{bmatrix} c_{11} & C_{1,2:n} \\ C_{1,2:n}^T & C_{2:n,2:n} \end{bmatrix} \tag{B.27}$$

Therefore, $z_{11}^2 = c_{11}$, $z_{11} Z_{1,2:n} = C_{1,2:n}$, and $Z_{1,2:n}^T Z_{1,2:n} + Z_{2:n,2:n}^T Z_{2:n,2:n} = C_{2:n,2:n}$.
Hence, $z_{11} = \sqrt{c_{11}}$, $Z_{1,2:n} = C_{1,2:n}/z_{11}$, and $Z_{2:n,2:n}^T Z_{2:n,2:n} = C_{2:n,2:n} - Z_{1,2:n}^T Z_{1,2:n}$.
Then, $Z_{1,2:n} = C_{1,2:n}/\sqrt{c_{11}}$ and $Z_{2:n,2:n}^T Z_{2:n,2:n} = C_{2:n,2:n} - C_{1,2:n}^T C_{1,2:n}/c_{11}$.
The matrix Z can be written in terms of elements in the matrix C as the equation B.22,

$$Z = \begin{bmatrix} \sqrt{c_{11}} & C_{1,2:n}/\sqrt{c_{11}} \\ 0 & Z_{2:n,2:n} \end{bmatrix} \tag{B.28}$$

where $Z_{2:n,2:n}^T Z_{2:n,2:n} = C_{2:n,2:n} - C_{1,2:n}^T C_{1,2:n}/c_{11}$.

From the equation B.28, the first row of the matrix Z can be determined. For the remaining part of the matrix Z, the matrix $Z_{2:n,2:n}$, since the matrix $Z_{2:n,2:n}$ is the $(n-1) \times (n-1)$ upper triangular matrix and the matrix $C_{2:n,2:n} - C_{1,2:n}^T C_{1,2:n}/c_{11}$ is the $(n-1) \times (n-1)$ symmetric matrix, the recursive Cholesky decomposition can be used to find the first row of the matrix $Z_{2:n,2:n}$ such that $Z_{2:n,2:n}^T Z_{2:n,2:n} = C_{2:n,2:n} - C_{1,2:n}^T C_{1,2:n}/c_{11}$. Then, remaining part of the matrix Z becomes the $(n-2) \times (n-2)$ upper triangular matrix. The similar process can be done recursively until the remaining part of the matrix Z becomes the 2×2 matrix. Then, the decomposition for a 2×2 matrix can be applied.